

Cool-Season Moderate Precipitation Events
in the Northeastern United States

Abstract of
a thesis presented to the Faculty
of the University at Albany, State University of New York
in partial fulfillment of the requirements
for the degree of
Master of Science
College of Arts & Sciences
Department of Earth and Atmospheric Sciences

Keith R. Wagner
2006

ACKNOWLEDGMENTS

During the last three years many people have played a significant role in allowing me to accomplish this important goal. The following is an attempt to identify some of the people that have provided immeasurable help and support along the way and to show them how much I appreciate it.

First of all I would like to thank my two advisors, Lance Bosart and Dan Keyser. Without their scientific knowledge, insight, and patience, none of this would have been possible. I have gained a wealth of knowledge from my interactions with them that I will undoubtedly use in my future endeavors. I am sure Lance will never forget our Yankees-Red Sox rivalry and the Real Estate Channel. I also immensely enjoyed being Dan's teaching assistant for three semesters. I am sure they will have a tremendous positive impact on my future.

This research would not have been possible without the financial support provided by NOAA as part of the Collaborative Science, Technology, and Applied Research (CSTAR) program. CSTAR allows for an opportunity to exchange valuable student research with forecasters at the National Weather Service. Both parties benefit greatly from this continued interaction. Specifically within the NWS, I would like to thank my focal point, Mike Evans from NWS BGM. Our interactions have resulted in many research opportunities and have helped shape this research into a form which is beneficial for both the NWS and the research community. It has been a great pleasure to work with Mike. I would also like to thank Warren Snyder, Ken Lapenta, and Tom Wasula from NWS ALB for their help in the case study aspect of this research. Each of

them were extremely helpful in setting up the Weather Event Simulator, and their efforts were most appreciated.

The results from this research would not have been possible without the help of many people within the department. First of all, I would like to thank my CSTAR colleagues Heather Archambault and Matt Greenstein for all of their help through the process. Matt and I have had innumerable conversations on frontogenesis and instability, among other unrelated topics. I would also like to offer my thanks to all other graduate students, especially Eric Kelsey, Nick Metz, Alan Srock, Amy Maddox, Carl Schreck, Gareth Berry, and Kay Shelton for all the help and good times. A special thanks goes to my officemate, Michael Tanu, for putting up with my shenanigans over the past few years. Also, a big thank-you goes to Celeste, Sharon, and Lynn for all of their help with the administrative details, and to Kevin Tyle and Dave Knight for the technical support I frequently needed.

Finally, I would like to thank my parents, grandparents, and aunt for all of their support over the years and for providing me with the opportunities that few people are lucky enough to have. Thank you to everyone who has helped make this research and more possible.

1. Introduction

1.1 Overview

Moderate precipitation events, defined as event total liquid precipitation amounts of 0.6–1.3 cm or snowfall accumulations of 6.4–19 cm, contribute a significant percentage of all cool-season precipitation events in the northeast United States. While most of the public, and many forecasters, tend to focus on heavy cool-season precipitation events, the lesser events may have a greater long-term impact. Moderate events during the cool season help build up the water table and reservoirs, thus providing crucial water supplies during dry summers. Conversely, frequently occurring moderate events can cause problems for humans and wildlife. Areas that experience consistent moderate snowfalls will build up the snowpack, thus increasing the likelihood for flooding from snowmelt. Frequent moderate rain events can also lead to flooding, especially when followed by a heavy rain event. Such situations can lead to property damage or even loss of life.

Up to this point, no known study has provided a climatology of Northeast cool-season moderate precipitation events. Also, very few studies have focused on the structure and evolution of such events. Past research in this area is overwhelmingly focused on heavy events (e.g., Nicosia and Grumm 1999). However, it is essential to investigate the climatology and structure of cool-season moderate events because 1) they are relatively common, 2) they tend to occur in relatively weak synoptic-scale forcing regimes, and 3) they can be challenging to forecast (e.g., Homan and Uccellini 1987;

Evans 2006). The timing of these events is also important (Call 2005). A moderate 8–10 cm snowfall during the late afternoon can bring traffic in metropolitan areas to a halt. The purpose of this research, through use of a climatology and case studies, is to determine the spatial and temporal characteristics of cool-season moderate precipitation events in the Northeast, and to examine the synoptic-scale and mesoscale forcing that governs when and where these events occur.

1.2 Literature Review

1.2.1 Precipitation Climatologies

Precipitation climatologies have long been used to study seasonal and diurnal distributions of precipitation. For example, Brooks and Stensrud (2000) noted that the forecasting process is greatly assisted by a better knowledge of the climatology of precipitation, especially heavy events. They argued that having a general knowledge of when and where these events occur would greatly help forecasters with individual events. This statement could easily be applied to moderate events as well.

Several recent rainfall climatologies have examined trends in precipitation amount across the United States (US). According to Karl and Knight (1998), precipitation amount has increased 10% across the contiguous US since 1910. An increase in precipitation has occurred because of an increase in the frequency of days with precipitation along with a general increase in rainfall amount on those days. The increased frequency of occurrence is not just for heavy events, but for all categories of

precipitation amount. However, Karl and Knight (1998) noted that the percentage of precipitation from heavy events is increasing relative to moderate events. They found that heavy and extreme events are the primary cause of the 10% increase in precipitation amount. Groisman et al. (2005) confirmed the widespread increase in frequency of occurrence of very heavy (upper 0.3%) precipitation events during the last 50 to 100 years. Both Groisman et al. (2005) and Karl (2006) showed that climate model simulations with enhanced greenhouse gas forcing show a strong and consistent signal of an increasing number of very heavy precipitation events. They argued that one possible cause of the observed increase in frequency and amount of precipitation may be global warming due to an increase in concentration of greenhouse gases in the atmosphere during the past few decades.

Other recent rainfall climatologies have focused on seasonal and diurnal variations in precipitation. The frequency of heavy rain and flash flood events was found to experience a seasonal cycle beginning with a maximum near the Gulf Coast during the cool season and shifting to the Midwest and Northeast during the warm season (Brooks and Stensrud 2000). Fracasso (2004) constructed a climatology of precipitation associated with 500 hPa cool-season cutoff cyclones in the Northeast and found that precipitation amount associated with these lows decreased in midwinter. These results suggest that very heavy precipitation occurs less frequently in the Northeast during the cool season. Wallace (1975) found that heavy precipitation during the cool season showed a nocturnal maximum over the Northeast, while the maximum occurrence of lighter precipitation was near sunrise.

Several climatologies have been constructed for winter-type precipitation. A climatology of freezing rain in the US was developed by Changnon and Karl (2003). They found that national maxima of freezing rain occurred in parts of Pennsylvania and New York, the Midwest, the eastern Appalachians, and the Pacific Northwest. Cortinas et al. (2004) constructed an analysis of sleet, freezing rain, and freezing drizzle across the US and Canada. They found that freezing precipitation exhibits a large spatial variability across the US and is affected by factors such as topography, proximity to water, and the synoptic storm track.

Climatologies are also available for winter cyclones. Colucci (1976) studied winter cyclone frequencies over the eastern US and western Atlantic from 1964–1973. He found that the synoptic-scale storm track favored three main regions: a band from Cape Hatteras to New England, the northern edge of the Gulf Stream current, and the eastern Great Lakes (Fig. 1.1). In an attempt to relate precipitation patterns to the movement of a center of low pressure, Businger et al. (1990) produced a storm-following climatology of winter cyclones that originated over the Gulf of Mexico and produced heavy precipitation (> 25 mm liquid equivalent). They found that the frequency of moderate to heavy precipitation for cyclones tracking up the Atlantic coast was generally highest to the north of the low center. A climatology of heavy banded snowfall in the Northeast revealed that the highest frequency of banding (and thus heavy precipitation) occurred northwest of the surface cyclone (Novak et al. 2004).

A detailed climatology of significant winter-type weather events in the contiguous US from 1982–1994 was presented by Branick (1997). Significant winter-type weather includes heavy snow, freezing rain, blizzards, and damaging wind events. Branick

(1997) found that an annual mean of 128 significant winter events occurred across the contiguous US. He also found that the maximum frequency of these events occurred from late November to late January, with a sharp rise in frequency from October to November.

1.2.2 Mechanisms for Producing Precipitation

Precipitation climatologies are useful for understanding a general pattern of when and where precipitation is most likely to occur. An equally important concept is understanding what mechanisms produce the precipitation. Many studies (e.g., Doswell et al. 1996) have determined that three main ingredients are necessary to produce precipitation: moisture, lift, and instability.

1.2.2.1 Moisture

The importance of sufficient moisture is noted in nearly all precipitation case studies (e.g., Homan and Uccellini 1987; Nicosia and Grumm 1999; Jurewicz and Evans 2004). If the air is very dry, precipitation will not form. Many instabilities, such as conditional symmetric instability, will not be released without sufficient moisture (Schultz and Schumacher 1999). The term “conditional” means that the air must be saturated. While saturation is usually thought to occur when relative humidity reaches 100%, values of 80% are often sufficient for considering that saturation has occurred. A

value of relative humidity lower than 100% is used to account for data errors and inadequacies in the model being used (Schultz and Schumacher 1999).

1.2.2.2 Lifting Mechanisms

The second ingredient for precipitation production is lift. Forcing for ascent can result from anything from a large-scale trough to the ageostrophic circulation around a front. For synoptic-scale features, the amount of lift is often diagnosed using the vertical velocity, ω , obtained from the quasi-geostrophic (QG) ω -equation as expressed in Holton (1992), Eq. (6.29):

$$\left(\nabla^2 + \frac{f_0^2}{\sigma} \frac{\partial^2}{\partial p^2} \right) \omega = \frac{f_0}{\sigma} \frac{\partial}{\partial p} \left[\vec{V}_g \cdot \vec{\nabla} \left(\frac{1}{f_0} \nabla^2 \Phi + f \right) \right] + \frac{1}{\sigma} \nabla^2 \left[\vec{V}_g \cdot \vec{\nabla} \left(-\frac{\partial \Phi}{\partial p} \right) \right], \quad (1)$$

where ω is the vertical velocity, σ is the static stability parameter, \vec{V}_g is the geostrophic wind vector, Φ is the geopotential, f is the Coriolis parameter, and f_0 is a reference value typically taken to be 10^{-4} s^{-1} . The first term on the right-hand side (RHS) of (1) represents differential vorticity advection while the second term on the RHS of (1) is the horizontal Laplacian of thickness advection. Therefore, vertical motion ($\omega < 0$) occurs with increasing cyclonic vorticity advection with height or in the presence of warm advection. However, these two terms often exhibit a large degree of internal cancellation. Therefore, a second way to analyze QG vertical motion is through the use of Q-vectors. The Q-vector form of the ω -equation [(Holton 1992), Eq. 6.35)] is given by:

$$\sigma \nabla^2 \omega + f_0^2 \frac{\partial \omega}{\partial p^2} = -2 \vec{\nabla} \cdot \vec{Q}, \quad (2)$$

where $-2\vec{\nabla}\cdot\vec{Q}$ is the Q-vector convergence and other terms are as defined above. \vec{Q} is defined by:

$$\vec{Q} \equiv (Q_1, Q_2) \equiv \left(-\frac{R}{p} \frac{\partial \vec{V}_g}{\partial x} \cdot \vec{\nabla} T, -\frac{R}{p} \frac{\partial \vec{V}_g}{\partial y} \cdot \vec{\nabla} T \right), \quad (3)$$

where R is the gas constant for dry air and T is temperature. Forcing for upward motion from (2) can be expected whenever there is Q-vector convergence. Q-vectors have become an accepted method to diagnose forcing for vertical motion. For example, Gyakum (1987) used Q-vectors to diagnose forcing for ascent associated with a light-to-moderate snow event in the US Midwest. In his study, the magnitude of the Q-vector convergence was not impressive, but was sufficient to correspond to lighter precipitation.

Mesoscale forcing for ascent is often the result of frontogenesis producing an ageostrophic circulation about a frontal boundary. Frontogenesis is the process by which a front forms or strengthens (e.g., Bluestein 1993, p. 248). The Petterssen (1956) two-dimensional (2D) scalar frontogenesis function used by Nicosia and Grumm (1999) can be defined mathematically as

$$F = \frac{1}{|\nabla\theta|} \left[-\left(\frac{\partial\theta}{\partial x}\right)^2 \frac{\partial u}{\partial x} - \frac{\partial\theta}{\partial y} \frac{\partial\theta}{\partial x} \frac{\partial v}{\partial x} - \frac{\partial\theta}{\partial x} \frac{\partial\theta}{\partial y} \frac{\partial u}{\partial y} - \left(\frac{\partial\theta}{\partial y}\right)^2 \frac{\partial v}{\partial y} \right], \quad (4)$$

where θ is potential temperature, and u and v are the components of the total wind in the x and y directions, respectively. The Petterssen 2D frontogenesis is based on shearing and stretching deformation of the horizontal wind field and its action on the horizontal potential temperature gradient. The effects of horizontal divergence on the horizontal potential temperature gradient are also included. When the potential temperature gradient

increases in (4), frontogenesis is implied. Maximum frontogenesis occurs when the axis of dilatation and the isentropes are parallel.

Sawyer (1956) asserted that frontogenesis is in progress with most active fronts. Regions of confluence act to tighten the horizontal potential temperature gradient and to decrease the vertical wind shear (e.g., Sanders and Bosart 1985). As the potential temperature gradient continues to tighten, it becomes too large for the associated vertical wind shear, thus disrupting the thermal wind balance. In order to restore thermal wind balance, the atmosphere produces a thermally direct ageostrophic circulation about the frontal boundary (Sanders and Bosart 1985). In general, the ascent on the warm side of the front is broad and gentle. However, Jurewicz and Evans (2004) showed that frontogenetically forced heavy snowbands in the presence of QG forcing were more narrow and intense than those removed from QG forcing. Therefore, QG forcing for ascent is sometimes an important aid for precipitation production, but is not always necessary.

1.2.2.3 Instability

The third important ingredient in precipitation formation is instability. Three common instabilities are gravitational (convective), inertial, and symmetric. Gravitational instability for dry air is defined as the potential temperature, θ , decreasing with height ($\partial\theta/\partial z < 0$), while inertial instability is defined as $\partial M_g / \partial x < 0$, where $M_g = v_g + f x$ is the geostrophic absolute angular momentum (e.g., Schultz and Schumacher 1999). For conditional gravitational (or symmetric) instability, θ is replaced with θ_{es} , the

saturation equivalent potential temperature. Symmetric instability arises from an imbalance between the pressure gradient, Coriolis, and buoyancy forces in baroclinic flows (e.g., Seltzer et al. 1985). It has been shown that symmetric instability is equivalent to dry gravitational instability evaluated along an M_g surface (e.g., Schultz and Schumacher 1999). A stratification that is gravitationally and inertially stable may be unstable with respect to slantwise parcel displacements as a result of symmetric instability. The condition for symmetric instability is that M_g surfaces slope less steeply (are less upright) than θ surfaces. Any parcel that is displaced at an angle between these two surfaces will release the symmetric instability. Figure 1.2 illustrates how symmetric instability works. The stratification is inertially and gravitationally stable for pure horizontal and vertical displacements of parcels A and B. However, parcel C is displaced in a slantwise manner such that it is between surfaces of constant M_g and θ . The resulting acceleration then has a component in the direction of the displacement.

A special kind of symmetric instability is conditional symmetric instability (CSI). CSI theory was originally developed by Bennetts and Hoskins (1979) and Emanuel (1983a,b). Bennetts and Hoskins (1979) found that when a layer of air is lifted to saturation and thus becomes conditionally symmetrically unstable, the instability manifests itself as rolls along the thermal wind, leading to banded cloud structures. Emanuel (1983a,b) assessed CSI by lifting an air parcel through an ambient atmosphere that is assumed to remain unaffected by the displacement. He found that CSI is a combination of gravitational and inertial forces and results in a slantwise motion along surfaces on which the buoyancy of the ascending air is near zero. Schultz and Schumacher (1999) point out that it is important to distinguish between CSI and

slantwise convection. Slantwise convection is the process by which the instability, CSI, is released.

Like symmetric instability, CSI is equivalent to dry gravitational instability evaluated along an M_g surface, except that θ is replaced with θ_{es} (Schultz and Schumacher 1999). CSI is generally evaluated using a cross section taken normal to the thermal wind or geopotential thickness contours by displaying lines of constant M_g and θ_{es} (e.g., Moore and Lambert 1993; Wiesmueller and Zubrick 1998). CSI is considered to occur locally at each level where $\partial\theta_{es}/\partial z < 0$ along an M_g surface (Schultz and Schumacher 1999). In other words, if lines of constant θ_{es} are more upright than lines of M_g at a given level, then CSI is present at that location. In practice, however, CSI may be anticipated in regions where lines of constant θ_{es} and constant M_g are nearly parallel, indicating weak or neutral CSI.

Schultz and Schumacher (1999) showed that discrepancies in interpreting the existence of CSI in cross sections could arise from the assumptions made using the θ_{es} - M_g relationship (see their section 3c for a complete list of assumptions). To avoid such problems, they recommend using a concept employed by Moore and Lambert (1993) known as equivalent potential vorticity (EPV) to diagnose CSI. Moore and Lambert (1993) define the three-dimensional (3D) form of EPV as

$$EPV = -g\eta \cdot \nabla \theta_e, \quad (5)$$

where g is gravity and η is the three dimensional vorticity vector. Expanding (5), assuming geostrophic flow, and neglecting terms with ω and variations with respect to y yields

$$EPV = g \left[\left(\frac{\partial M_g}{\partial p} \frac{\partial \theta_e}{\partial x} \right) - \left(\frac{\partial M_g}{\partial x} \frac{\partial \theta_e}{\partial p} \right) \right]. \quad (6)$$

Current literature has shown the form of EPV given by (6) is actually evaluating potential symmetric stability. If $EPV < 0$ and the atmosphere is potentially stable ($\partial \theta_e / \partial p < 0$), then that region is potentially symmetrically unstable. However, the form of EPV in (6) is 2D and thus requires use of the assumptions referred to above. McCann (1995) developed a 3D form of the EPV equation by expanding (5) and making use of the thermal wind relationship. He showed that EPV in a saturated environment is a function of horizontal and vertical temperature gradients. While conceptually simple, the equation using this method proved difficult to compute.

In order to be consistent with the above definitions of CSI, Schultz and Schumacher (1999) and Jurewicz and Evans (2004) recommended that θ_e be replaced by θ_{es} in (6) in order to correctly diagnose CSI. The result is an equation for the saturation equivalent potential vorticity (EPV*), which is sometimes referred to as moist potential vorticity (MPV) and is expressed in 2D form as

$$EPV^* = g \left[\left(\frac{\partial M_g}{\partial p} \frac{\partial \theta_{es}}{\partial x} \right) - \left(\frac{\partial M_g}{\partial x} \frac{\partial \theta_{es}}{\partial p} \right) \right]. \quad (7)$$

The criterion that satisfies CSI requires that the absolute vorticity is negative on a θ_{es} surface, or equivalently that $EPV^* < 0$ (Moore and Lambert 1993). Therefore, Snook (1992) stated that $EPV^* < 0$ determines the potential for CSI. However, the second term in (7) must be looked at carefully. If $\partial \theta_{es} / \partial p > 0$, then the atmosphere is conditionally unstable to vertical displacements. In this case, assuming $\partial M_g / \partial x > 0$, EPV^* will be negative. However, since conditional instability (CI) has a faster growth rate than CSI,

CI will dominate and the diagnosis of CSI becomes irrelevant (Moore and Lambert 1993). Schultz and Schumacher (1999) showed that CSI and CI can coexist in the same region, but not in the same exact location, as shown in Fig. 1.3. Therefore, although EPV* is a quick and effective method for diagnosing regions of instability, it should be used in conjunction with the M_g - θ_{es} analysis along with cross sections of relative humidity to differentiate between regions of CSI and CI.

Wiesmueller and Zubrick (1998) discussed atmospheric criteria that can result in CSI. Regions in which the vertical wind shear is on the order of $10\text{--}20\text{ m s}^{-1}$ in the lowest 1–2 km of the atmosphere are favorable for CSI because M_g surfaces are strongly tilted. CSI usually occurs in the presence of low static stability ($\partial\theta/\partial p$) in the middle troposphere with a statically stable boundary layer. This type of stability profile is often found north of surface frontal boundaries. Therefore, a thermodynamic profile that is nearly saturated and close to moist adiabatic in the middle troposphere is necessary. These conditions often occur near a warm front or ahead of large-scale upper troughs. Also, upper-level absolute vorticity tends to be weak or near zero in many regions where CSI is present. Therefore, while CSI often occurs near frontal boundaries or synoptic-scale troughs, it may sometimes be operating in a seemingly “quiet” environment.

Several theoretical studies have shown that there appears to be a strong correlation between regions of instability and forcing for ascent. Negative EPV* is often associated with an intensified frontogenetical circulation (e.g., Nicosia and Grumm 1999). Xu (1989) showed that frontogenesis in the presence of negative EPV* can produce long lasting mesoscale bands. The theory behind these observations was developed by Emanuel (1985). He showed that the thermally direct circulation around a

frontal zone (as described in section 1.2.2.2) is concentrated and enhanced on the warm side of the frontal zone when that side corresponds with a region of weak MPV or EPV*, as shown in Fig. 1.4. Regions of weak MPV or EPV* may also be referred to as regions of weak moist symmetric stability, or WMSS (Novak et al. 2006). These results were confirmed by Thorpe and Emanuel (1987), who showed that in an atmosphere characterized by WMSS, frontogenesis proceeds at an increased rate while the horizontal scale of the ascent in the warm air is considerably reduced. Therefore, it appears that frontogenetical forcing is driving banded precipitation, while WMSS and even negative EPV* are modulating factors that intensify and localize the band.

1.2.3 Ingredients-based Methodologies

1.2.3.1 History of Ingredients-based Methodologies

Doswell et al. (1996) stated that an ingredients-based methodology (IBM) is a logical choice for the application of scientific understanding to the forecast task. Wetzel and Martin (2001) showed that IBMs are useful because they offer forecasters an alternative to empirically derived rules of thumb. IBMs have been used operationally for several decades in the context of warm-season convection and heavy rain. The three main ingredients for deep convection are moisture, instability, and lift (e.g., McNulty 1978, 1995; Doswell 1987; Johns and Doswell 1992). McNulty (1978) included upper-level wind maxima and their associated divergence fields as additional ingredients for severe weather. Doswell et al. (1996) developed an IBM for flash flooding. He asserted

that heavy precipitation results from sustained high rainfall rates. Based on this premise, the rainfall rate, R , was defined as $R = Ewq$, where E is the precipitation efficiency, w is the vertical velocity, and q is the mixing ratio. Total precipitation (P) was then defined as the product of R and the duration of precipitation. An IBM for cloud heads, a precursor of rapid cyclogenesis, was developed by Dixon et al. (2002). Their IBM was designed to provide a measure of the “vertically integrated extent of realizable symmetric instability” (VRS). The VRS is defined as the number of layers (every 50 hPa) where $EPV^* < 0$, relative humidity is $>95\%$, vertical velocity is upward, and the geostrophic absolute vorticity on an isobaric surface is positive. The greater the magnitude of the VRS, the more likely cloud heads will develop.

Adapting the approach used by Doswell et al. (1996), an IBM for snowfall was developed by Nietfeld and Kennedy (1998). They proposed that air temperature, snowfall rate, and snowfall duration are the three ingredients in a snow event. The same equation for rainfall rate, $R = Ewq$, as used by Doswell et al. (1996), was applied to snowfall. In this case, q is the forecasted mixing ratio due to moisture advection, w is the vertical velocity, and E combines effects of the degree of saturation of the air mass, cloud physics, and the snow to liquid water ratio. Janish et al. (1996) developed an IBM to diagnose the areal distribution of winter weather precipitation type. Their method involves the use of winter weather composite charts to combine maps of moisture, temperature profiles, and vertical motion into a single chart. Wetzell and Martin (2001) expanded the method of Janish et al. (1996) in an attempt to make use of more physically relevant ingredients involved in winter weather production. They selected five key

ingredients for a winter weather precipitation event: QG forcing for ascent, moisture, instability, precipitation efficiency, and temperature.

The first three ingredients selected by Wetzell and Martin (2001) have been discussed in detail in the previous sections. Their fourth ingredient, precipitation efficiency, is identical to E in Nietfeld and Kennedy (1998) and is best described using cloud microphysics. Certain ice crystal habits (e.g., dendrites, plates, needles) are more conducive to large snow accumulations. It has been shown that dendritic ice crystals are usually the lowest density crystal type (Power et al. 1964; Roebber et al. 2003). Lower densities suggest the possibility for higher snow accumulations. Once ice crystal growth has been initiated, the growth rate of those crystals by deposition is greatest at a temperature within a few degrees of -15°C (Mossop 1970; Rogers and Yau 1989, p. 161). This temperature range also happens to be where dendritic crystals form (Power et al. 1964). Therefore, high snow accumulations are favored when the maximum vertical velocity coincides with a region where the temperature is near -15°C (Auer and White 1982). The fifth ingredient selected by Wetzell and Martin (2001) is temperature, which will determine whether the precipitation falls as rain, snow, sleet, or freezing rain. If the wet-bulb temperature remains below zero everywhere, then the precipitation will fall as snow. As seen above, temperature also plays a major role in precipitation efficiency. Therefore, temperature not only determines what type of precipitation will fall, but also how much.

1.2.3.2 Empirical Use of IBMs

Several IBMs for snowfall prediction have been employed operationally over the last few decades. Goree and Younkin (1966) used a synoptic climatology method to find favored areas of snow in relation to the 500 hPa vorticity maximum and surface low. They found the most likely area of snow to be about 7° latitude downstream and 2.5° latitude to the left of the vorticity maximum, and 5° latitude along and 2.5° latitude to the left of the path of the surface low. Browne and Younkin (1970) expanded on this work by relating regions of snowfall to the track of the 850 hPa low. They noted that the greatest probability of heavy snow lies approximately 170 km to the left of the 850 hPa low center. An IBM for snowfall amounts using 200 hPa warm advection was developed by Cook (1980). He suggested that snow accumulations (in inches) during the next 24-h time period are roughly equal to the 200 hPa temperature increase implied by warm advection in °C day⁻¹ during that period. Maximum snowfall would then occur near the coldest 200 hPa temperature that is downstream of the warmest 200 hPa temperature. A “magic chart” was developed by Sangster and Jagler (1985), which relates snowfall amounts to the net vertical displacement (NVD) of an air parcel over a 12-h period for a parcel based at 700 hPa. They found that if the NVD exceeded 80 hPa, heavy snow should be predicted, while a NVD of less than 80 hPa meant light to moderate snow was likely. Wetzel (2000) summarized a snowfall accumulation IBM originally developed by Garcia (1994). Wetzel (2000) stated that the 12-h snowfall (in inches) equals twice the average mixing ratio (in g kg⁻¹) on an isentropic surface that intersects the forecast area between 700–750 hPa. Garcia (2000) revised his original method to allow for high snow to liquid water ratios and for jet streak induced events. Finally, Gordon (1998) developed a winter weather checklist in which he describes the LEMO technique. The LEMO

technique relates snow accumulations to the speed of the associated absolute vorticity maximum. Each of the above techniques has some merit. However, they generally focus on only one or two parameters and do not take into account all of the ingredients that may be producing the precipitation.

1.2.4 Heavy Snow in the Presence or Absence of an Intense Cyclone

Classic eastern US cyclogenesis has been studied extensively in the literature (e.g., Kocin and Uccellini 1990, 2004a, chapters 3–4; Maglaras et al. 1995, section 4). The classic setup for rapid cyclogenesis and heavy snow usually includes a strong surface high pressure system over southeastern Canada, a deep upper-level trough across the central US, and a surface low pressure center near the southeast or mid-Atlantic coast. Coupled jet streak interactions and their associated circulations are also favorable for cyclogenesis and heavy snow production (Uccellini and Kocin 1987). Readers are referred to the above works for details concerning synoptic-scale aspects of US east coast cyclogenesis. The ingredients discussed in previous sections usually coincide best in storms such as these. However, sometimes heavy snow occurs in association with weak surface lows or even with no surface low at all.

1.2.4.1 Ingredients Applied to Intense Cyclones

Precipitation structure in a cyclone was initially described by Bjerknes (1919). He showed that moving cyclones typically have a broad shield of stratiform precipitation

ahead of the warm front and north or northwest of the surface low, with a squall line ahead of the cold front. Novak et al. (2004) showed that heavy bands of snow are often found to the northwest of surface cyclones. Correspondingly, Sanders (1986) found that lower-tropospheric frontogenesis occurs in the banded region northwest of the surface low. Frontogenesis, in turn, increases the geostrophic vertical wind shear, making M_g surfaces flatter, thus making the region more prone to CSI (Wiesmueller and Zubrick 1998). It appears, therefore, that banded regions northwest of intense surface cyclones have three necessary ingredients for heavy precipitation: sufficient moisture, lift, and instability. Since precipitation in the following cases was in the form of snow, temperature was not an issue other than its relation to precipitation efficiency.

The Megalopolitan snowstorm of February 1983, which produced a band of very heavy snow (30–60 cm) across most major northeastern US cities, was studied by Sanders and Bosart (1985). They found that maximum ascent in the band was the result of a thermally direct circulation that formed in response to frontogenetical forcing. Maximum ascent occurred in a band parallel to the axis of frontogenesis, and narrowed and intensified due to its collocation with a region of WMSS. These results confirmed the theoretical work of Emanuel (1985).

Reuter and Yau (1990) provided evidence that CSI or CI-related banding to the northwest of cyclones was not a rare phenomenon. During a three-month period in early March 1986, seven cases of CSI or CI-related heavy banded precipitation that affected Nova Scotia or the nearby Atlantic Ocean were observed. The idea that this situation occurs frequently is supported by numerous recent observational studies that attribute heavy banded snow to frontogenetical forcing in the presence of WMSS or negative

EPV*. Studies by Seltzer et al. (1985), Nicosia and Grumm (1999), Novak et al. (2004), and Jurewicz and Evans (2004) all showed that heavy banded snow northwest of intense surface cyclones was the result of a frontogenetical circulation being concentrated and intensified in the presence of WMSS or negative EPV*. Figure 1.5 shows a cross section through a heavy snowband northwest of an intense surface cyclone. The cross section is taken normal to the geopotential thickness contours (approximately perpendicular to the band). The heavy snow is associated with an intense, upright frontogenesis maximum that coincides with a deep region of WMSS and negative EPV*.

1.2.4.2 Ingredients Applied to Weak or Nonexistent Cyclones

Other observational studies, and some of the studies mentioned in the previous section, have shown that heavy snow also can occur with weak cyclones or with no obvious surface cyclone at all. Seltzer et al. (1985), Moore and Blakely (1988), Jurewicz and Evans (2004), Moore et al. (2004), and Evans (2006) present cases where heavy snow occurred in the absence of an intense cyclone. The results from their case studies mirror the results of the classic intense cyclone case studies described above. While frontogenesis and CSI have their favored locations (i.e., northwest of intense cyclones), their presence is not limited to these regions. As noted by Sawyer (1956), frontogenesis is occurring with most active fronts. Therefore, heavy snowbands can occur with weaker lows or baroclinic zones not associated with an obvious surface low. The driving force for these cases is a frontogenetical circulation. The vertical component of that circulation is concentrated and enhanced by regions of WMSS or CSI (i.e., negative EPV*), leading

to heavy precipitation exactly as seen in the classic cyclone cases. Figure 1.6, taken from Moore et al. (2005), shows a schematic cross section through a heavy snowband (with or without an intense surface cyclone). The key features (assuming saturation and sufficiently cold temperatures) are a deep, intense, and upright region of frontogenesis whose vertical circulation is collocated with a deep region of WMSS or negative EPV*.

Novak et al. (2004) and Jurewicz and Evans (2004) documented cases with weaker bands or nonbanded precipitation. They found that cases that exhibited lower precipitation totals were characterized by weaker and less upright frontogenesis maxima. Gyakum (1987) and Homan and Uccellini (1987) examined three cases of light-to-moderate snow events. Gyakum (1987) showed that a frontal circulation and the susceptibility of the atmosphere to slantwise convection were likely reasons for the observed precipitation. Homan and Uccellini (1987) examined differences in the low-level thermal fields for their two cases, but did not discuss mesoscale lifting mechanisms or instabilities.

1.3 Research Goals and Thesis Synopsis

The above literature review has surveyed some key aspects of precipitation production, especially as they relate to winter storms. A review of precipitation climatologies was presented to show their utility to the forecasting community. In this sense, it is important to create such climatologies for weaker precipitation events since we observe them to occur frequently and often find them difficult to forecast. Mechanisms for precipitation production were discussed and it was shown how attempts

have been made to use them in IBMs within the operational community. Theoretical and observational studies have shown the importance of sufficient moisture, synoptic-scale lift, and instability in producing precipitation. For bands of snow producing heavy precipitation totals, an important factor was an intense, upright frontogenetical circulation that is concentrated and enhanced in the presence of a deep region of WMSS or negative EPV*. This configuration of frontogenetical forcing and instability was observed for bands associated with classic intense cyclones, as well as weak or nonexistent surface cyclones.

To that end, the goals of this research are to 1) construct a climatology of cool-season moderate precipitation events in the Northeast in order to determine their spatial and temporal characteristics and 2) examine the synoptic-scale and mesoscale forcing that governs when and where these events occur. The second goal will be accomplished through the use of case studies by applying elements of the IBMs discussed above in a manner similar to observational studies of heavy snow discussed in sections 1.2.4.1 and 1.2.4.2.

The remainder of the thesis is organized as follows: Chapter 2 discusses the data and methodology used in the climatology and cases studies. Chapter 3 presents results of the moderate event climatology. Chapter 4 provides results of four moderate event case studies. A discussion of the climatology and case studies is presented in chapter 5. Chapter 6 offers some concluding remarks and suggestions for future work.

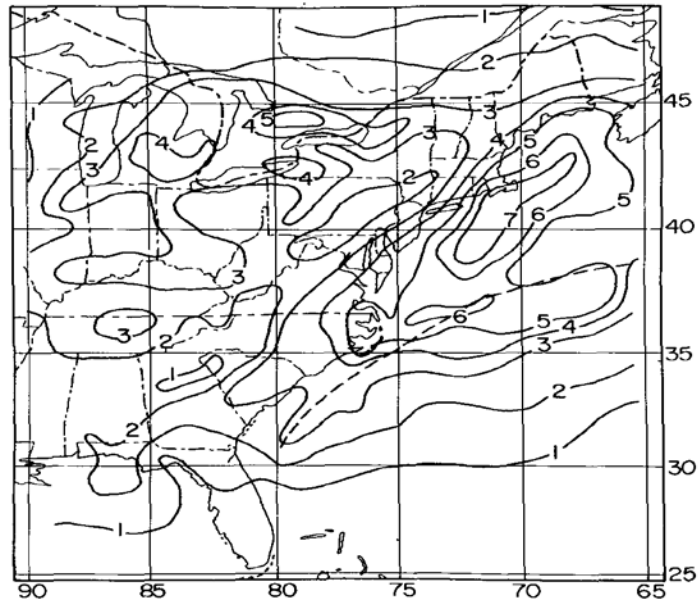


Fig. 1.1. Winter cyclone frequencies for January 1964–December 1973. Contour values should be multiplied by 10. Source: Colucci (1976), Fig. 1.

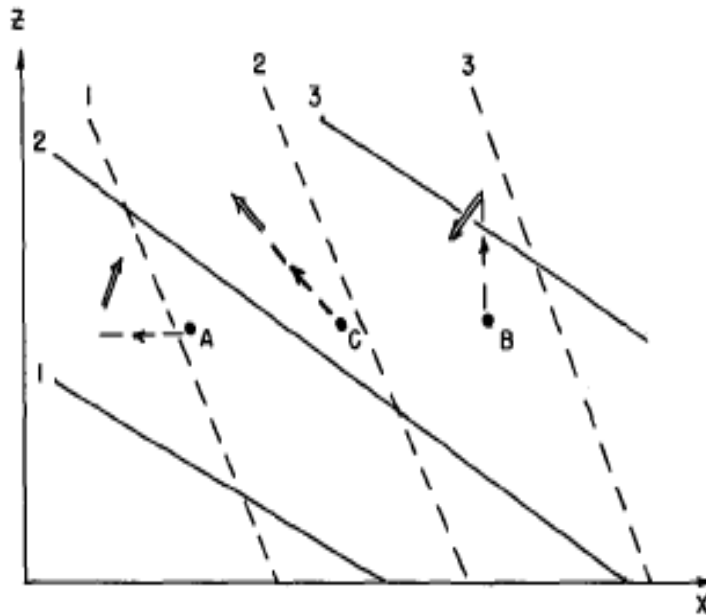


Fig. 1.2. Schematic vertical cross section illustrating symmetric instability. Solid lines represent absolute momentum, M , while dashed lines represent potential temperature. Letters show sample displacements (dashed) and accelerations (arrows). This configuration of absolute momentum and potential temperature is symmetrically unstable to the slantwise displacement shown for parcel C. Source: Sanders and Bosart (1985), Fig. 4.

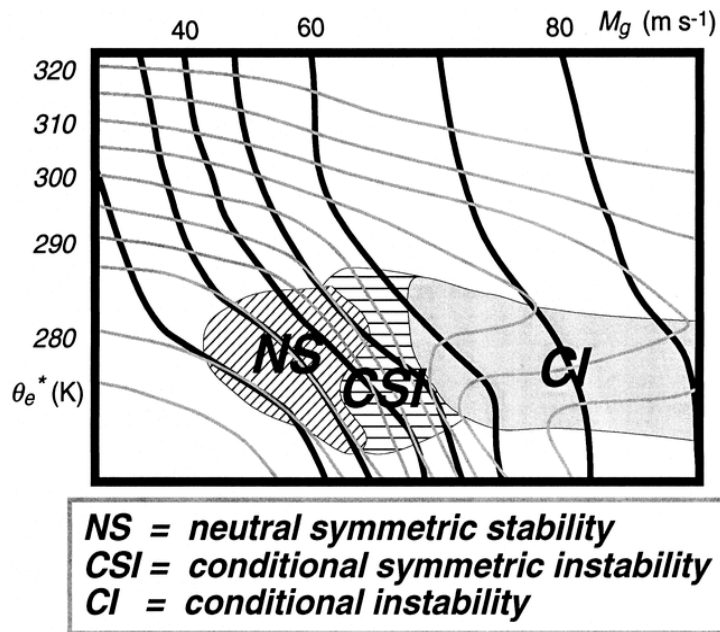


Fig. 1.3. Stability regimes often observed near frontal zones. Contours represent typical values: M_g (thick black lines) and θ_e^* (θ_{es}) (thin gray lines). Source: Schultz and Schumacher (1999), Fig. 4.

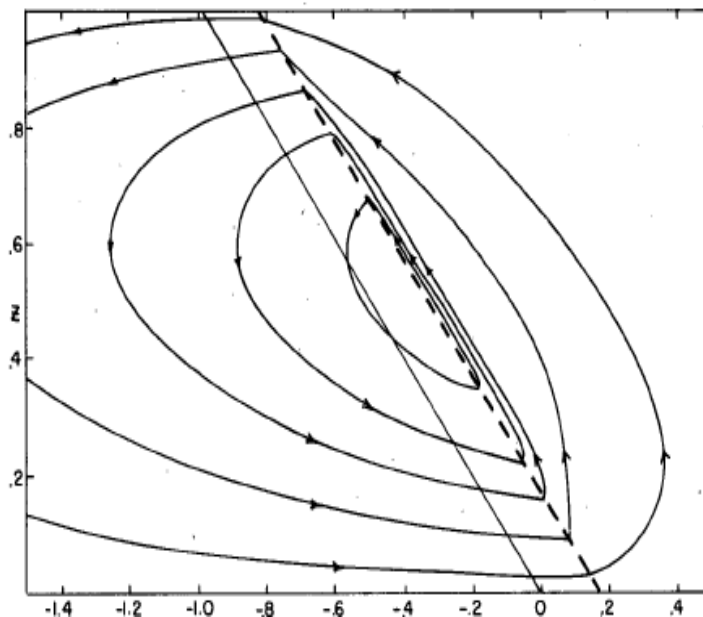


Fig. 1.4. Vertical cross section of the vertical circulation around a sloping frontal zone (dashed line) in the presence of weak moist symmetric stability (to the right of the frontal zone). Source: Emanuel (1985), Fig. 5.

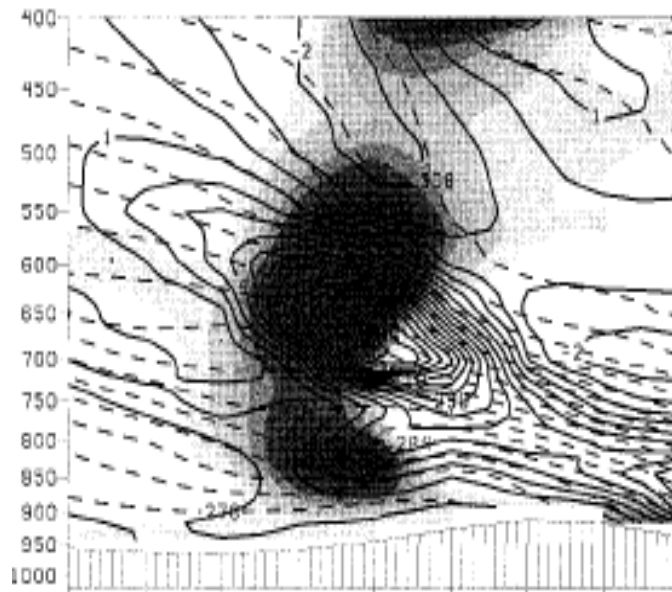


Fig. 1.5. Cross section through a heavy snowband depicting strong, upright frontogenesis (solid contours), saturation equivalent potential temperature (dashed contours), and saturation equivalent potential vorticity (negative values shaded) for a 12-h forecast valid at 0000 UTC 5 February 1995. Source: Nicosia and Grumm (1999), Fig. 5c.

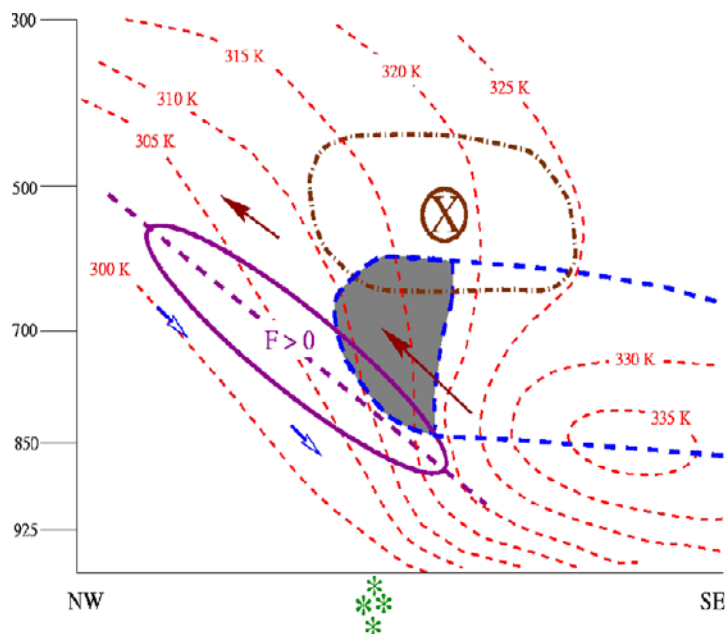


Fig 1.6. Schematic cross section through a heavy snowband showing steeply sloped midlevel frontogenesis (solid purple ellipse) and conditionally unstable region (dashed blue line). Region of WMSS is shaded. X represents the dry conveyor belt. Arrows indicate sense of slantwise circulation. Source: Moore et al. (2005), Fig. 15b.

2. Data and Methodology

2.1 Data Sources

2.1.1 Climatology

Data for the moderate event climatology were obtained from the National Climatic Data Center (NCDC) Local Climatological Data (LCD) and Hourly Precipitation Data (HPD). The LCD and HPD used in this study have been quality controlled by NCDC. Daily precipitation amounts obtained from the LCD are recorded from midnight to midnight local standard time. The LCD contains daily liquid precipitation amounts as well as daily snowfall accumulations. Only a handful of days at certain observing stations had missing daily liquid precipitation data. Gaps in the snowfall data were slightly more prevalent, especially at Allentown, PA (ABE), Wilkes Barre-Scranton, PA (AVP), and Worcester, MA (ORH), where several months were missing daily snowfall accumulations. However, many days when snowfall data were missing, but liquid precipitation data were recorded, had temperatures that were unlikely to support snow. Overall, the missing data had a minimal impact on the climatology.

2.1.2 Case Studies

Data for all moderate event case studies came from several sources. Each of the case studies used the 40 km Eta model (e.g., Black 1994), available at 3-h intervals. Data

were previously archived at the Albany and Binghamton National Weather Service (NWS) Forecast Offices. Horizontal maps and cross-sectional analyses using these data were displayed using the NWS Weather Event Simulator (WES), version 4.0. The WES displays data processed by the NWS Advanced Weather Information Processing System (AWIPS). Additional synoptic-scale maps were produced using the National Centers for Environmental Prediction (NCEP)/National Center for Atmospheric Research (NCAR) reanalysis dataset (Kalnay et al. 1996; Kistler et al. 2001). The NCEP/NCAR global reanalysis dataset has a 2.5° latitude–longitude spatial resolution and a 6-h temporal resolution. Archived NCDC radar reflectivity data were also used in the case studies, while atmospheric soundings were obtained from the University of Wyoming Department of Atmospheric Science website (<http://weather.uwyo.edu/>).

2.2 Methodology

2.2.1 Climatology

The climatology began by defining the cool season as October through April. A cool-season moderate precipitation event was then defined as a precipitation event occurring during this time period that had an event liquid precipitation total of 0.6–1.3 cm (± 0.1 cm) or snowfall total of 6.4–19.0 cm. The domain considered as the Northeast in this research was bounded on the west by a north–south line passing through Detroit, MI (DTW), and on the south by an east–west line passing through Charleston, WV (CRW). Stations located north and east of these lines were considered for the climatology. It was

then decided that only stations which were defined as first-order and had sufficient daily and hourly precipitation data going back several decades would be used in the study. First-order stations were defined as those stations that have an automated surface observing system (ASOS) and are locations of NWS forecast offices or ASOS-NWS cooperative stations. Based on these criteria, 35 first-order stations were identified in the domain. The locations and three-letter identifiers of these stations are shown in Fig. 2.1. A noticeable gap between stations occurs over central Pennsylvania. However, State College, PA, did not fit the criteria of a first-order station, and Williamsport, PA, had insufficient hourly data. Therefore, it was decided to leave a gap in that region.

Once stations were selected, the time period of 1994–2004 was chosen to conduct the climatology, beginning with October 1994 and ending with April 2004. This time period was chosen due to the availability of Weather Surveillance Radar-1988 Doppler (e.g., Crum et al. 1993). The LCD were then consulted for each of the 35 stations on a daily basis. If the precipitation amount for a certain day fell within the moderate range, that day was considered to have a moderate event. The moderate precipitation total could come from either the liquid or the snowfall data. For example, if the liquid equivalent was only 0.4 cm, but the snowfall total was 7 cm, then the event was considered moderate. However, if the liquid equivalent was 1.2 cm (in the moderate range), but snowfall amounts were 22 cm (above the moderate range), then the event was not considered to be moderate. The HPD were used to refine the event selection process for potentially ambiguous cases. For example, if two consecutive days individually had precipitation amounts that were in the moderate range, but collectively were above the range, then the HPD were consulted. If a gap in measurable precipitation was found

between the two days that lasted for six hours or longer, then it was considered that two separate moderate events had occurred. If the gap was less than six hours, the precipitation was considered to have come from the same event, and therefore a moderate event had not occurred. As another example, the HPD were also consulted if two consecutive days individually had precipitation amounts that were below the moderate range, but collectively were in the range. If the gap in precipitation was less than six hours, then the precipitation was considered to come from one event, and thus, a moderate event had occurred. This method of determining whether two, one, or no moderate events had occurred was used for all ambiguous cases.

Histograms of the climatology results were produced similar to those presented in Cortinas et al. (2004). The histograms show the distribution of moderate events by month, station, state, and geographic region. Also, a horizontal map summarizing the distribution of moderate events by geographic region over the 10-year period was produced.

2.2.2 Case Studies

Possible cases for further study were selected based on the criteria that the event total precipitation at stations near the precipitation region was in the moderate range. The precipitation amount was confirmed using the LCD and HPD. Also, the precipitation associated with each case could not obviously be associated with an intense cyclone. It was determined that four main types of systems (excluding lake-effect precipitation) produce moderate precipitation events during the cool season across the Northeast:

Alberta Clippers, weak Ohio Valley cyclones, inverted troughs, and 500 hPa cutoff cyclones. Hutchinson (1995) showed that Alberta Clippers are often associated with light-to-moderate precipitation and impact the northern US between late fall and early spring. Weak Ohio Valley cyclones, such as those studied by Homan and Uccellini (1987), can be considered to be those cyclones with minimum central pressure greater than 1000 hPa and that track in a general northeast or east-northeast direction in the Ohio Valley region. These systems often have a shield of light-to-moderate precipitation ahead of the surface warm front and north of the surface low pressure center. Keshishian et al. (1987) discussed the formation of cyclones with inverted troughs over interior North America, while Keshishian and Bosart (1987) discussed inverted troughs associated with coastal fronts. These studies showed that frontogenesis occurs in conjunction with inverted troughs; thus, assuming moisture is present precipitation is likely to occur. Fracasso (2004) showed that 500 hPa cutoff cyclones are often associated with moderate precipitation, especially across New England.

Based on the criteria presented above, four cases were selected for further study: 27 December 2004 (inverted trough), 8 January 2005 (weak Ohio Valley cyclone), 26 January 2005 (Alberta Clipper), and 21 February 2005 (Alberta Clipper/Ohio Valley hybrid). No 500 hPa cutoff cyclones were used in the case studies. These cases were selected in order to compare and contrast the different types of synoptic-scale systems that produce moderate events.

Horizontal maps for each case were constructed to assess the synoptic-scale features associated with the precipitation. Maps of sea level pressure, 500 hPa geopotential height and absolute vorticity, 1000–500 hPa thickness, low-level vertical

motion, and low-level Q-vector divergence [refer to Eq. (2) in section 1.2.2.2] were constructed on WES using the 40 km Eta model. Upper-level winds (300 hPa) were calculated using NCEP/NCAR reanalysis data. Atmospheric soundings were also obtained for locations near the precipitation to determine any possible thermodynamic influence on the precipitation.

Radar data were used to delineate areas of possible moderate precipitation for each case. Cross sections were taken perpendicular to the 1000–500 hPa thickness contours and through the precipitation region, in accordance with the guidelines set forth in previous CSI literature as discussed in section 1.2.2.3, using forecast data corresponding to the time closest to when the precipitation was observed. The cross sections were constructed in order to assess mesoscale forcing for the observed precipitation. Vertical cross sections were produced showing Petterssen frontogenesis [refer to Eq. (4) in section 1.2.2.2], vertical velocity, EPV*, relative humidity (RH), and temperature. Separate cross sections were made showing the M_g - θ_{es} relationship in order to determine if regions of negative EPV* were due to CI or CSI. Additionally, a composite schematic cross section through a moderate precipitation band was produced to compare features of moderate events to features observed in heavy events. The above methods were used since they closely follow methods used to diagnose synoptic-scale and mesoscale features in heavy snow events as described in sections 1.2.4.1 and 1.2.4.2.

It is important to note that Petterssen frontogenesis was calculated using the total wind instead of the geostrophic wind because ageostrophic winds may be significant near frontal zones (e.g., Nicosia and Grumm 1999). The EPV* calculation from WES/AWIPS was based on the 2D version given by (7) in section 1.2.2.3. The form of EPV* in (7) is

based on approximations using the geostrophic wind (e.g., Schultz and Schumacher 1999, section 3c). In contrast, Jurewicz and Evans (2004) and Novak et al. (2004) provided arguments for using the total wind to calculate EPV*. Jurewicz and Evans (2004) noted that the potential for slantwise acceleration of air parcels relative to an evolving and unbalanced environment can be better described using EPV* calculated with the total wind. Consistent with this reasoning, Novak et al. (2004) used the total wind to calculate EPV* since it is more representative of the curved flow associated with cyclones. Using the total wind requires that some minor changes be made to (7). The geostrophic absolute angular momentum, M_g , is replaced by the absolute angular momentum, M , where $M = v + fx$. This modification results in the 2D form of the EPV* equation calculated using the total wind, which is given by

$$EPV^* = g \left[\left(\frac{\partial M}{\partial p} \frac{\partial \theta_{es}}{\partial x} \right) - \left(\frac{\partial M}{\partial x} \frac{\partial \theta_{es}}{\partial p} \right) \right]. \quad (8)$$

The interpretation of (8) is the same as that of (7): $EPV^* < 0$ indicates the existence of CI or CSI. This form of EPV* was used by WES/AWIPS to calculate EPV* for each case study.



Fig 2.1. Location and three-letter identifier for all 35 first-order stations used in the cool-season moderate event climatology across the Northeast.

3. Climatology Results

3.1 Seasonal Trends

Using the methodology described in Chapter 2, a list of moderate events that occurred at each first-order station during the cool season from 1994-2004 was created. Based on this list, histograms were produced for each station in order to reveal any trends within the cool season. Figures 3.1 and 3.2 show the frequency of occurrence of cool-season moderate precipitation events at Albany, NY (ALB), for 1999–2000 and 2000–2001, respectively. The frequency of occurrence at Buffalo, NY (BUF), for the 2000–2001 and 2003–2004 cool seasons are given in Figs. 3.3 and 3.4, respectively. Histograms such as these were produced for each cool season at every station. However, this method of representing the distribution of moderate events by month did little to reveal any trends in the data. For example, Figs. 3.1 and 3.4 show peaks in frequency of occurrence for December, while Figs. 3.2 and 3.3 show minima in December. Note that BUF had no moderate events during December 2001 (Fig. 3.3).

In order to determine if any seasonal trends existed within the cool season, histograms were produced for the entire 10-yr period at each station. The 10-yr cool-season monthly totals at BUF (Fig. 3.5) exhibited a general peak in frequency of occurrence of moderate events from November–January with fewer events for other months. However, Elkins, WV (EKN), and ALB featured dual peaks in frequency of occurrence: one in early to midwinter and a second in early to midspring (Figs. 3.6 and 3.7, respectively). The appearance of dual peaks in frequency of occurrence was also

noted in the combined 10-yr monthly totals for all seven first-order stations in New York State (Fig. 3.8). Nearly 160 events occurred at these stations during December and January, while approximately 150 events occurred during March and April. Conversely, there were distinct minima across the state during October and February, with October having significantly fewer events than February. A sharp rise in the number of events occurred with the transition from mid to late autumn. The sharp increase was similar to the increase in frequency of significant winter weather events across the contiguous US from October to November that was noted by Branick (1997). Similar dual peaks in frequency with pronounced midwinter minima occurred for the combined 10-yr monthly totals for all five stations in Pennsylvania (Fig. 3.9) and Ohio (Fig. 3.10). This trend was also evident for the combined 10-yr monthly totals comprising all 35 stations (Fig. 3.11). Again, a sharp increase was noted early in the cool season, with over 200 more events occurring in December than October. Also, February had between 150–200 fewer events than the months surrounding it. Figure 3.11 shows that the March/April peak in frequency of occurrence had a greater magnitude than the December/January peak when all 35 stations were considered.

These results show that variations in the frequency of occurrence of moderate precipitation events exist within the cool season across the Northeast. In general, minimum frequency occurs at the beginning of the cool season, followed by a rapid increase in frequency during early winter. A pronounced minimum then occurs in midwinter, followed by an even larger peak in frequency during early spring.

3.2 Geographical Trends

In addition to monthly variations within the cool season, variations by station and geographic region over the 10-yr period were also studied. Erie, PA (ERI), received the most cool-season moderate precipitation events over the past 10 years (197), while Baltimore, MD (BWI), received the least (95). The seven first-order stations in New York State (see Fig. 2.1) represent a good example of the variation in frequency of moderate events across the domain. Figure 3.12 shows the number of events that occurred over the 10-yr period for each station in New York State, beginning in the west at BUF and continuing east and south to New York City (JFK/LGA). The four western most stations [BUF, Rochester (ROC), Syracuse (SYR), and Binghamton (BGM)] received between 140 and 180 events, while the eastern and southern portions of the state received less than 120 events. A steady decrease in the number of events occurred while moving east and south across the state.

Other geographical regions were examined to determine if there was a common signal of fewer moderate events in the eastern or southern portions of the domain. The results for northern New England (Fig. 3.13) revealed that approximately 120–180 events occurred. Caribou, ME (CAR), the northernmost of the four stations, had nearly 40 more moderate events than the next station to the south. Consistent with these results, stations in southern New England (Fig. 3.14) received approximately 95–125 moderate events over the 10-yr period. This range was much smaller than for northern New England. The three stations in the Washington, DC, area [Wilmington, DE (ILG), BWI, and Washington Reagan National Airport (DCA)] had only 95–105 moderate events (Fig. 3.15). In fact, the stations in the southeastern part of the domain had the lowest

frequency of occurrence of all geographic regions. Stations located on or near the Atlantic coast (Fig. 3.16) recorded approximately 95–125 moderate events, with the highest number of events occurring at the northernmost station [Portland, ME (PWM)]. With the exception of DTW, stations across the western region (Ohio/Michigan) received between 120 and 160 moderate events (Fig. 3.17), which was a much higher frequency than along the Atlantic coast.

The results of the 10-yr climatology of cool-season moderate precipitation events at each station are summarized in Fig. 3.18. During the 10-yr period, a mean of 132.5 events occurred when all stations were considered. The numbers at each first-order station in Fig. 3.18 represent the ratio of the total number of events at that station to the mean number of events for all stations. For example, a value of 1.31 means that 1.31 times the mean number of events occurred at that location (in this case, 174 events). The 1.00 contour begins in southern Maine and curves westward and southward into central Virginia, roughly following the shape of Atlantic coast. All stations south and east of this contour received less than the mean number of events. All stations to the north and west of the 1.00 contour, with the exception of DTW and Akron, OH (CAK), received more than the mean number of events. Three distinct regions of enhanced frequency of occurrence within the general high frequency region can be seen in Fig. 3.18. These enhanced regions are east of Lake Erie, along the US/Canadian border, and along the spine of the Appalachians. Based on Fig. 3.18, it appears that a general decrease in the frequency of occurrence of moderate events occurs as one moves south and east across the domain.

Albany 1999-2000 Moderate Precipitation Events

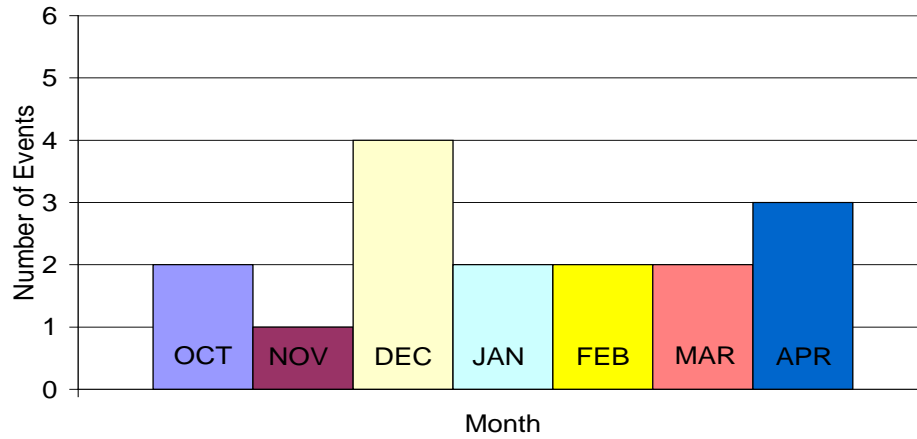


Fig. 3.1. Frequency of occurrence of moderate precipitation events at ALB for the 1999–2000 cool season.

Albany 2000-2001 Moderate Precipitation Events

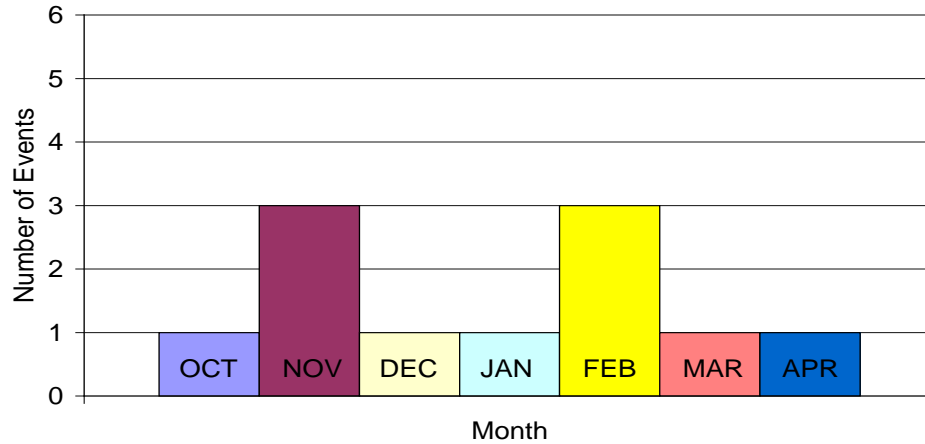


Fig. 3.2. As in Fig. 3.1 except for 2000–2001.

Buffalo 2001-2002 Moderate Precipitation Events

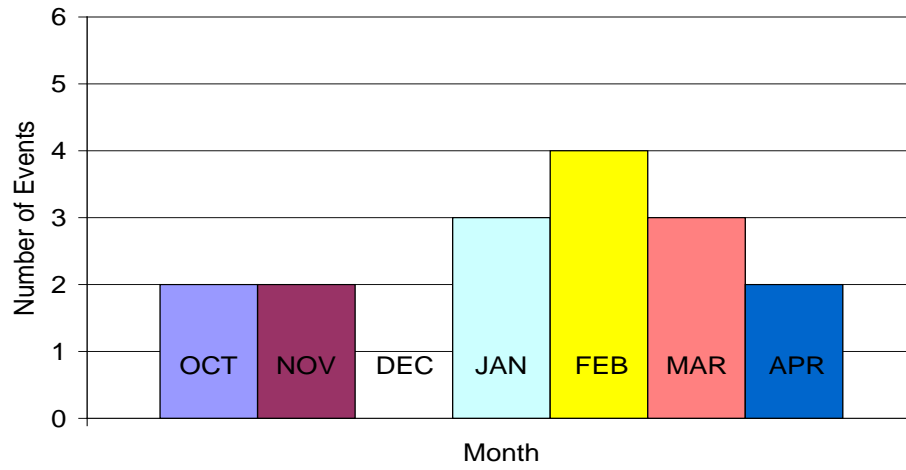


Fig. 3.3. As in Fig. 3.1 except at BUF for 2001–2002.

Buffalo 2003-2004 Moderate Precipitation Events

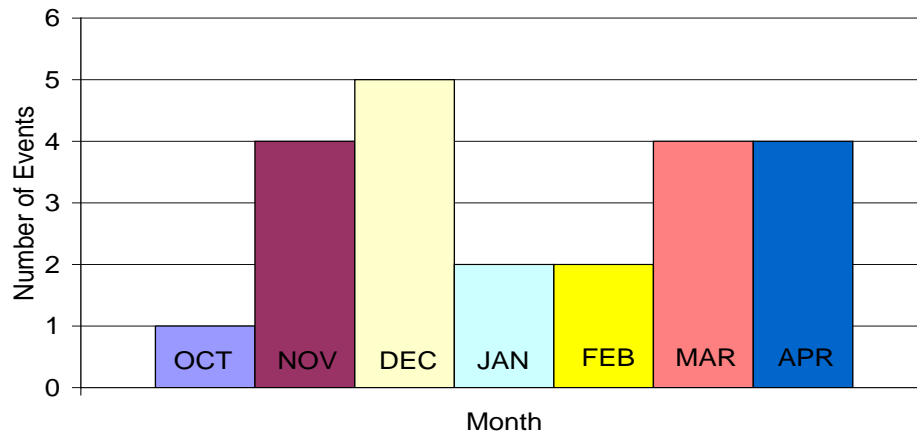


Fig. 3.4. As in Fig. 3.3 except for 2003–2004.

**Buffalo Moderate Precipitation Events By Month:
1994-2004**

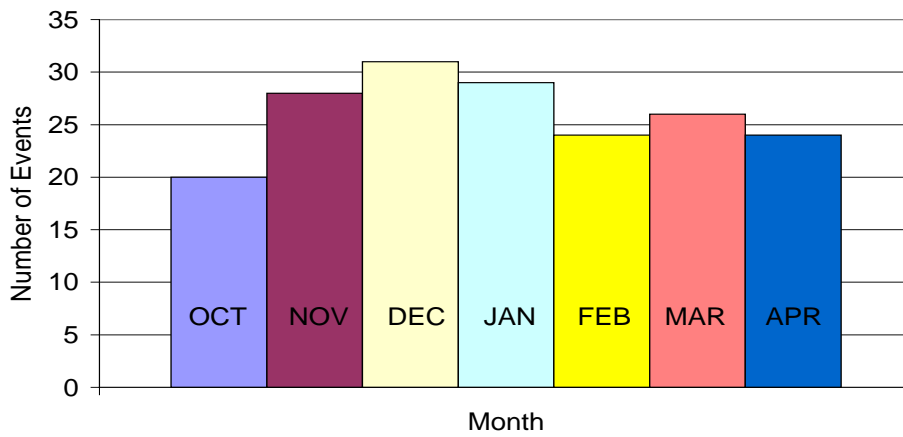


Fig. 3.5. Frequency of occurrence of moderate events at BUF for the 10-yr period 1994–2004.

**Elkins Moderate Precipitation Events By Month:
1994-2004**

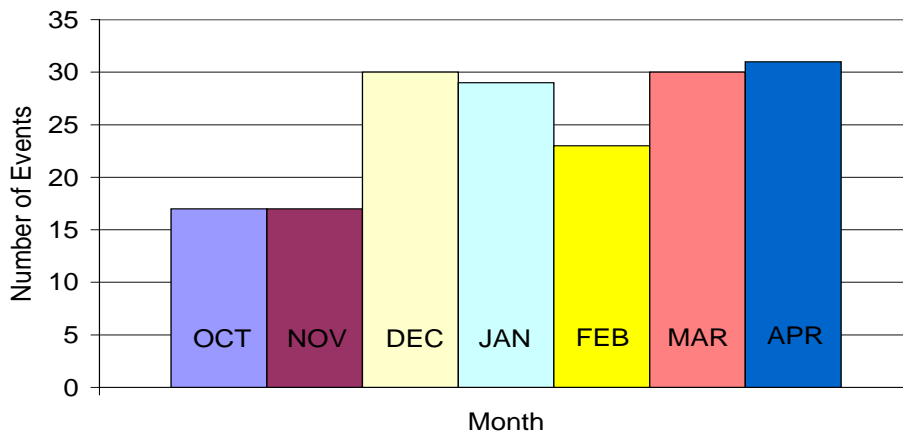


Fig. 3.6. As in Fig. 3.5 except at EKN.

**Albany Moderate Precipitation Events By Month:
1994-2004**

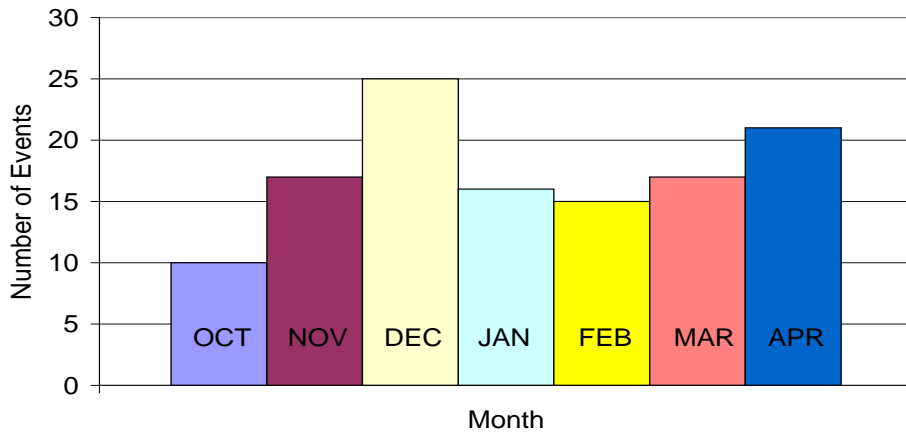


Fig. 3.7. As in Fig. 3.5 except at ALB.

**New York State Moderate Precipitation Events By
Month: 1994-2004**

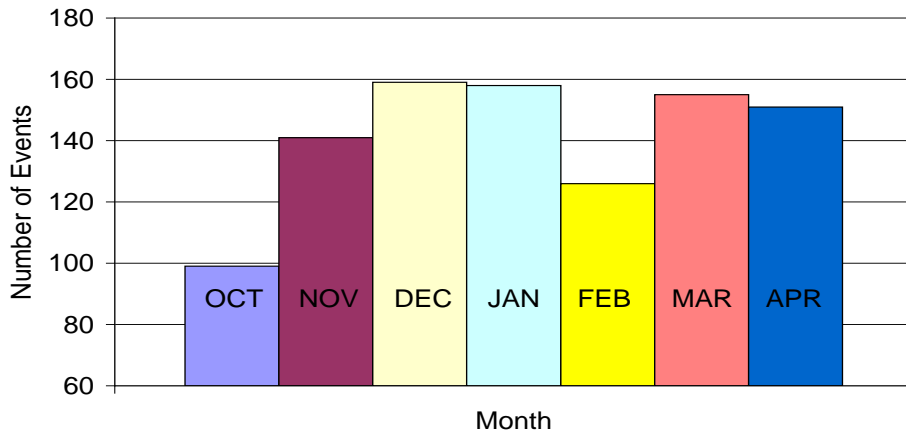


Fig. 3.8. As in Fig. 3.5 except for all seven first-order stations in New York State.

Pennsylvania Moderate Precipitation Events By Month: 1994-2004

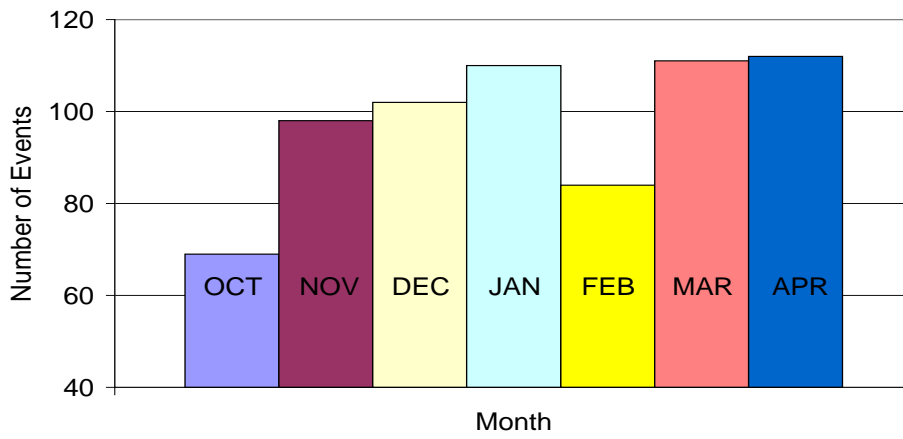


Fig. 3.9. As in Fig. 3.5 except for all five stations in Pennsylvania.

Ohio Moderate Precipitation Events By Month: 1994-2004

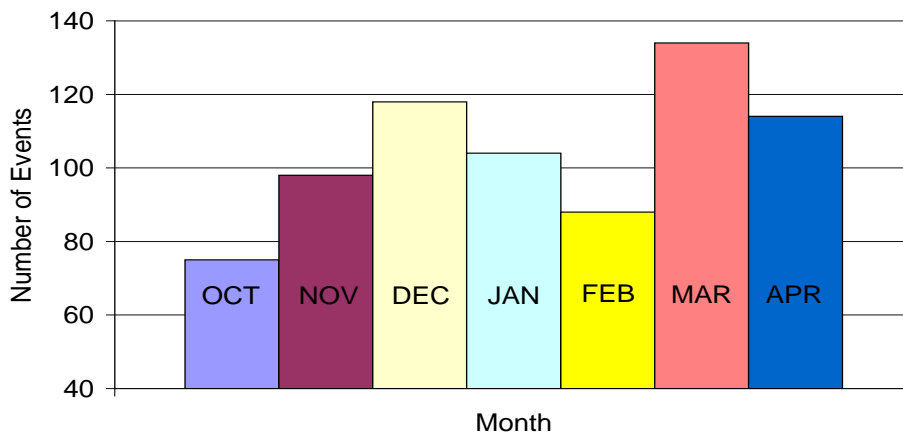


Fig. 3.10. As in Fig. 3.5 except for all five station in Ohio.

Moderate Precipitation Events For All Stations By Month: 1994-2004

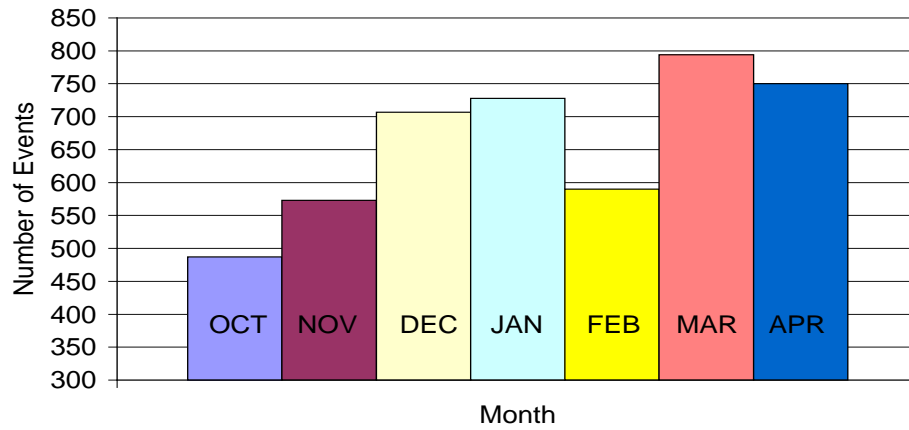


Fig. 3.11. As in Fig. 3.5 except for all 35 stations across the Northeast.

New York Moderate Precipitation Events: 1994-2004

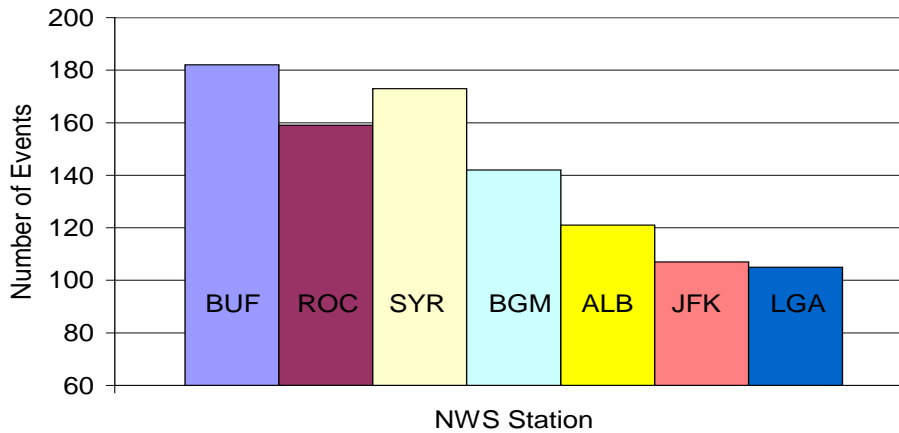


Fig. 3.12. Number of cool-season moderate events at each station in New York State for the 10-yr period 1994–2004.

**Northern New England Moderate Precipitation
Events: 1994-2004**

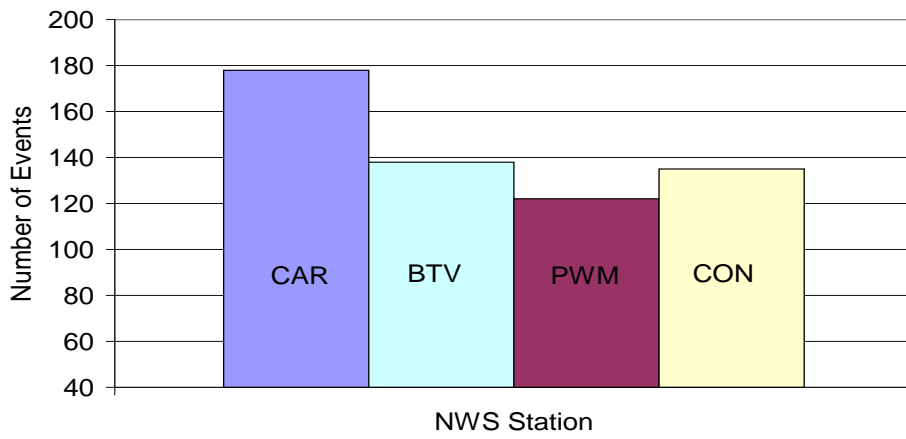


Fig. 3.13. As in Fig. 3.12 except for northern New England.

**Southern New England Moderate Precipitation
Events: 1994-2004**

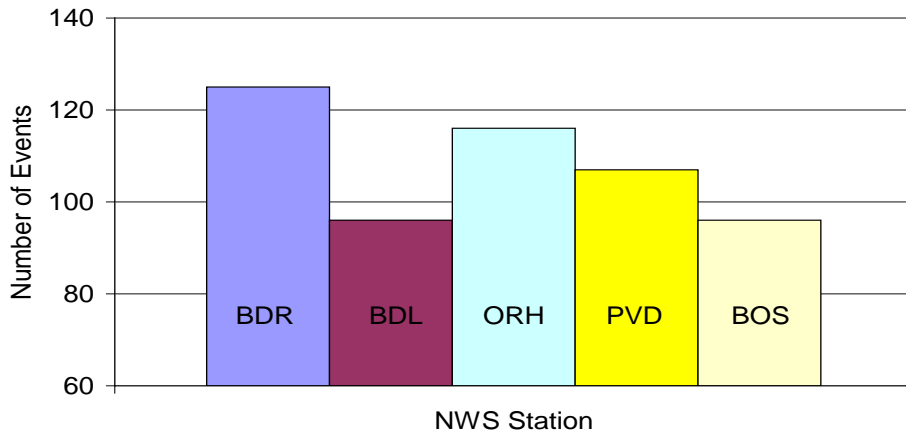


Fig. 3.14. As in Fig. 3.12 except for southern New England.

Washington, DC, Area Moderate Precipitation Events: 1994-2004

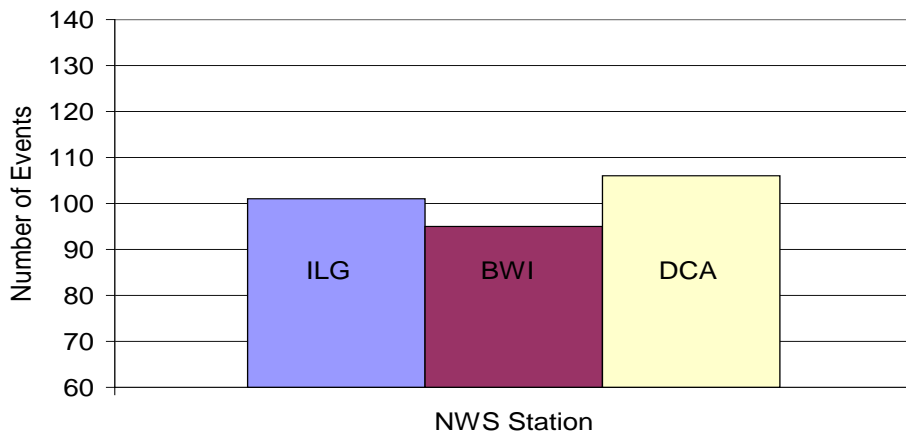


Fig. 3.15. As in Fig. 3.12 except for the Washington, DC, area.

Atlantic Coast Moderate Precipitation Events: 1994-2004

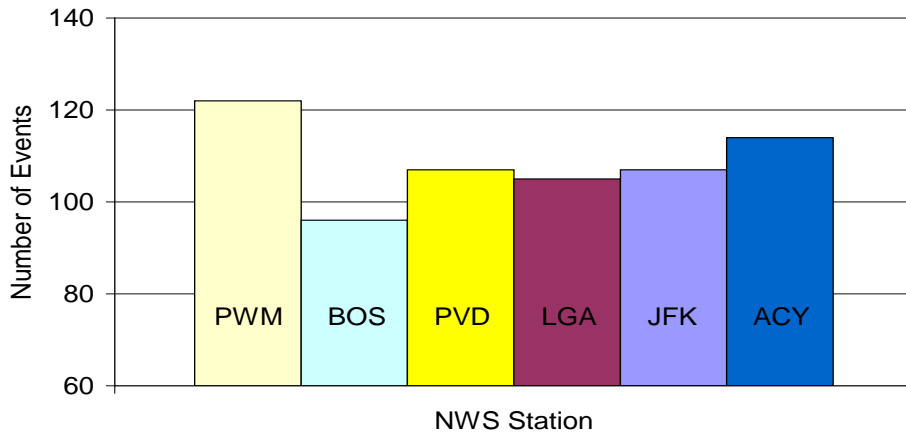


Fig. 3.16. As in Fig. 3.12 except for stations near the Atlantic coast.

**Western Region Moderate Precipitation Events:
1994-2004**

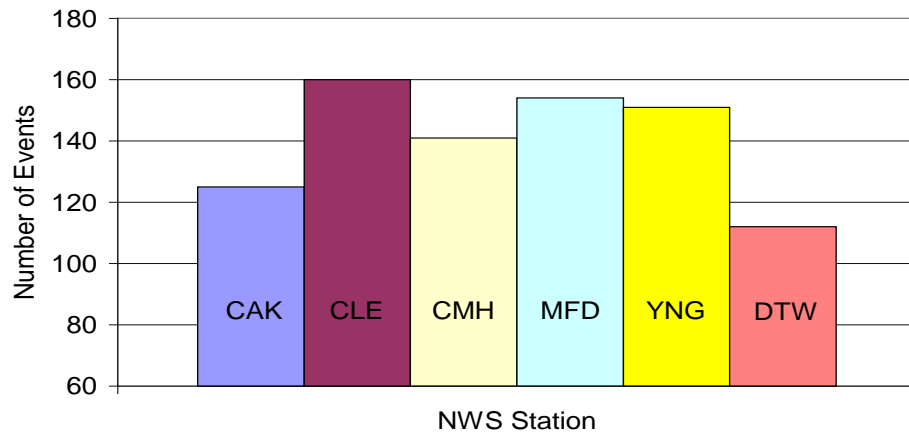


Fig. 3.17. As in Fig. 3.12 except for the western region.

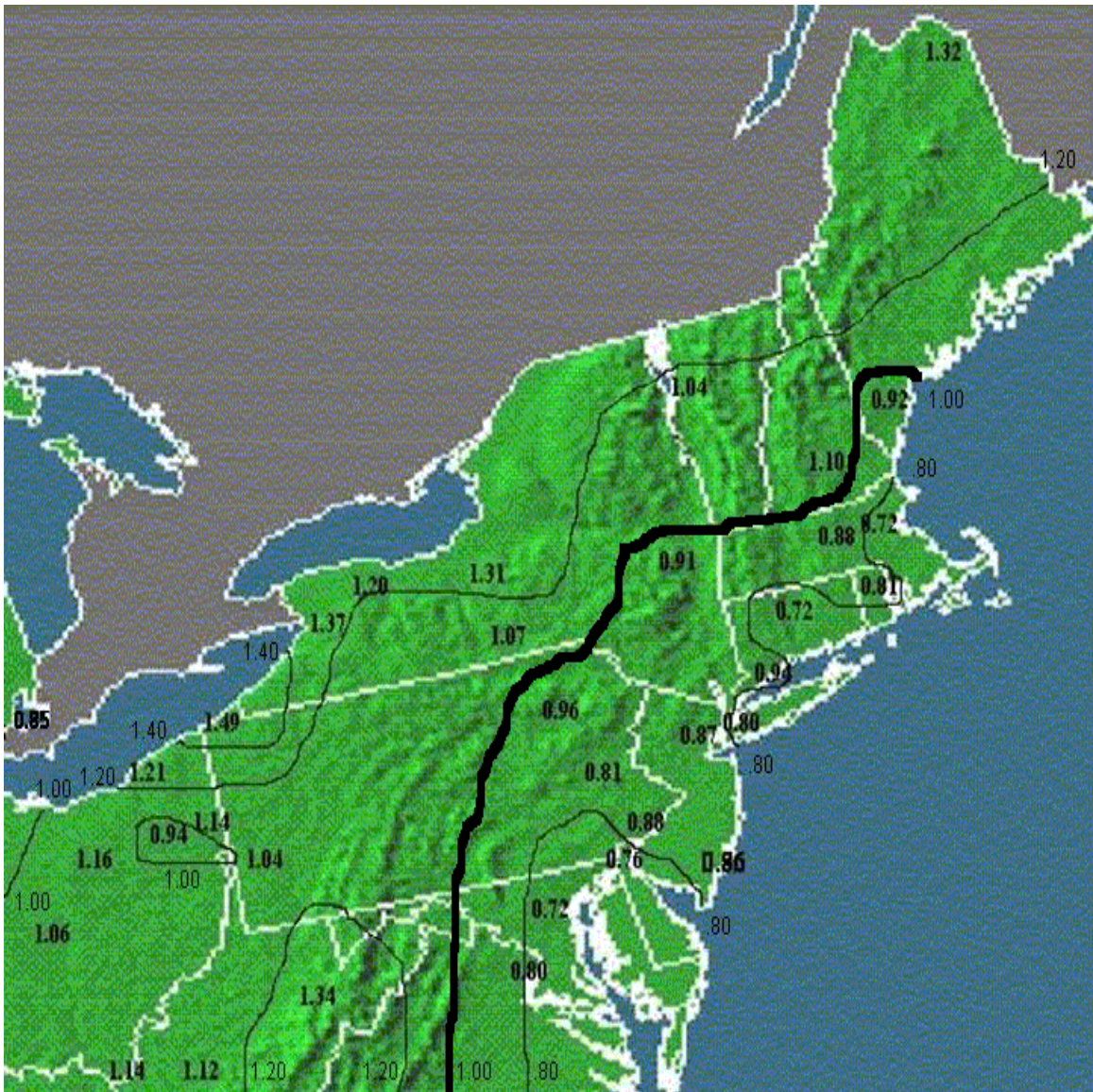


Fig. 3.18. Ratio of the number of events at each station to the mean number of events for all stations (132.5). Contours drawn about the mean at 0.20 intervals. The mean number of events is defined by the 1.00 contour.

4. Case Studies

4.1 Overview

As previously mentioned in section 2.2.2, four cool-season moderate precipitation events that affected the Northeast were selected for further study. The cases included the 27 December 2004 inverted trough, the 8 January 2005 weak Ohio Valley cyclone, the 26 January 2005 Alberta Clipper, and the 21 February 2005 weak Ohio Valley cyclone/Alberta Clipper hybrid. These cases were chosen to compare and contrast different types of relatively weak synoptic-scale systems that produce moderate precipitation events. A synoptic-scale overview of each system is presented, followed by an analysis of the mesoscale features within the moderate precipitation region.

4.2 Case 1: 27 December 2004

Forecasts for 27 December 2004 in the Albany, NY (ALB), area called for a chance of light snow as an intense cyclone passed well south and east of the region with a weak inverted trough extending across eastern New York. Instead, ALB was surprised by nearly 17 cm of snow. This amount is on the upper bounds of the moderate range criteria. Since snowfall amounts of this magnitude were not expected, it is important to investigate what caused the event and to examine its mesoscale structure. The plots discussed in this section are from the 27 December initialized 0600 UTC Eta model unless otherwise noted.

4.2.1 Synoptic Overview

Figure 4.1 shows the Binghamton, NY (BGM), WSR-88D reflectivity image (Level II; 0.5° elevation angle) at 0300 UTC 27 December. A narrow north–south band of moderate precipitation (20–30 dBZ) exists just east of BGM. At 0600 UTC, the moderate band of precipitation is located over ALB, while by 0900 UTC the band has drifted slightly eastward and weakened considerably (Figs. 4.2a–b). The 9-h forecast of mean sea level pressure valid at 0300 UTC and the initialized 0600 UTC mean sea level pressure are shown in Figs. 4.3 and 4.4, respectively. The 26 December 1800 UTC Eta 9-h forecast (Fig. 4.3) features an intense 991 hPa surface cyclone several hundred kilometers off the New Jersey coast at 0300 UTC on 27 December. The initialized 0600 UTC Eta on 27 December places a 988 hPa cyclone approximately 75–100 km east-northeast of the 0300 UTC position (Fig. 4.4). Therefore, Eta model forecasts indicated that the cyclone would intensify but move away from the coast. However, the dashed white line in Fig. 4.4 denotes an inverted trough extending northwestward from the center of the surface low into eastern New York. Although this feature appears relatively innocuous, it serves as a focusing mechanism for precipitation.

Figure 4.5 shows the 1000–500 hPa thickness contours along with the cross section position (blue line) to be used in the next subsection. A strong thermal trough is located over the eastern Great Lakes. The 1000–500 hPa thickness at ALB is approximately 520 dam, which is sufficiently low enough for precipitation to fall as all snow. Winds at 300 hPa (Fig. 4.6) calculated using NCEP/NCAR reanalysis data reveal

that a strong jet streak is located well northeast of ALB and is not in a position to enhance upward motion. However, the wind vectors suggest that a negatively tilted trough is located over central New York, which helps provide forcing for ascent over eastern New York. The 500 hPa geopotential heights and absolute vorticity are shown in Fig. 4.7. Note that a trough and associated cyclonic vorticity maximum are located over western/central New York at this time. From this pattern, it can be inferred that cyclonic vorticity advection is occurring over eastern New York ahead of the trough. QG theory shows that vertical motion occurs in regions of cyclonic vorticity advection and in regions of warm advection (e.g., ahead of a 500 hPa trough) as given by (1) in section 1.2.2.2. Another method of analyzing forcing for vertical motion is through the use of Q-vectors [Eq. (2), section 1.2.2.2.]. Figure 4.8 displays average 850–700 hPa Q-vector divergence. A region of moderate 850–700 Q-vector convergence is found over eastern New York, indicative of forcing for ascent. Consistent with the results of Figs. 4.7 and 4.8, a region of upward vertical motion exists across eastern New York (Fig. 4.9). A maximum vertical velocity of $-8 \mu\text{b s}^{-1}$ is noted. The forcing for ascent and resulting vertical motion is not overly impressive, but is sufficient to correspond to light-to-moderate precipitation.

4.2.2 Mesoscale Aspects

A cross section was taken through the snowband and perpendicular to the 1000–500 hPa thickness contours (see Fig. 4.5) at 0600 UTC on 27 December. Figure 4.10 shows Petterssen frontogenesis and vertical velocity (ω) along the cross section. A

shallow frontogenesis maximum (approximately 50 hPa deep) is observed near 850 hPa over ALB. However, this frontogenesis region is not intense [approximately $1 \text{ K} (100 \text{ km})^{-1} (3 \text{ h})^{-1}$] and is very flat (i.e., it does not have significant vertical tilt). A maximum vertical velocity of $-8 \mu\text{b s}^{-1}$ is noted just above the frontogenesis maximum on the warm side of the circulation. A shallow, flat region of negative EPV* (blue shading) exists between 850–800 hPa, with another thinner region located at 700 hPa (Fig. 4.11). Figure 4.11 also shows that a shallow region of WMSS (dark green shading) exists between the two layers of negative EPV*. The deep regions of frontogenesis and negative EPV* located at 500 hPa on the extreme right of Figs. 4.10 and 4.11 are associated with the main shield of precipitation from the surface cyclone (not shown). Relative humidity (RH) and temperature are also plotted on Fig. 4.11. The atmosphere can be considered saturated ($\text{RH} \geq 80\%$) in the region of negative EPV* near 850 hPa, while the region of WMSS is nearly saturated.

Figure 4.12 shows absolute geostrophic momentum (M_g) and saturation equivalent potential temperature (θ_{es}) taken along the cross section, the latter of which is used to differentiate regions of CSI from regions of CI as discussed in section 1.2.2.3. Near 700 hPa (the upper area of negative EPV*), θ_{es} decreases with height, indicating a region of CI. Just above 850 hPa and extending to around 750 hPa, lines of constant θ_{es} are slightly more vertical or nearly parallel to lines of constant M_g . This orientation corresponds to thin regions of CSI and WMSS, respectively.

Also, as seen by comparing Figs. 4.10 and 4.11, maximum vertical motion (just above 850 hPa) is occurring in a region coincident with temperatures near -15°C , which supports maximum snow growth. Atmospheric soundings taken at ALB on 27 December

(Figs. 4.13a–b) confirm a nearly saturated and sufficiently cold atmosphere for snow production.

4.3 Case II: 8 January 2005

The forecast at BUF for 8 January 2005 called for light snow with accumulations generally under 3 cm across the region due to a weak cyclone passing by to the south. However, by late afternoon BUF and much of western New York had received nearly 8 cm of snow, while ALB had received almost 15 cm of snow. This analysis focuses on the precipitation across western New York. The figures discussed in the remainder of this section are from the 8 January initialized 1800 UTC Eta model unless otherwise noted.

4.3.1 Synoptic Overview

Figures 4.14a–b show the BUF radar reflectivity on 8 January 2005 at 1500 UTC and 1800 UTC, respectively. At 1500 UTC, a band of moderate-to-heavy snow stretches from Lake Erie across the Niagara Peninsula to Lake Ontario. By 1800 UTC, the band of snow has weakened slightly (20–35 dBZ), but has expanded over much of western New York. At this time, a weak 1014 hPa surface cyclone is located just off the New Jersey coast (Fig. 4.15) after moving east-northeastward up the Ohio Valley (not shown). Contours of 1000–500 hPa thickness and the position of the cross section to be used in the next subsection (white line) are given in Fig. 4.16. A region of 1000–500 hPa

thickness of 534–540 dam, which marginally supports snow, is located across western New York. A weak thermal trough is located over the eastern Great Lakes, while a thermal ridge is in place ahead of the surface low. A thickness value of 540 dam near BGM suggests that mixed precipitation is possible. Consistent with this value, BGM reported a mix of rain and snow from this system.

Figure 4.17 displays 300 hPa winds at 1800 UTC calculated using NCEP/NCAR reanalysis data. A 50 m s^{-1} jet streak is draped along the Atlantic coast, placing western New York near the left entrance region of the jet with a west to west-southwest flow. Geopotential heights and absolute vorticity at 500 hPa (Fig. 4.18) reveal that a short-wave trough and associated cyclonic vorticity maximum (PV hook) are located over western New York and western Pennsylvania. Although the strongest vorticity advection is occurring over central/eastern New York and Pennsylvania, enough is occurring over western New York to result in some synoptic-scale lift. Additionally, the strongest Q-vector forcing for upward motion is occurring over northeastern Pennsylvania and southeastern New York, with weaker Q-vector convergence over western New York (Fig. 4.19). Figure 4.20 shows the average 850–500 hPa vertical velocity across the Northeast. The strongest vertical motion is located over southern New England, but the Eta model is picking up on a “wraparound” region of $-3 - -5 \mu\text{b s}^{-1}$ vertical velocities over parts of western New York. Therefore, only weak synoptic-scale forcing is present across western regions of New York, resulting in the likelihood of light precipitation.

4.3.2 Mesoscale Aspects

A cross section was taken through the moderate snowband in the same manner as in Case I. Petterssen frontogenesis along the cross section is displayed in Fig. 4.21. A slanted region of frontogenesis is found between 500 and 250 hPa, but this region is very stable as EPV* (Fig. 4.22) is strongly positive. The more important region of frontogenesis is located from approximately 900–750 hPa just east of BUF and continuing southeast along the path of the cross section. While this frontogenesis maximum is slightly more intense and upright than in the 27 December 2004 case, it is still weak [$2 \text{ K (100 km)}^{-1} (3 \text{ h})^{-1}$], shallow, and flat. Maximum vertical velocities associated with the frontogenesis maximum (not shown) are $-5 \mu\text{b s}^{-1}$ in the 700–500 hPa layer east of BUF. EPV*, RH, and temperature along the cross section path are plotted in Fig. 4.22. An approximately 50 hPa-deep region of negative EPV* exists at 700 hPa near BGM and slopes upward to 600 hPa east of BUF. The region of frontogenesis and negative EPV* are saturated with RH in excess of 80%.

M_g and θ_{es} evaluated along the cross section are displayed in Fig. 4.23. CI is present at the southeastern end of the cross section since θ_{es} decreases with height in south-central New York and north-central Pennsylvania at the 700 hPa level. However, it is difficult to say what type of instability is causing the region of negative EPV* east of BUF due to the lack of a tight θ_{es} gradient in that area in Fig. 4.23.

As mentioned earlier, maximum vertical velocities occur in the 700–500 hPa layer. In terms of precipitation efficiency, Fig. 4.22 shows that the -15°C isotherm is located at approximately 600 hPa. However, a strong vertical temperature gradient exists, resulting in a narrow layer of optimal snow growth. The 1200 UTC sounding at

BUF (Fig. 4.24) shows a nearly saturated atmosphere with the temperature for optimal snow growth located at 550 hPa.

4.4 Case III: 26 January 2005

An Alberta Clipper dropped across the Great Lakes and slid eastward along the New York/Pennsylvania border on the morning of 26 January 2005. Snowfall amounts across New York State were in the 7–13 cm range. Alberta Clippers typically produce light-to-moderate snow accumulations, so the observed amounts were not out of the ordinary. This case was chosen to see how the structure of Alberta Clippers compares with other types of synoptic systems. The figures presented in this section are from the 26 January 0600 UTC Eta model 3-h forecast valid at 0900 UTC unless otherwise noted.

4.4.1 Synoptic Overview

Figure 4.25 displays the ALB radar reflectivity on 26 January 2005 at 0900 UTC. A shield of moderate snow is located approximately along the Massachusetts Turnpike (Interstate 90) and extends northwestward toward ALB before bending back to the southwest along Interstate 88. South of this region, a more cellular pattern is noted in the radar returns. The initialized 0600 UTC Eta places a 1000 hPa cyclone near DTW (Fig. 4.26). By 0900 UTC, the cyclone has moved eastward to near ERI and weakened slightly to 1001 hPa (Fig. 4.27). Contours of 1000–500 hPa thickness and the position of the cross section to be used in the next subsection are displayed in Fig. 4.28. A weak thermal

ridge is in place across New York State, suggestive of a warm advection pattern. Thickness values across New York State and southern New England are sufficiently cold for the precipitation to fall as snow. The 540 dam contour slices across north-central Pennsylvania, indicating a possible precipitation type transition zone.

NCEP/NCAR reanalysis 300 hPa winds at 1200 UTC are displayed in Fig. 4.29. An eastward propagating 55 m s^{-1} jet streak is located off the New England coast, placing portions of southeastern New York and eastern Pennsylvania in the equatorward entrance region of the jet. Geopotential heights and absolute vorticity at 500 hPa (Fig. 4.30) reveal that a fairly tight meridional geopotential height gradient exists across the Northeast with cyclonic vorticity advection likely over the northern half of New York State. Q-vector divergence at 700 hPa (Fig. 4.31) indicates that the strongest Q-vector forcing ahead of the cyclone is over southern Canada and extreme northern New York with a tail extending southward into eastern Maryland. The average 850–700 hPa vertical velocity maximum (Fig. 4.32) is actually located slightly farther south than the maximum Q-vector forcing. Peak vertical velocities of $-5 - -8 \mu\text{b s}^{-1}$ are found across southeastern New York and eastern Pennsylvania. Therefore, once again, only weak-to-moderate synoptic-scale forcing is present across eastern New York.

4.4.2. Mesoscale Aspects

A cross section taken through the precipitation region (see Fig. 4.28) displaying Petterssen frontogenesis and vertical velocity is shown in Fig. 4.33. Three distinct frontogenesis maxima (and corresponding vertical velocity maxima) are visible along the

length of the cross section. At the northern end of the cross section, a fairly weak 100 hPa-deep region of frontogenesis [$3 \text{ K (100 km)}^{-1} (3 \text{ h})^{-1}$] slopes from 700 hPa south of ALB to 500 hPa south of Montpelier, VT. Maximum vertical velocities associated with the warm side of the frontal circulation are $-8 \mu\text{b s}^{-1}$ in the 600–500 hPa layer over ALB. Closer to the New York/Pennsylvania border, a second region of frontogenesis is noted near 850 hPa. This region is not as deep as its northern counterpart and has almost no vertical tilt. Nonetheless, a vertical velocity of $-8 \mu\text{b s}^{-1}$ is seen near 850 hPa associated with this frontogenesis maximum. Also, a third frontogenesis maximum is seen in northeastern Pennsylvania in the 800–700 hPa layer. This maximum has almost no vertical tilt, yet a vertical velocity of $-12 \mu\text{b s}^{-1}$ occurs in the 700–500 hPa layer. The BGM radar (not shown) suggests that another band of snow is developing across northeastern Pennsylvania in association with this region of frontogenesis.

EPV*, RH, and temperature along the cross section are given in Fig. 4.34. As is the case with frontogenesis, several distinct regions of WMSS and negative EPV* exist. A region of negative EPV* is seen at 500 hPa at the northern end of the cross section, while a second region is noted just above 600 hPa across southern New York and into northern Pennsylvania. An area of WMSS exists between these two regions in the 500–400 hPa layer. The frontogenesis maximum near 850 hPa is in a stable region of positive EPV*, which may account for the decrease in precipitation intensity south of ALB as seen in Fig. 4.25. The entire troposphere is saturated below 500 hPa, so sufficient moisture is present for the formation of snow.

M_g and θ_{es} evaluated along the cross section are displayed in Fig. 4.35. The negative EPV* region near 500 hPa at the northern end of the cross section is difficult to

explain. The slopes of lines of constant M_g and θ_{es} suggest that a thin layer of WMSS is more likely to occur there. CSI is likely responsible for the southernmost region of negative EPV*, as lines of constant θ_{es} are more upright than lines of constant M_g .

As seen by comparing Figs. 4.33 and 4.34, the maximum vertical velocity at the northern end of the cross section occurs at temperatures of $-15 - -24^\circ\text{C}$. This range corresponds to temperatures that are near or slightly colder than those for optimal snow growth. Temperatures associated with the southernmost vertical velocity maximum are near or slightly warmer than -15°C . The ALB 1200 UTC sounding (Fig. 4.36) confirms the saturated lower troposphere and temperatures below -15°C at the level of maximum vertical velocity (600–500 hPa layer).

4.5 Case IV: 21 February 2005

On the morning of 21 February 2005, an Alberta Clipper/Ohio Valley cyclone hybrid slid eastward across the southern Great Lakes before stalling and weakening over western New York. The term hybrid was used because the storm was following a track between typical Alberta Clippers and Ohio Valley cyclones. Snowfall broke out across eastern New York and New England in the warm advection region well ahead of the surface low. Snow totals were in the 7–15 cm range. This case represents an example of weak-to-moderate synoptic-scale forcing interacting with moderate mesoscale forcing; however, the ingredients only align themselves in a favorable manner for a short period of time. The figures discussed in the remainder of this section are from the 21 February initialized 0600 UTC Eta model unless otherwise noted.

4.5.1 Synoptic Overview

The ALB radar on 21 February 2005 at 0600 UTC (Fig. 4.37) shows a shield of moderate precipitation across much of eastern New York and western New England. At this time, a 1005 hPa cyclone is located over western Lake Erie (Fig. 4.38). Twelve hours later, the cyclone is located over western New York and is considerably weaker (not shown). Contours of 1000–500 hPa thickness and the position of the cross section to be used in the next section are given in Fig. 4.39. A weak thermal ridge is located over the eastern Great Lakes, suggestive of a warm advection pattern. A fairly tight northeast–southwest thickness gradient is in place across much of the Northeast, with sufficiently low thickness values to correspond to snow across eastern New York.

NCEP/NCAR reanalysis 300 hPa winds (Fig. 4.40) reveal that eastern New York and New England appear to be in the right entrance region of a jet $60+ \text{ m s}^{-1}$ jet streak. Geopotential heights and absolute vorticity at 500 hPa (Fig. 4.41) indicate a short-wave trough and associated cyclonic vorticity maximum over Lake Huron and Lake Erie, with a ribbon of cyclonic vorticity stretching from Lake Ontario across northern New York into southern New England. This ribbon of vorticity is likely noise from the high resolution dataset since there is no signature in the geopotential height field that would result in such a pattern. Average 700–500 hPa Q-vector divergence (Fig. 4.42) shows a large region of Q-vector convergence across eastern New York and western New England extending westward across New York State. However, average 700–500 hPa vertical velocity maxima (Fig. 4.43) are inexplicably shifted southward across eastern

Pennsylvania. Nonetheless, ascent is occurring over eastern New York. Therefore, it appears that weak-to-moderate synoptic-scale forcing is in place across much of the region.

4.5.2 Mesoscale Aspects

Petterssen frontogenesis and vertical velocity taken along the cross section in Fig. 4.39 are shown in Fig. 4.44. In this figure, upward vertical motion is given by the dashed yellow lines. An intense region of frontogenesis [approximately $13 \text{ K (100 km)}^{-1} (3 \text{ h})^{-1}$] slopes from approximately 700 hPa near the New York/Pennsylvania border to 500 hPa north of ALB. Associated with this frontogenesis maximum is a nearly upright region of $-8 \mu\text{b s}^{-1}$ upward vertical velocity over the ALB region in the 550–350 hPa layer. A second region of more intense, upright vertical motion is located over northeastern Pennsylvania. This vertical motion is not associated with any apparent frontal circulation. EPV*, RH, and temperature are displayed in Fig. 4.45. A deep region of WMSS and negative EPV* is seen south of ALB and extending into northeastern Pennsylvania. Over the ALB region, an area of WMSS (and a tiny region of negative EPV*) exists in the 500–400 hPa layer. This WMSS region corresponds to the location of maximum vertical velocity on the warm side of the frontal circulation. Figure 4.45 also shows that the atmosphere is saturated in the frontogenetical region, while the zone of WMSS is nearly saturated.

A cross section of M_g and θ_{es} is shown in Fig. 4.46. A small portion of the negative EPV* region is the result of CSI (e.g., southwest of ALB near 550 hPa), while

many locations exhibit θ_{es} contours that are nearly parallel to M_g contours (e.g., near ALB at 500 hPa and across northeastern Pennsylvania near 700 hPa), indicating regions of WMSS. Additional θ_{es} contours are needed to determine if the deep region of negative EPV* over northeastern Pennsylvania is the result of CI or CSI, but doing so would make the remainder of the plot unreadable.

Revisiting Fig. 4.45, the maximum vertical velocity which occurred over ALB in the 550–350 hPa layer is noted to occur at temperatures in the $-20 - -40^\circ\text{C}$ range. These temperatures are much colder than those needed for optimal snow growth. The 0000 UTC and 1200 UTC ALB soundings (Figs. 4.46a–b) confirm that temperatures in the region of maximum vertical velocity are much colder than needed for optimal snow growth.

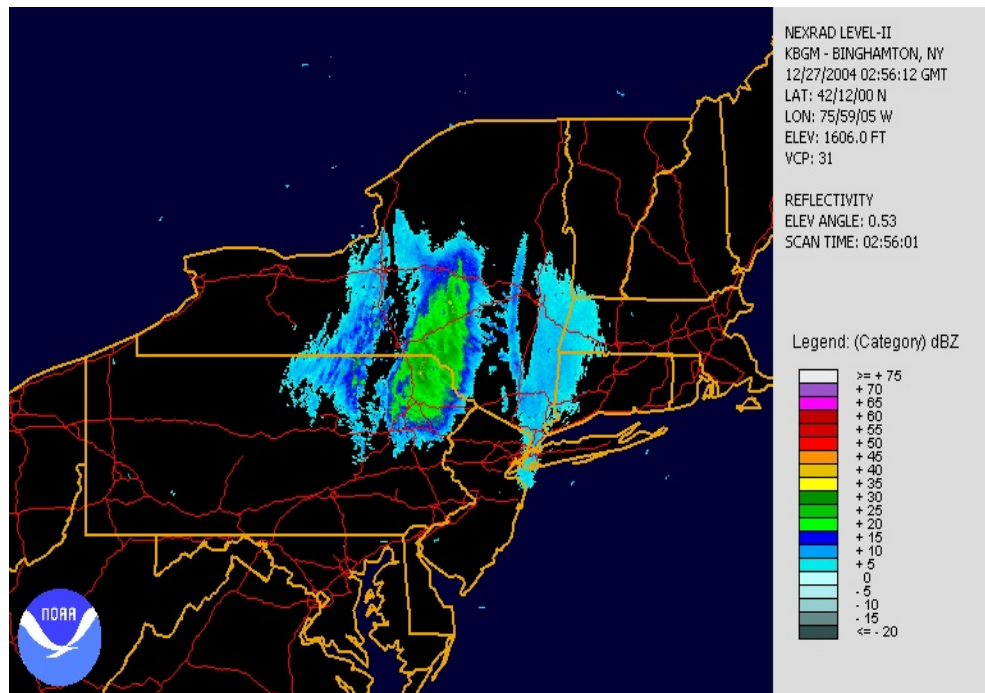


Fig. 4.1. BGM WSR-88D (Level II) reflectivity image at 0300 UTC 27 December.

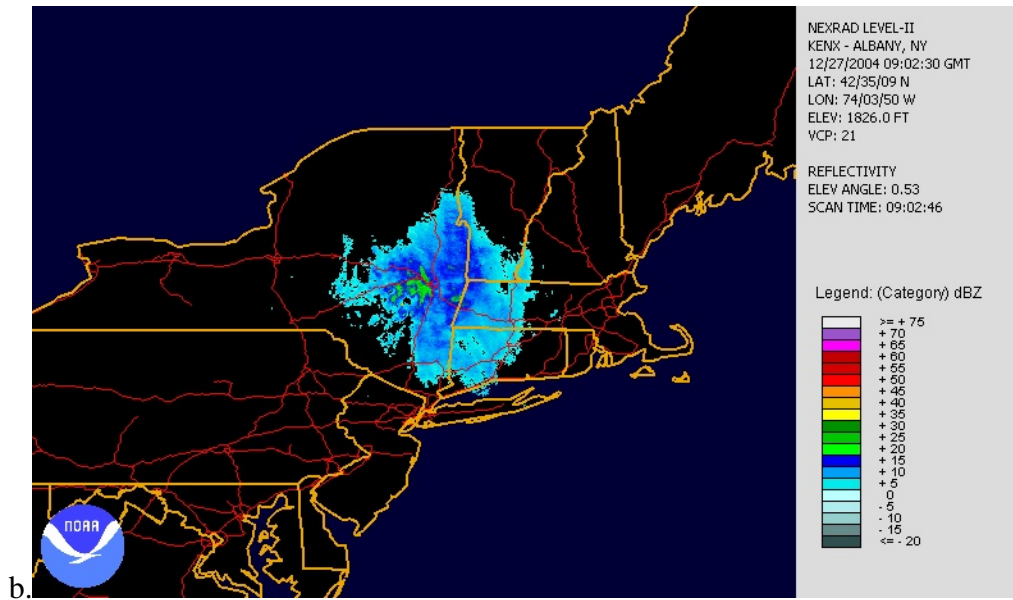
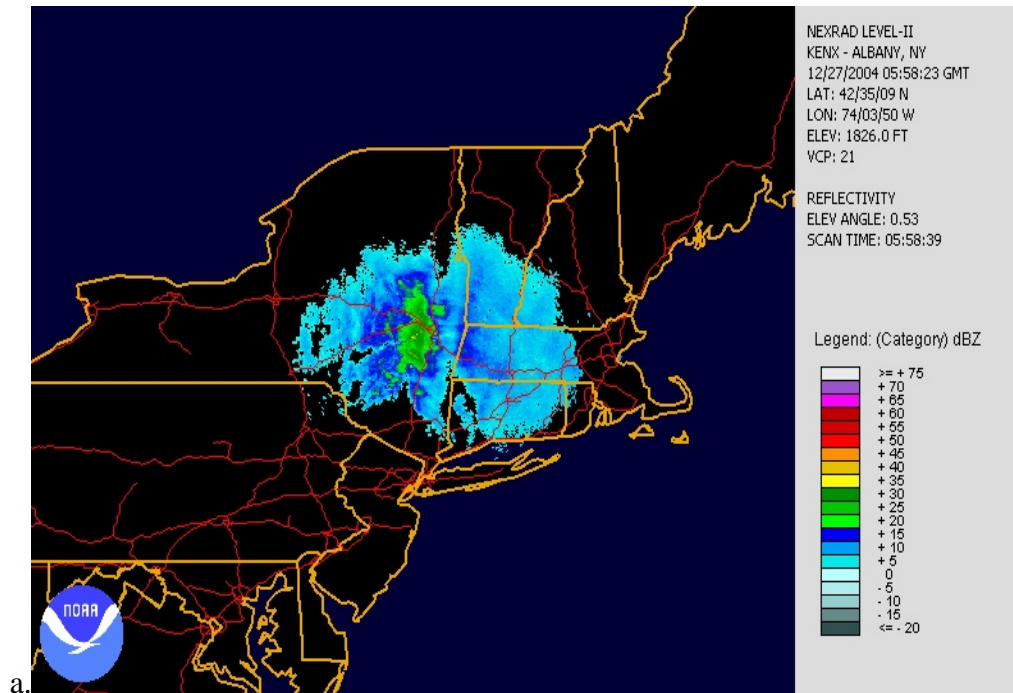


Fig. 4.2a–b. ALB WSR 88-D (Level II) reflectivity image on 27 December 2004 at: a) 0600 UTC and b) 0900 UTC.

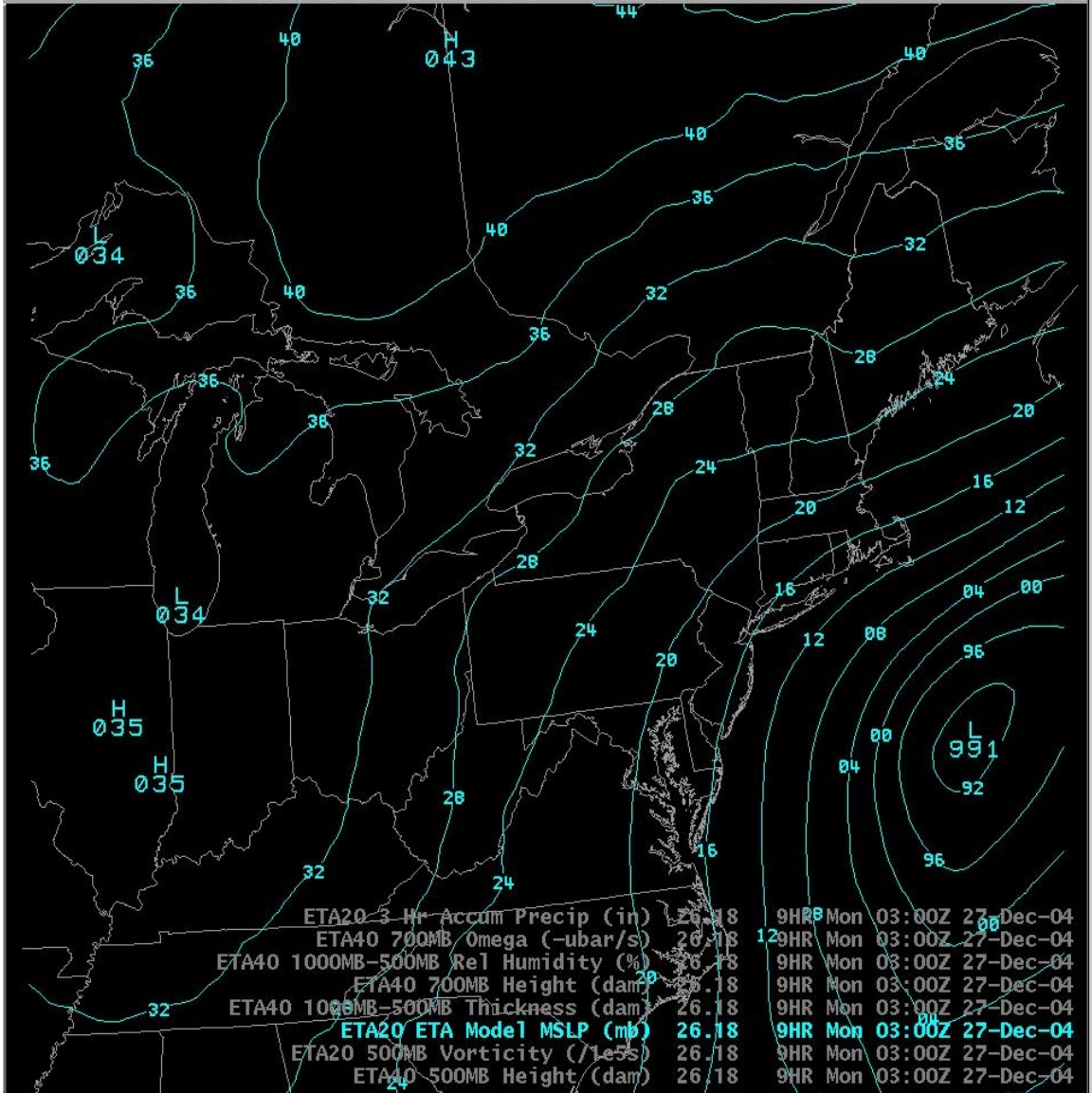


Fig. 4.3. 26 December 1800 UTC Eta 9-h forecast of mean sea level pressure (hPa) valid at 0300 UTC on 27 December 2004.

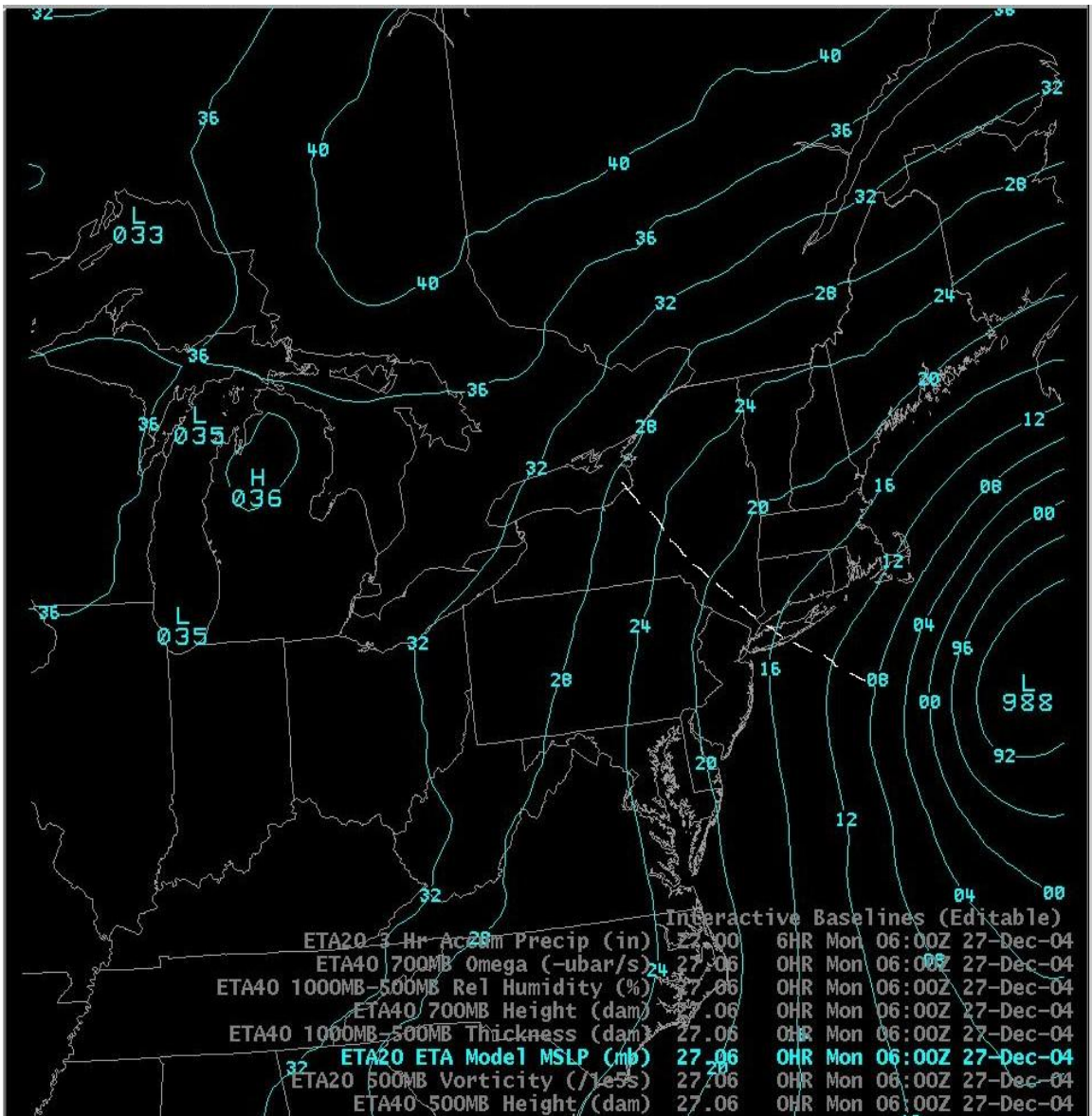


Fig. 4.4. 27 December initialized 0600 UTC Eta mean sea level pressure (hPa). Dashed white line marks location of an inverted trough.

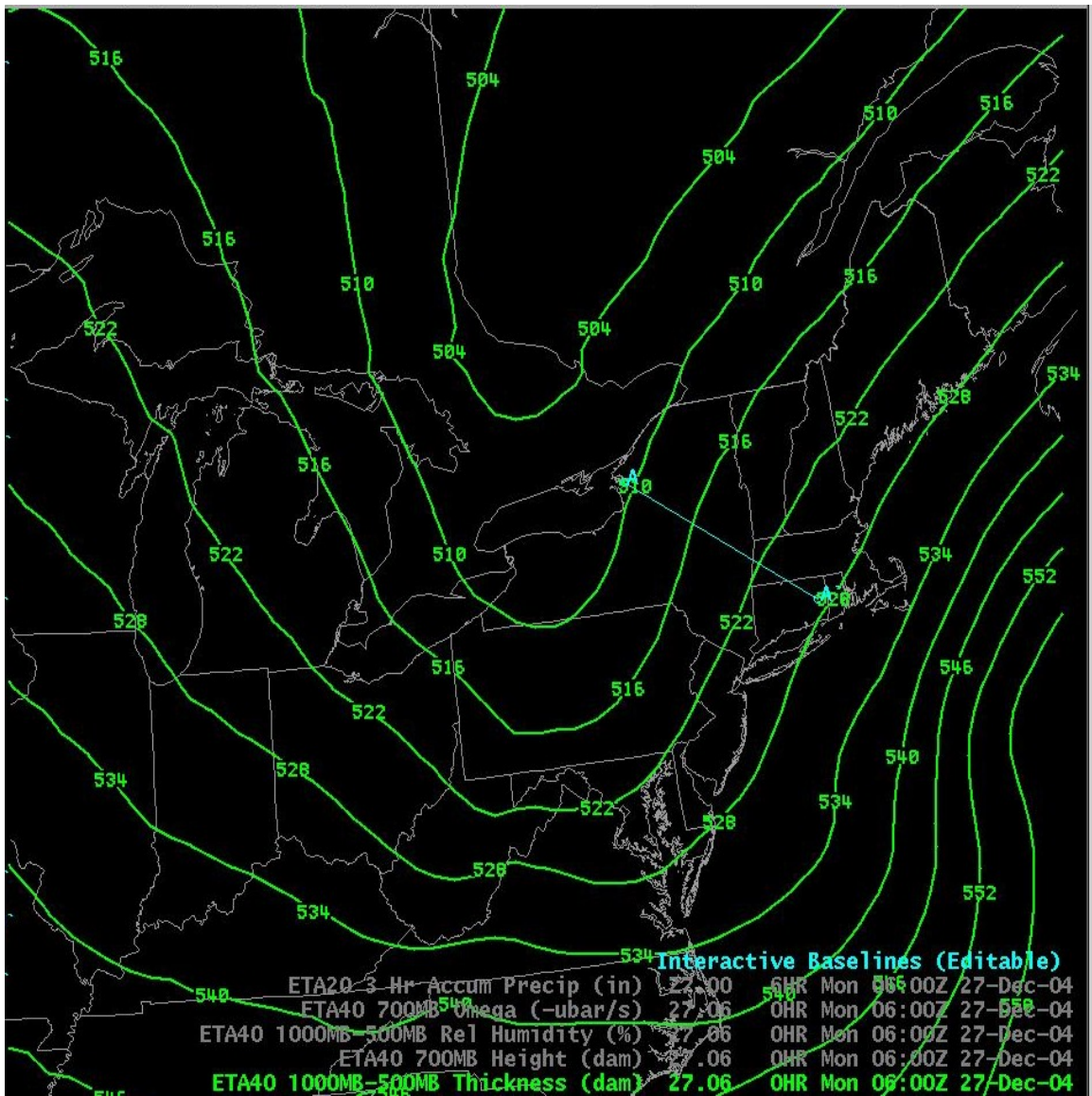


Fig. 4.5. 27 December initialized 0600 UTC Eta 1000–500 hPa thickness (green contours). Blue line marks location of cross section.

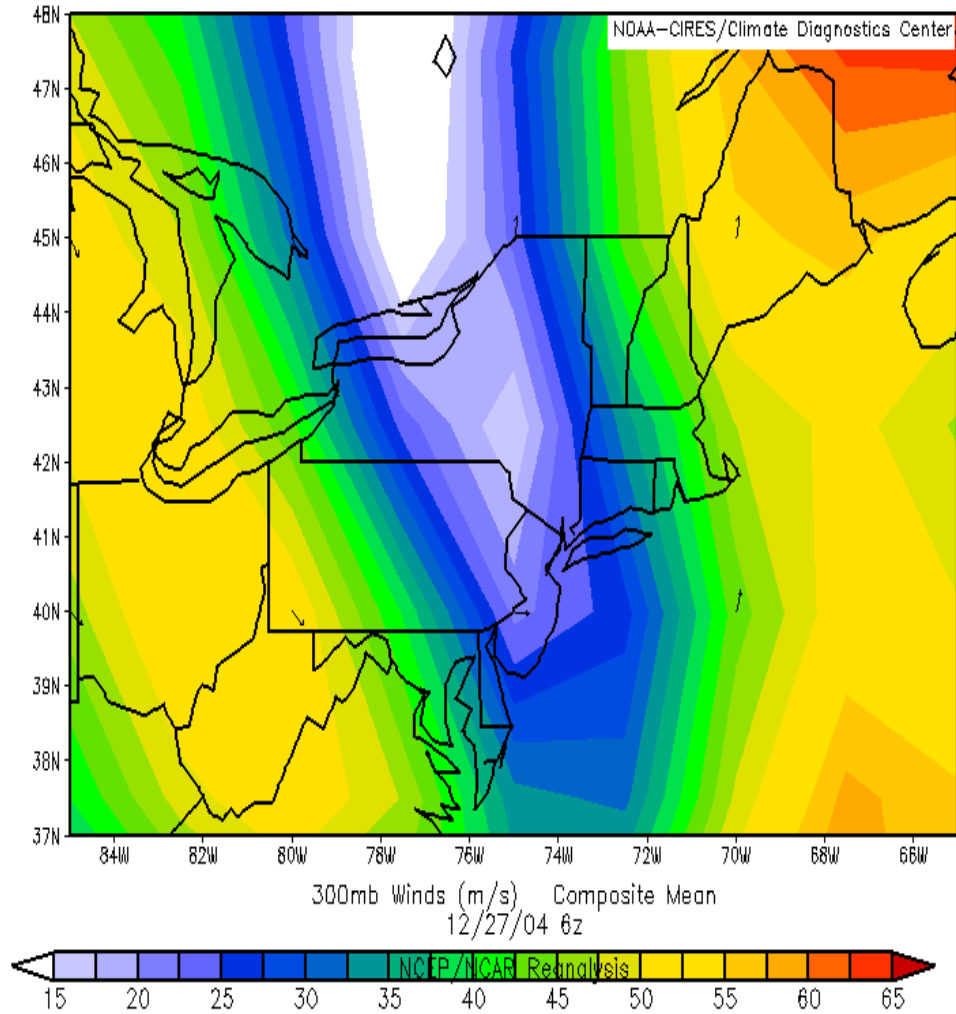


Fig. 4.6. 27 December 0600 UTC NCEP/NCAR reanalysis 300 hPa winds. Wind direction given by black arrows.

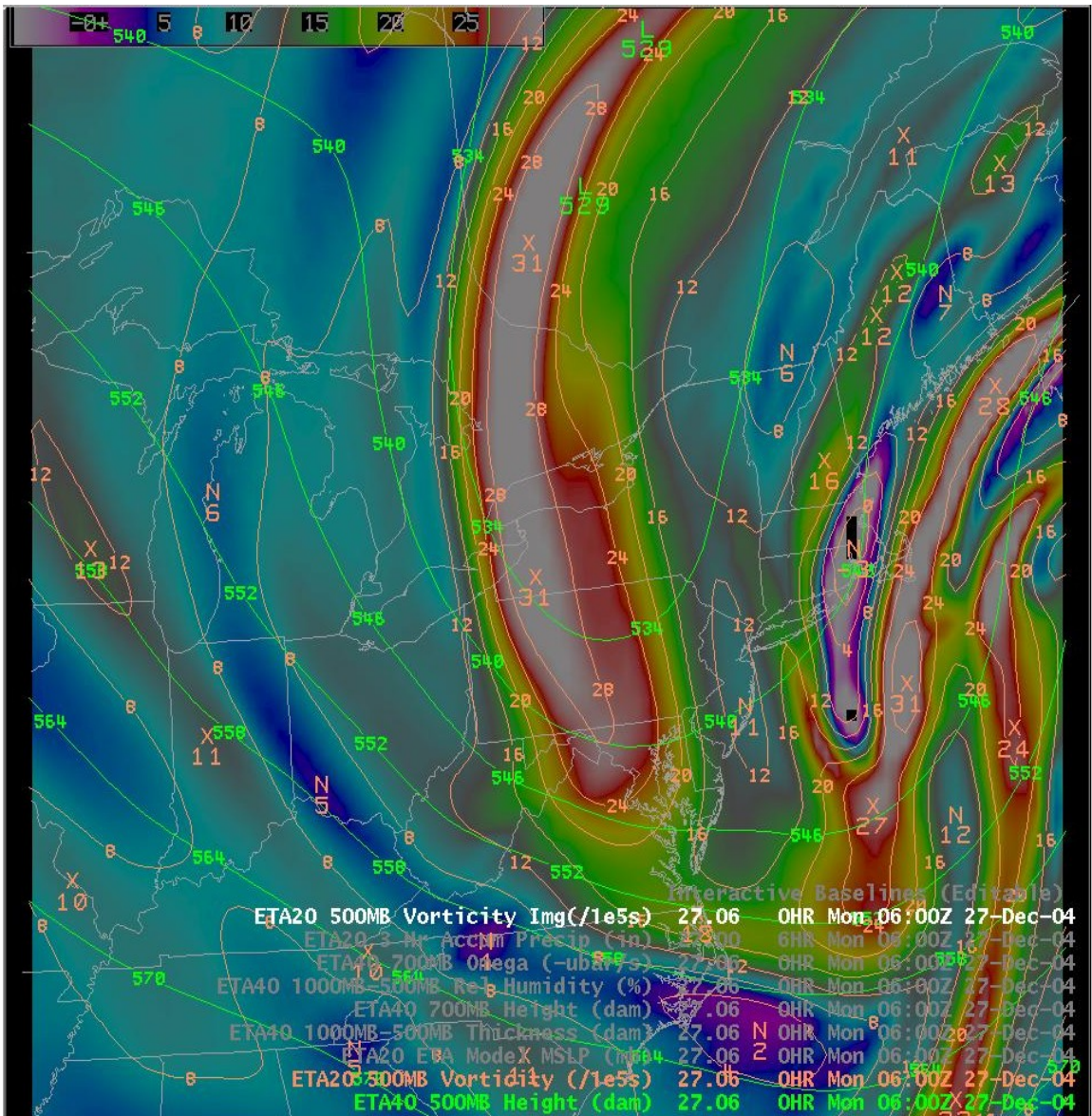


Fig. 4.7. 27 December initialized 0600 UTC Eta 500 hPa geopotential height (green contours, dam) and absolute vorticity (brown contours, shaded, 10^{-5} s^{-1}).

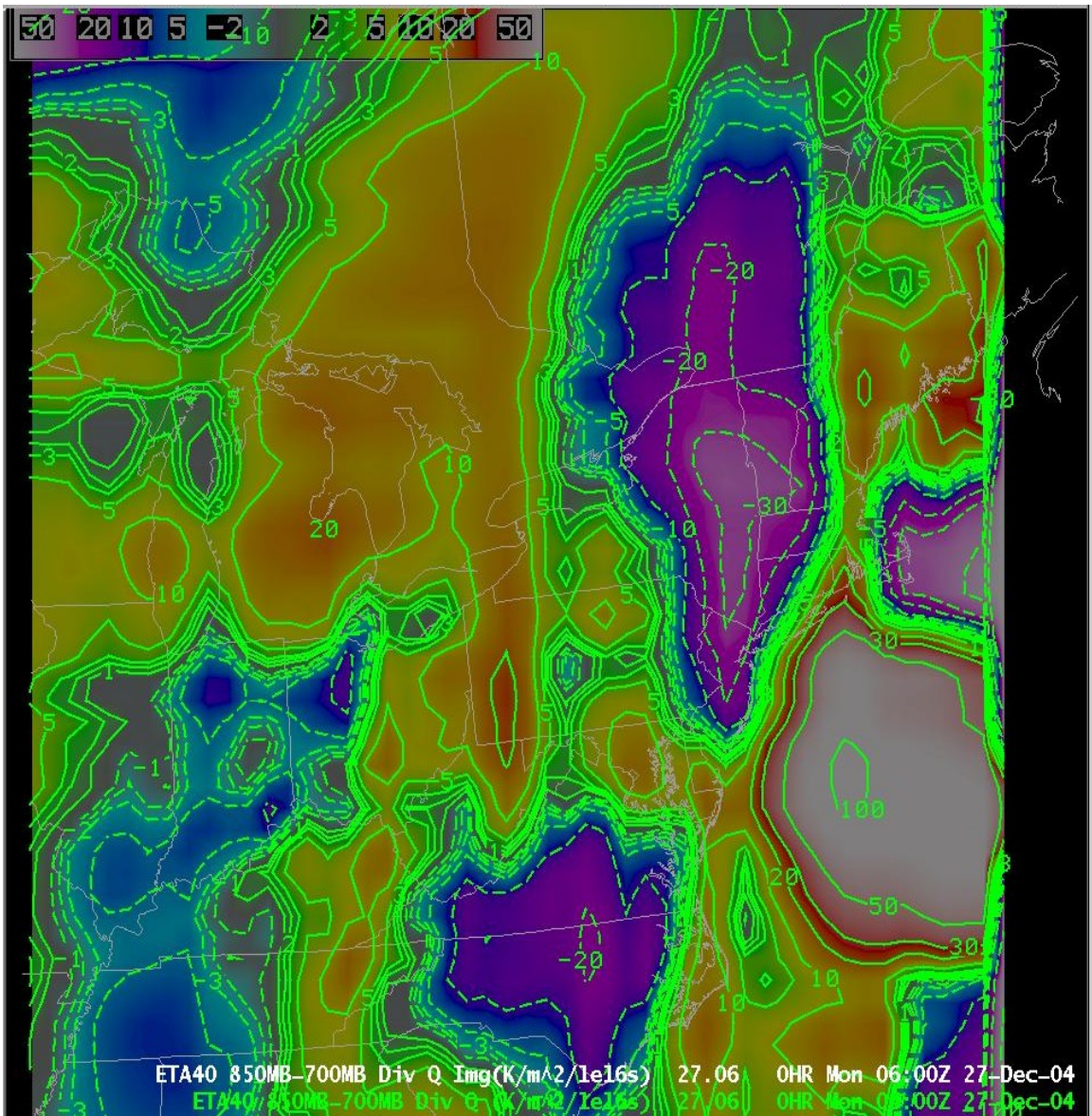


Fig. 4.8. 27 December initialized 0600 UTC Eta 850–700 hPa average Q-vector divergence (solid green contours, shaded, $10^{-16} \text{ K m}^{-2} \text{ s}^{-1}$). Q-vector convergence is given by dashed green contours.

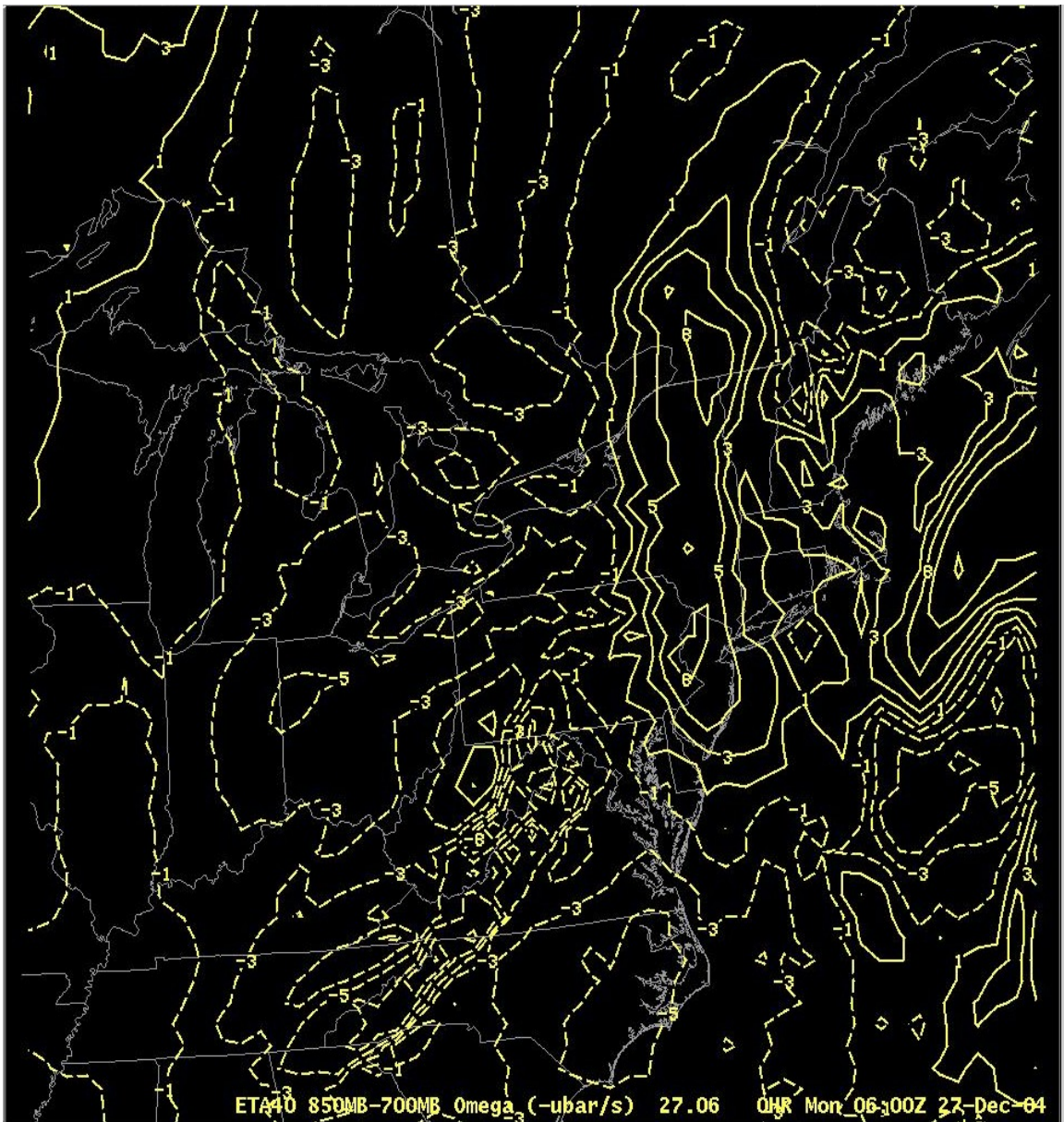


Fig. 4.9. 27 December initialized 0600 UTC Eta 850–700 hPa average vertical velocity (yellow contours, $-\mu\text{b s}^{-1}$). Upward motion is given by solid contours.

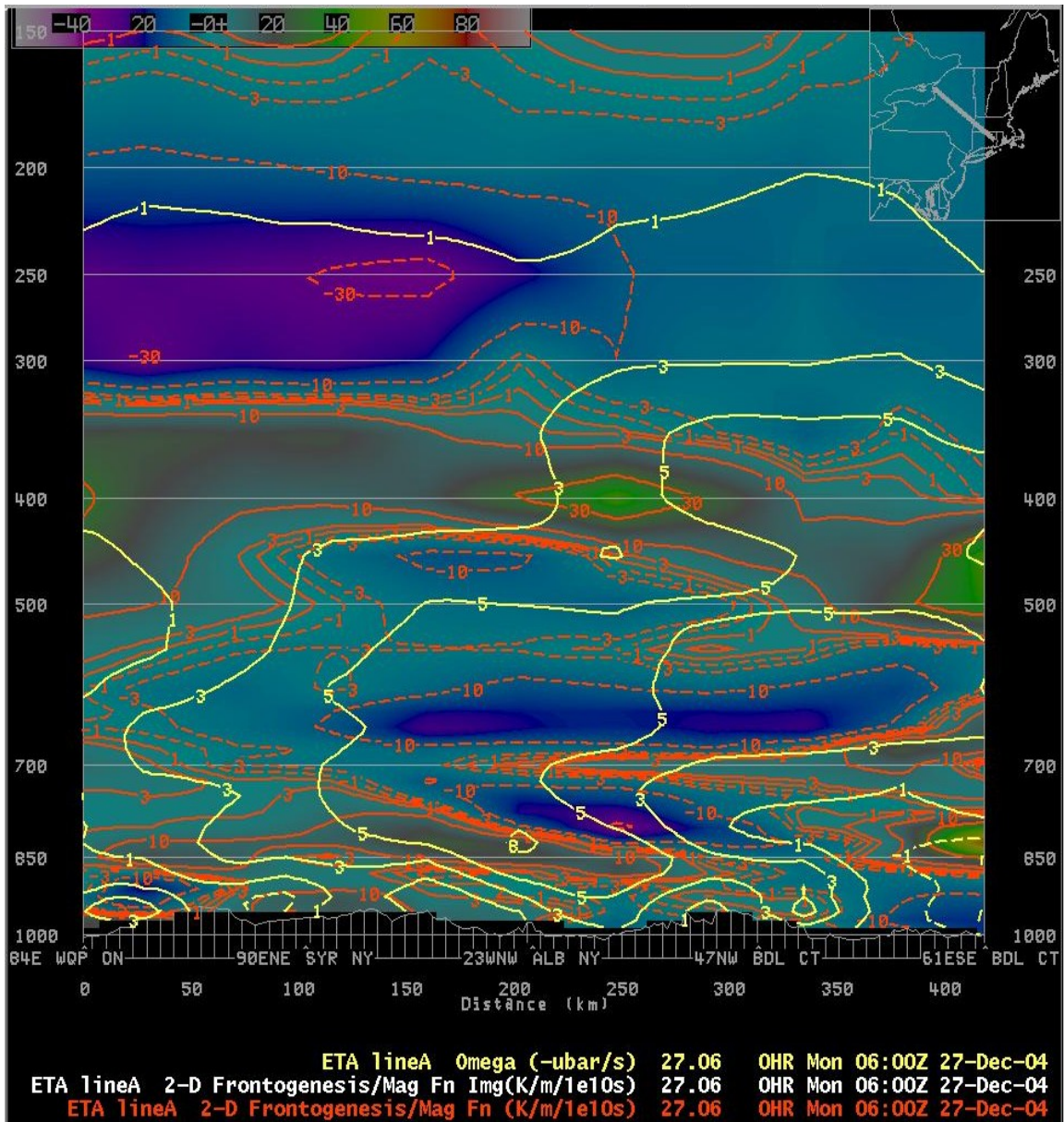


Fig. 4.10. 27 December initialized 0600 UTC Eta Petterssen frontogenesis (red contours, shaded, $10^{-10} \text{ K m}^{-1} \text{ s}^{-1}$) and vertical velocity (yellow contours, $-\mu\text{b s}^{-1}$). Regions of frontogenesis are given by solid red contours and green shading. Upward vertical motion is depicted by solid yellow contours.

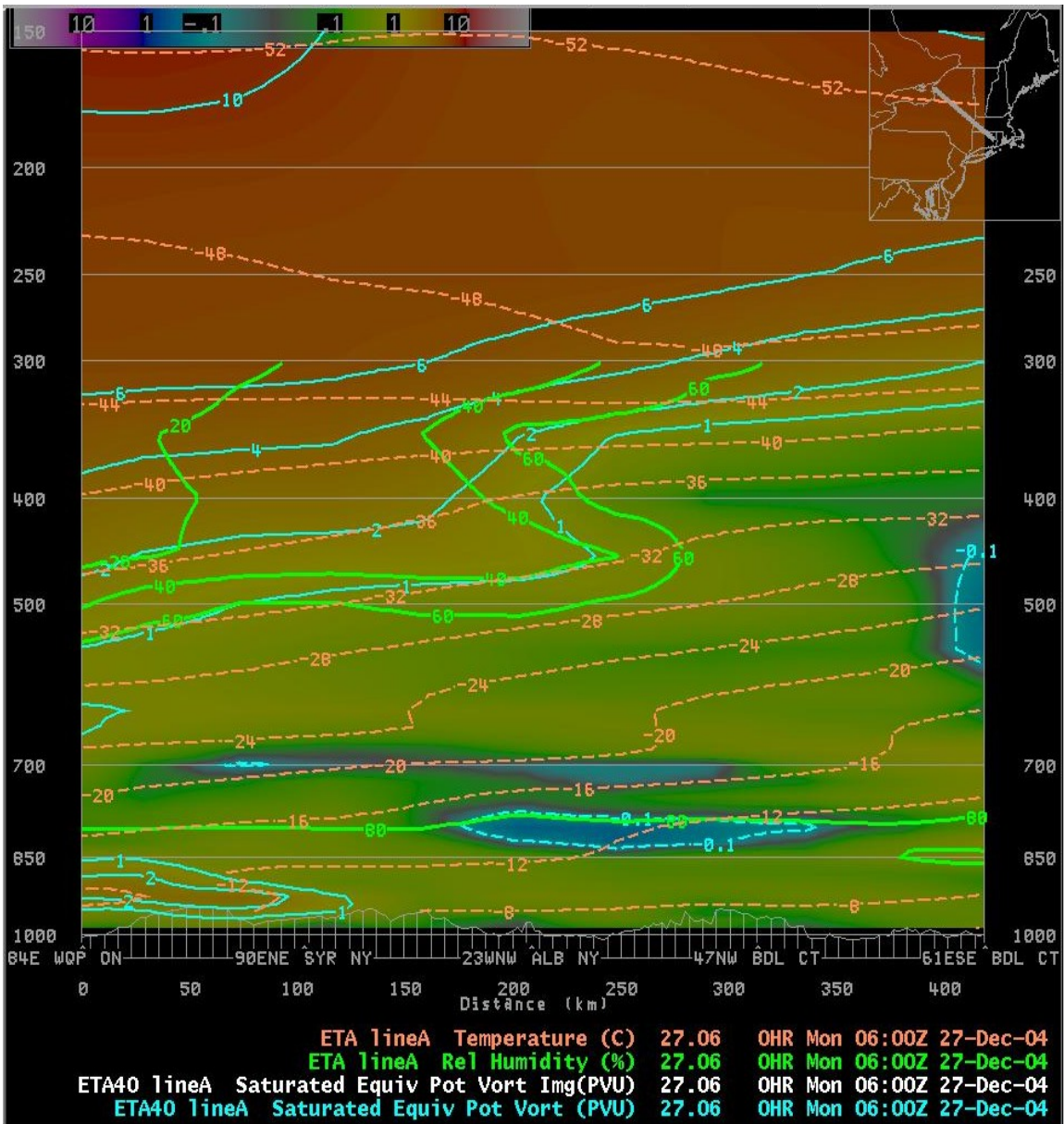


Fig. 4.11. 27 December initialized 0600 UTC Eta saturation equivalent potential vorticity (blue contours, shaded, PVU), relative humidity (green contours, %), and temperature (dashed orange contours, °C). Regions of negative EPV* are shaded blue, while regions of WMSS are shaded dark green.

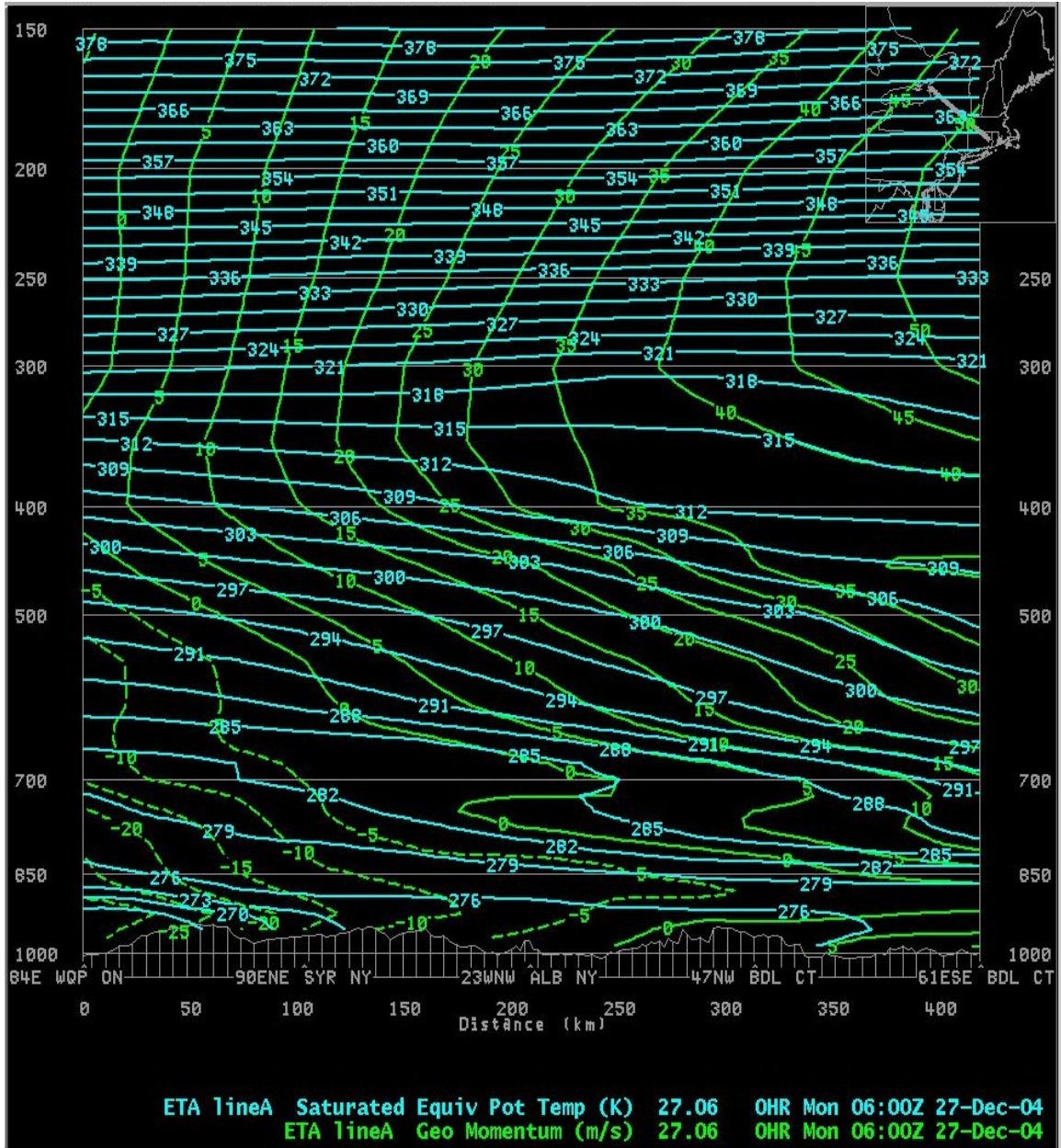
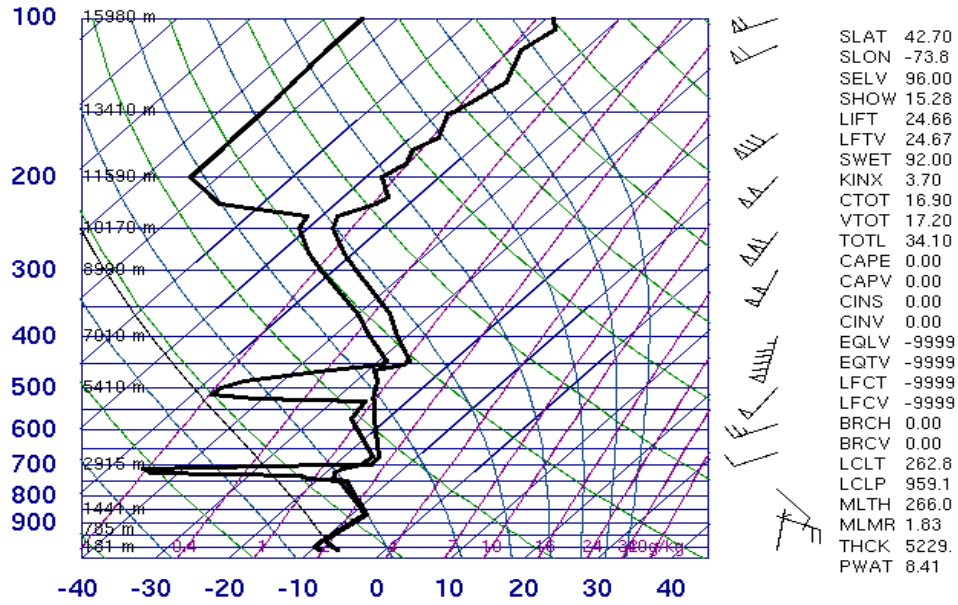


Fig. 4.12. 27 December initialized 0600 UTC Eta absolute geostrophic momentum (green contours, m s^{-1}) and saturation equivalent potential temperature (blue contours, K).

72518 ALB Albany

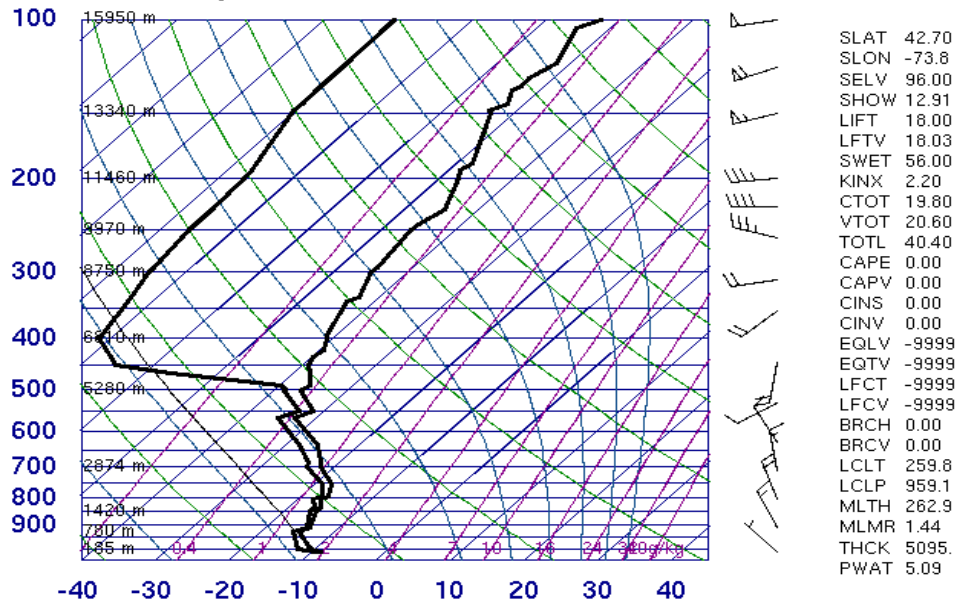


00Z 27 Dec 2004

University of Wyoming

a.

72518 ALB Albany

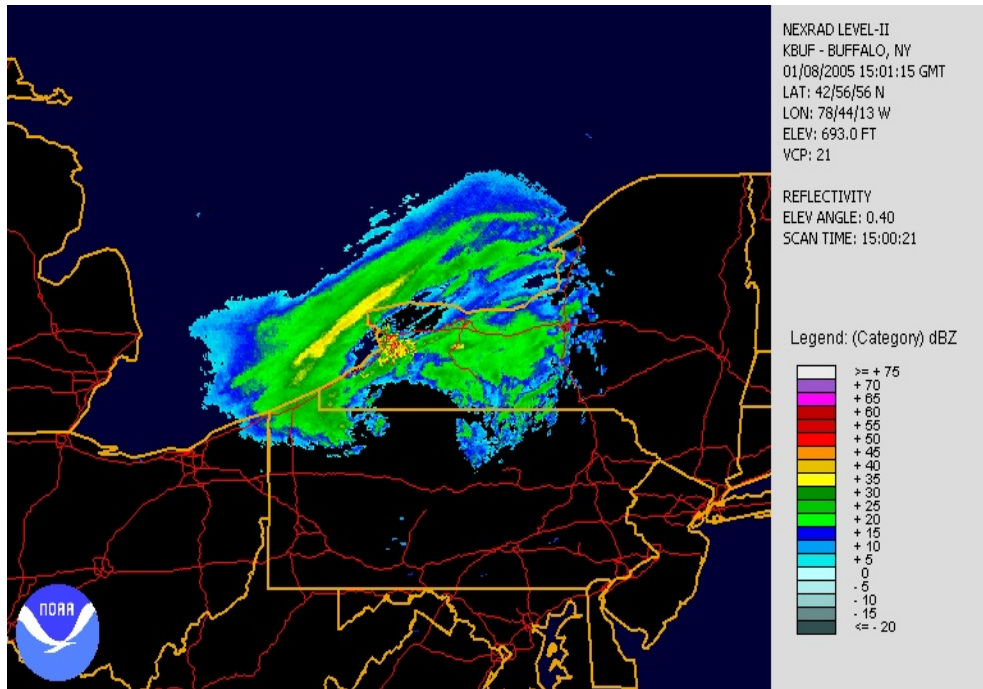


12Z 27 Dec 2004

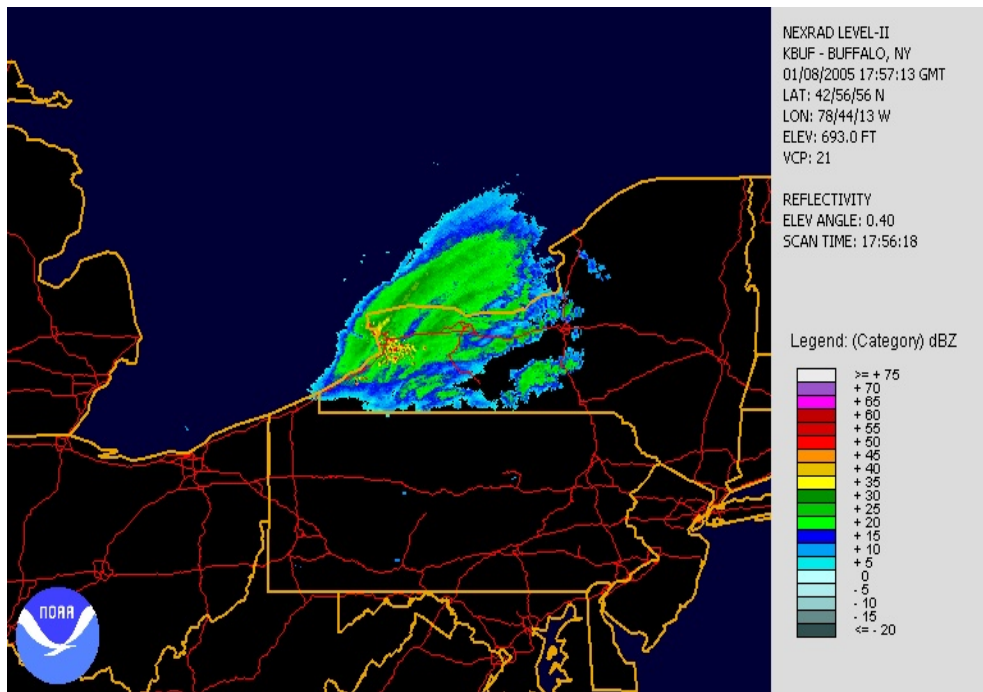
University of Wyoming

b.

Fig. 4.13a–b. Atmospheric soundings taken at ALB on 27 December at: a) 0000 UTC and b) 1200 UTC.



a.



b.

Fig. 4.14a–b. BUF WSR 88-D reflectivity image on 8 January 2005 at: a) 1500 UTC and b) 1800 UTC.

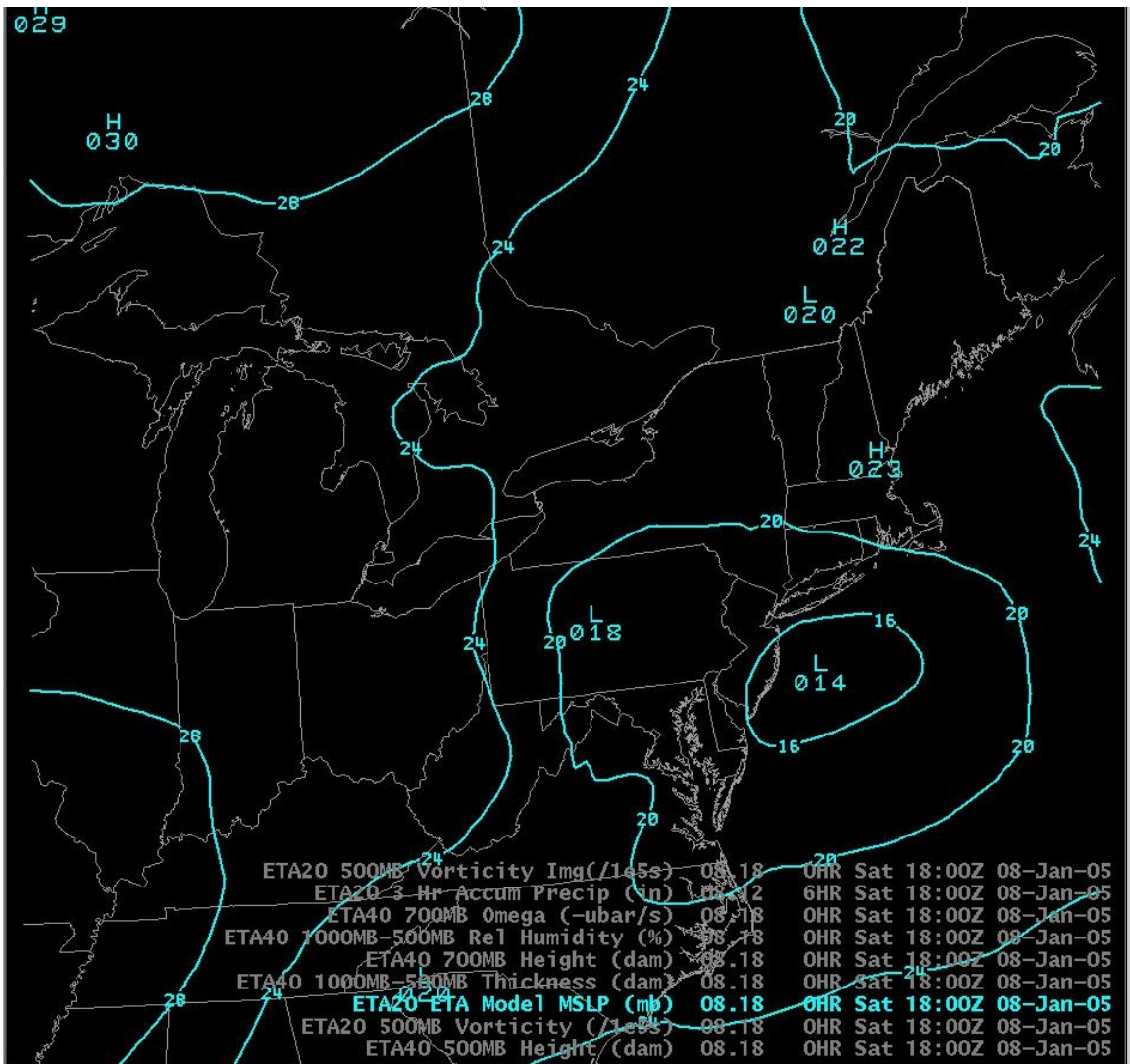


Fig. 4.15. As in Fig. 4.4 except for 8 January initialized 1800 UTC Eta.

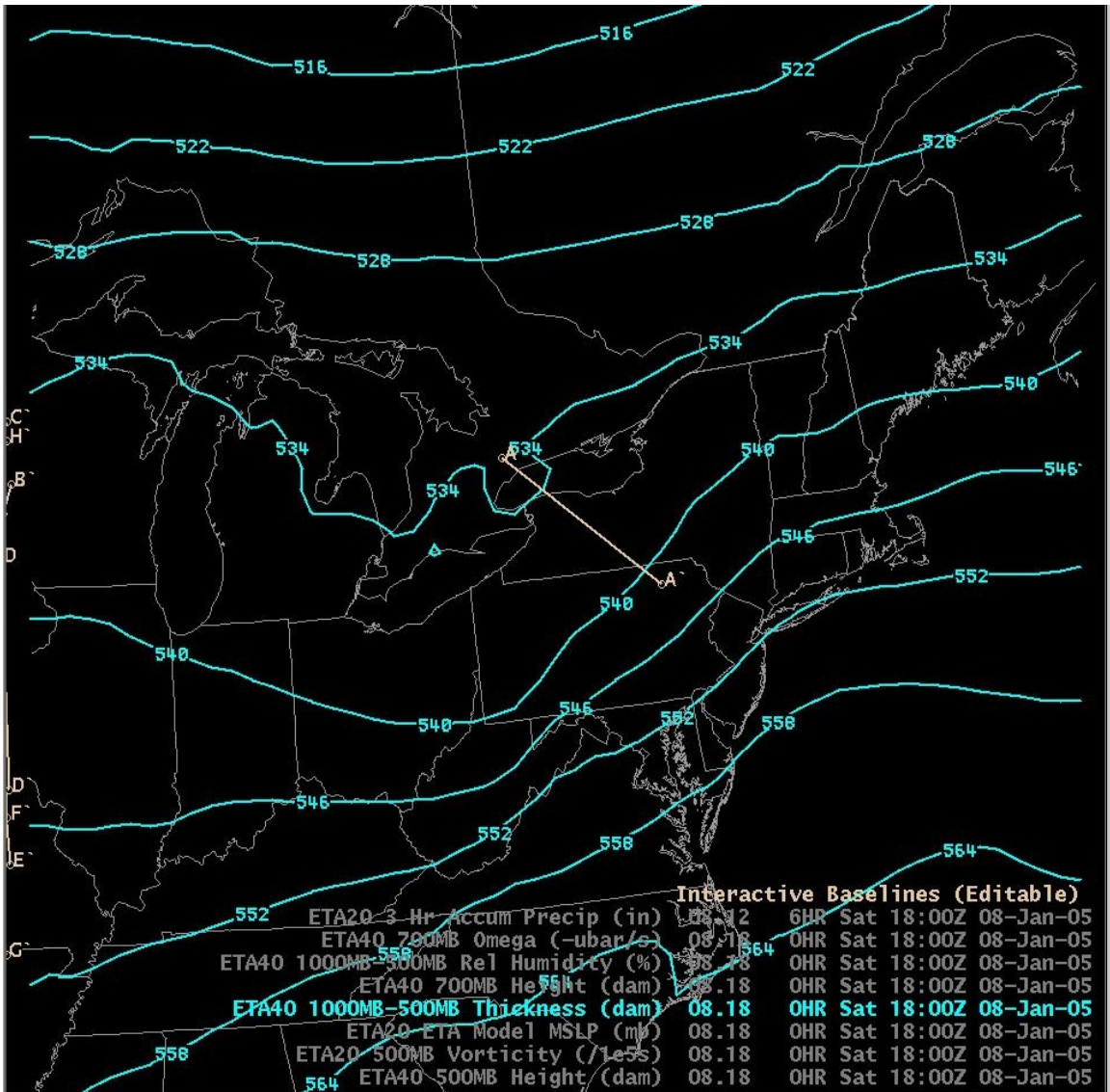


Fig. 4.16. 8 January initialized 1800 UTC Eta 1000–500 hPa thickness (blue contours, dam). White line marks location of cross section.

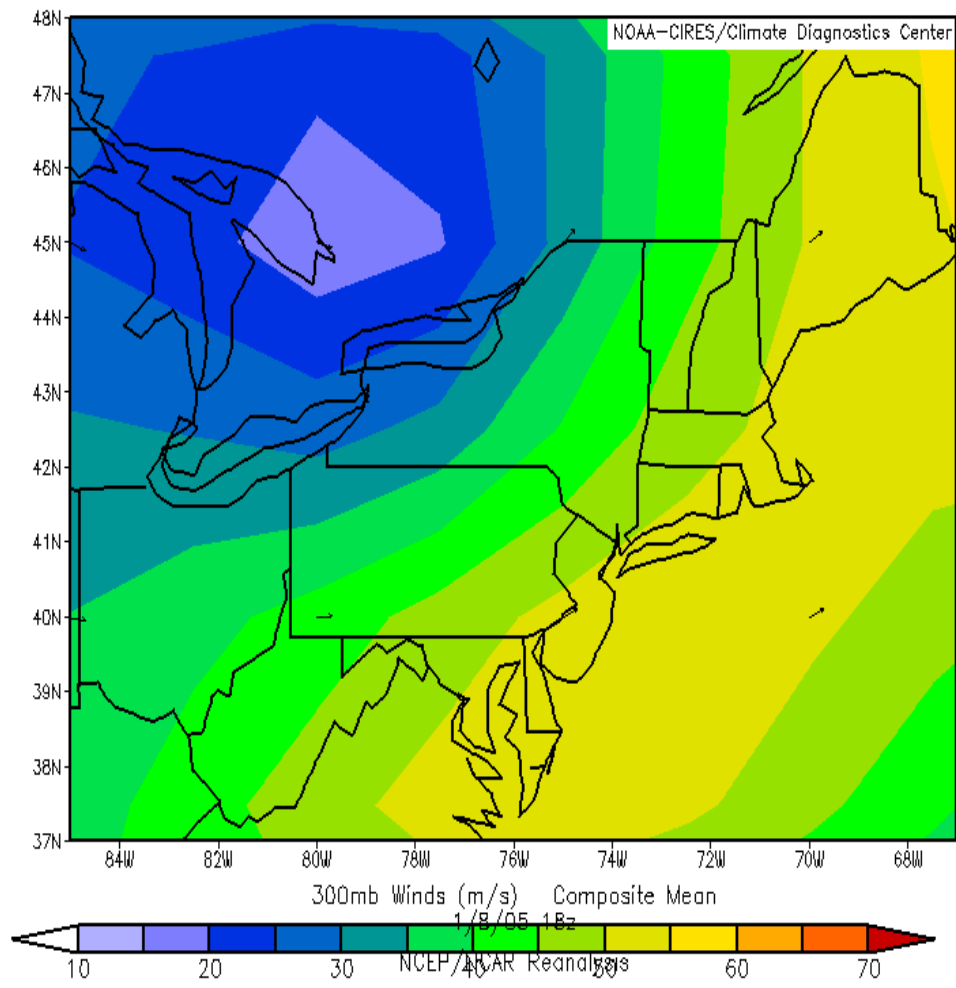


Fig. 4.17. As in Fig. 4.6 except for 8 January 1800 UTC.

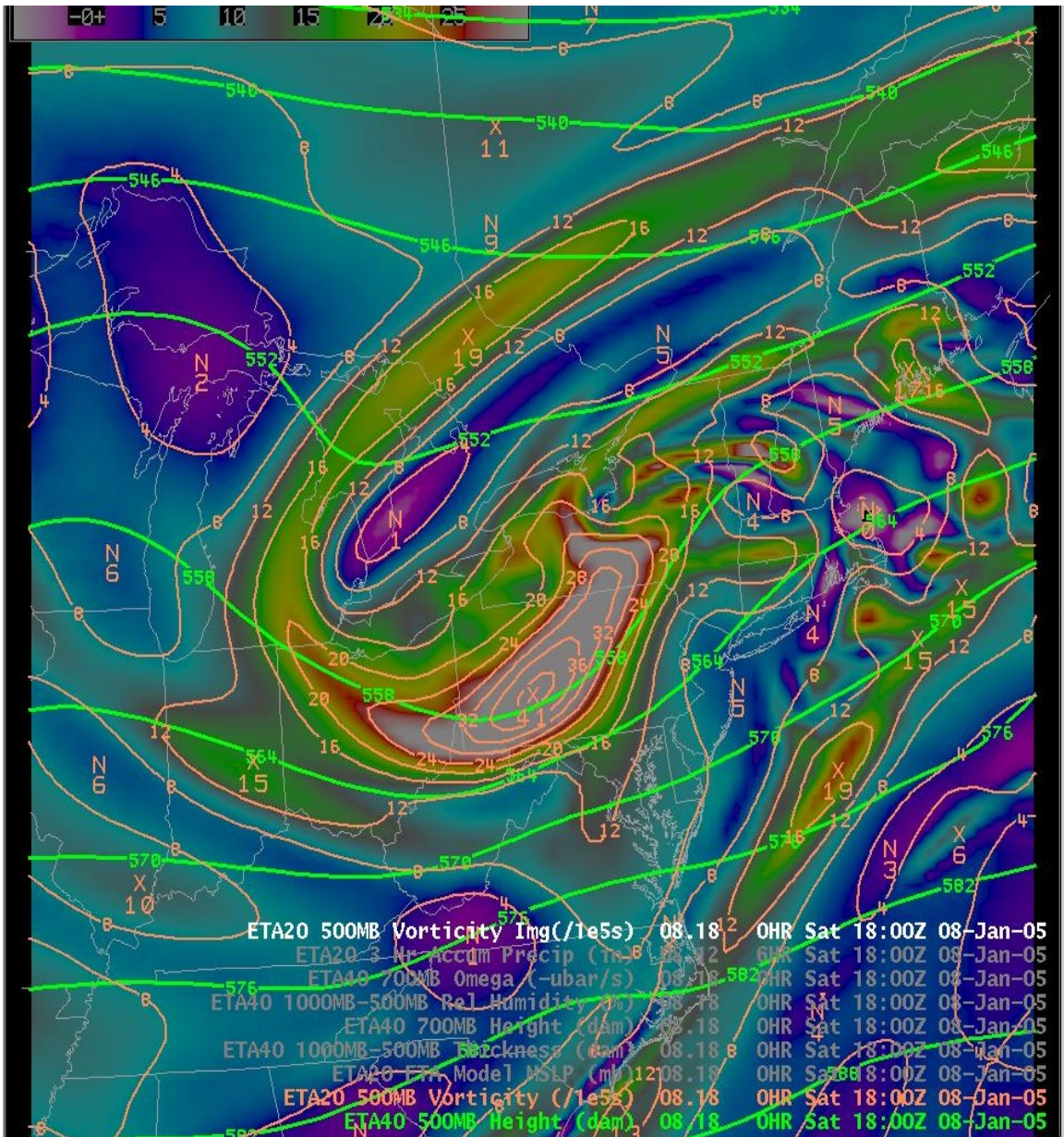


Fig. 4.18. As in Fig. 4.7 except for 8 January using the initialized 1800 UTC Eta.

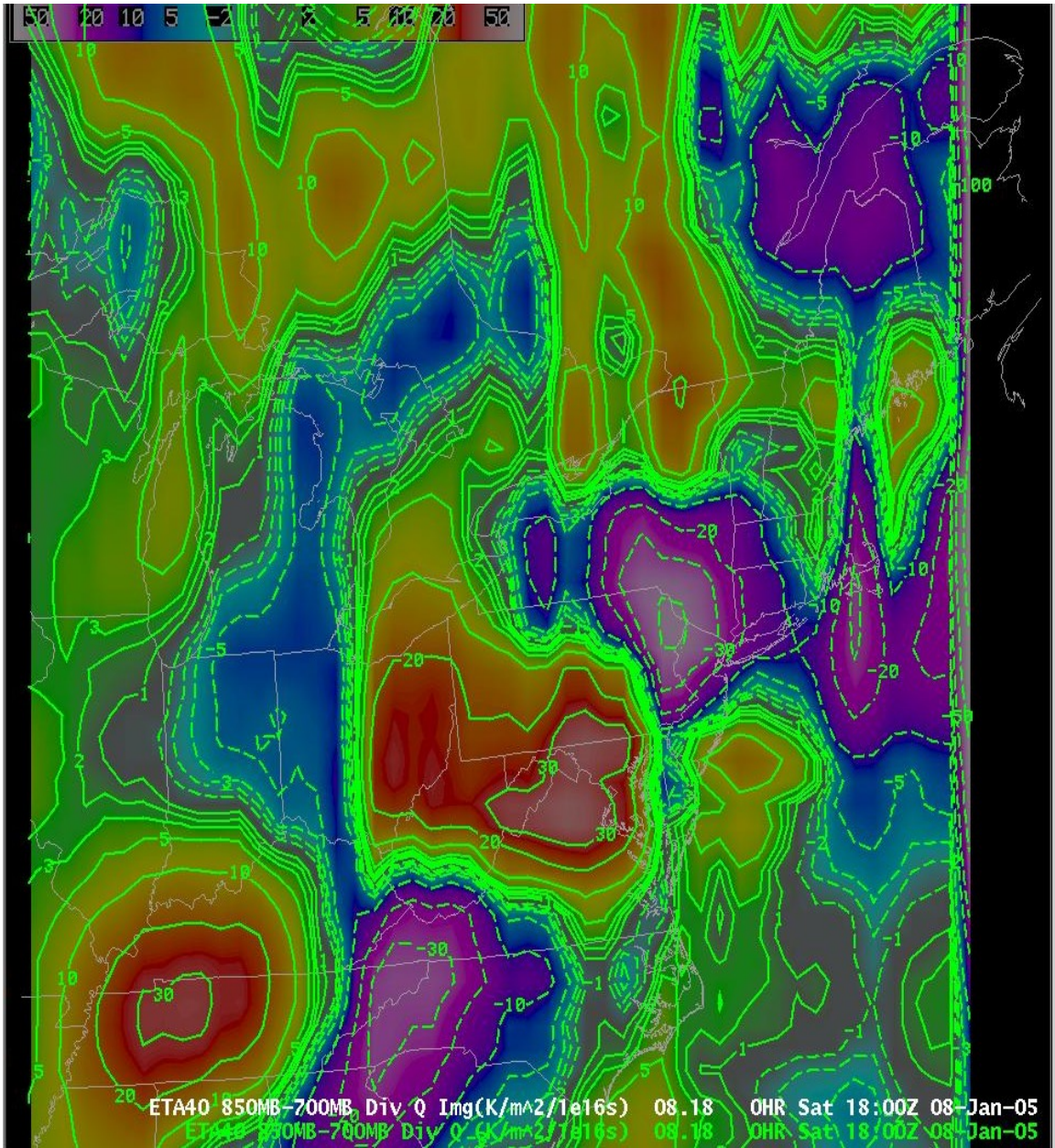


Fig. 4.19. As in Fig. 4.8 except for 8 January using the initialized 1800 UTC Eta.

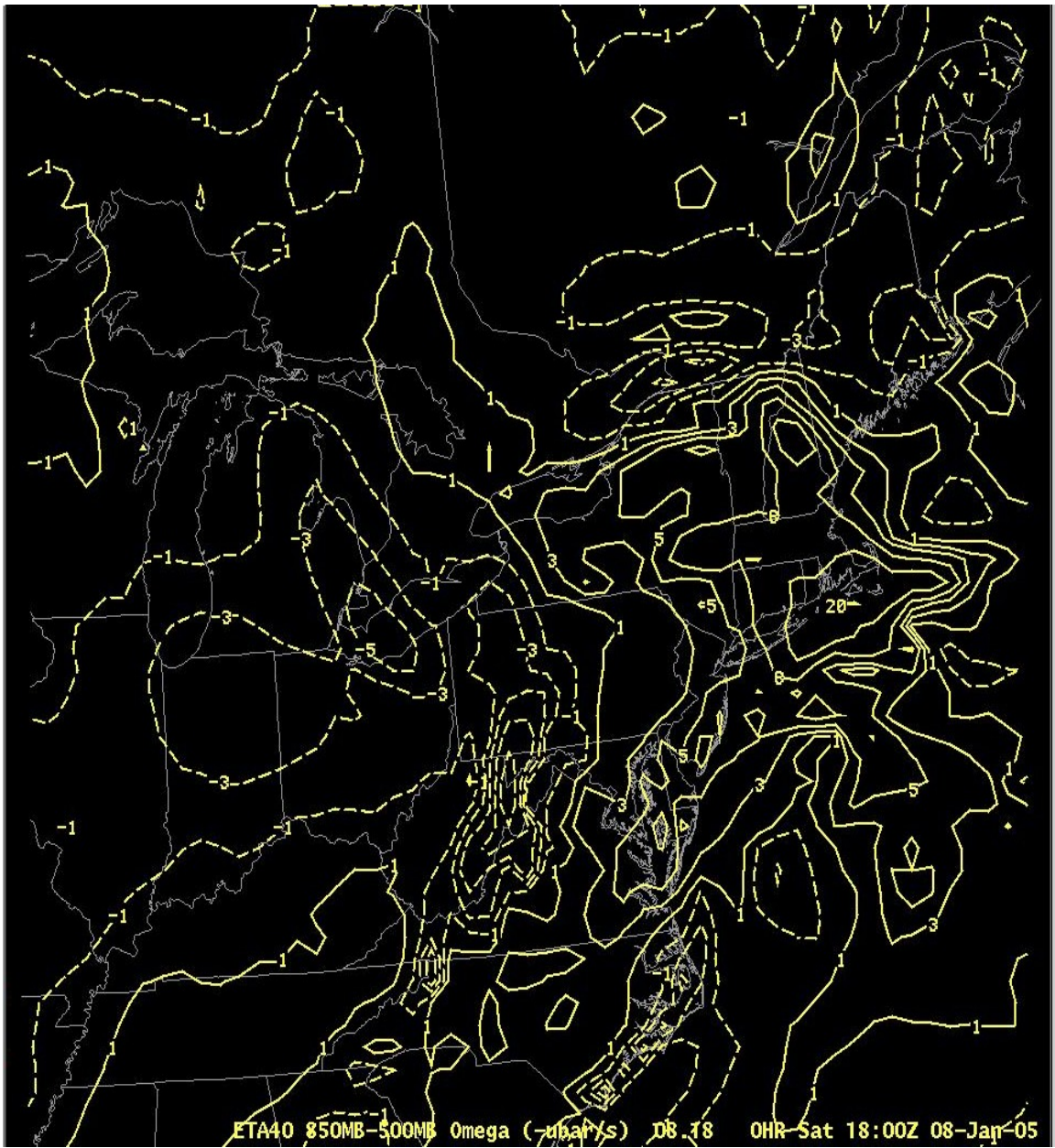


Fig. 4.20. 8 January initialized 1800 UTC Eta 850–500 hPa average vertical velocity (yellow contours, $-\mu\text{b s}^{-1}$). Upward motion is given by solid contours.

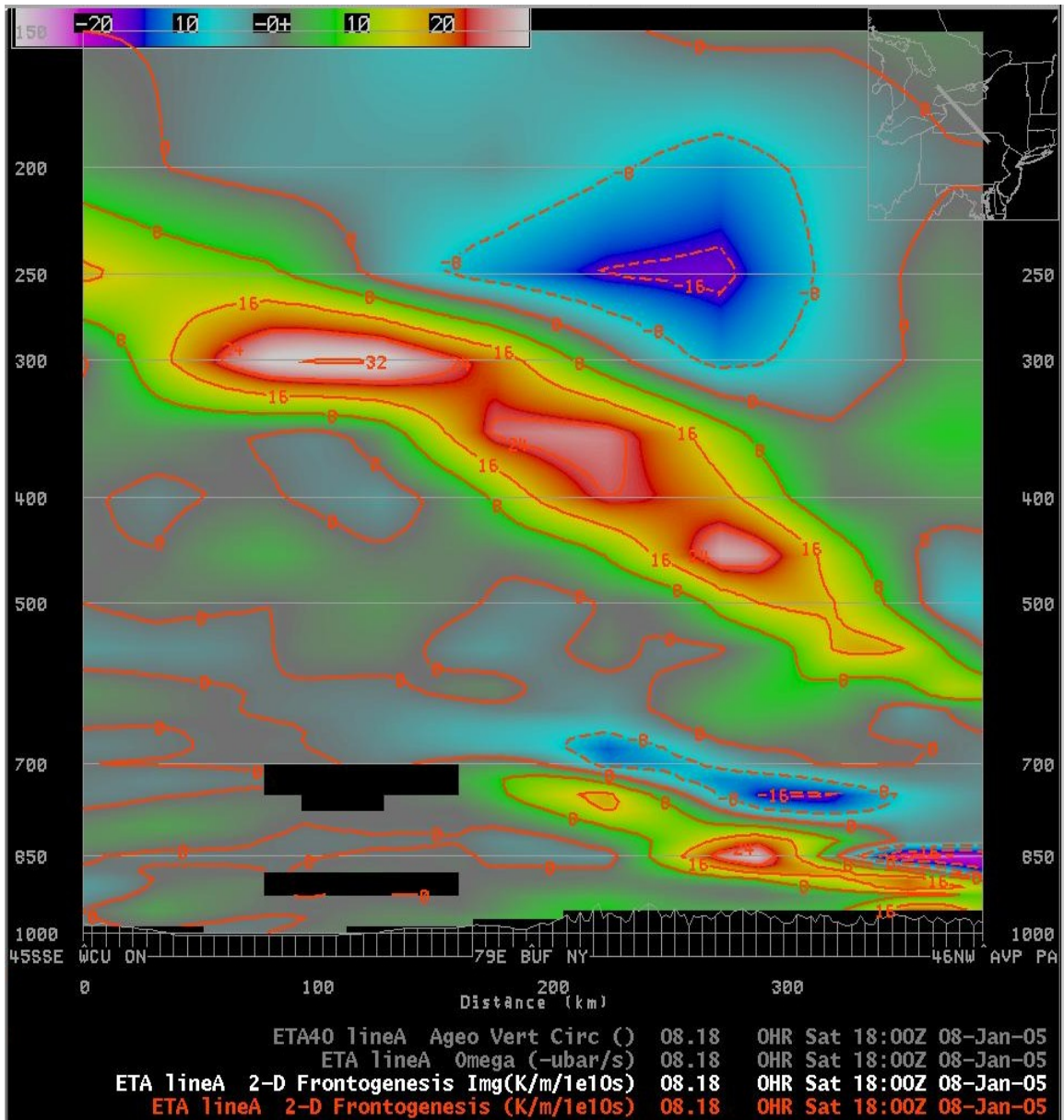


Fig. 4.21. 8 January initialized 1800 UTC Eta Petterssen frontogenesis (red contours, shaded, $10^{-10} \text{ K m}^{-1} \text{ s}^{-1}$). Regions of frontogenesis are given by solid red contours and shaded warm colors.

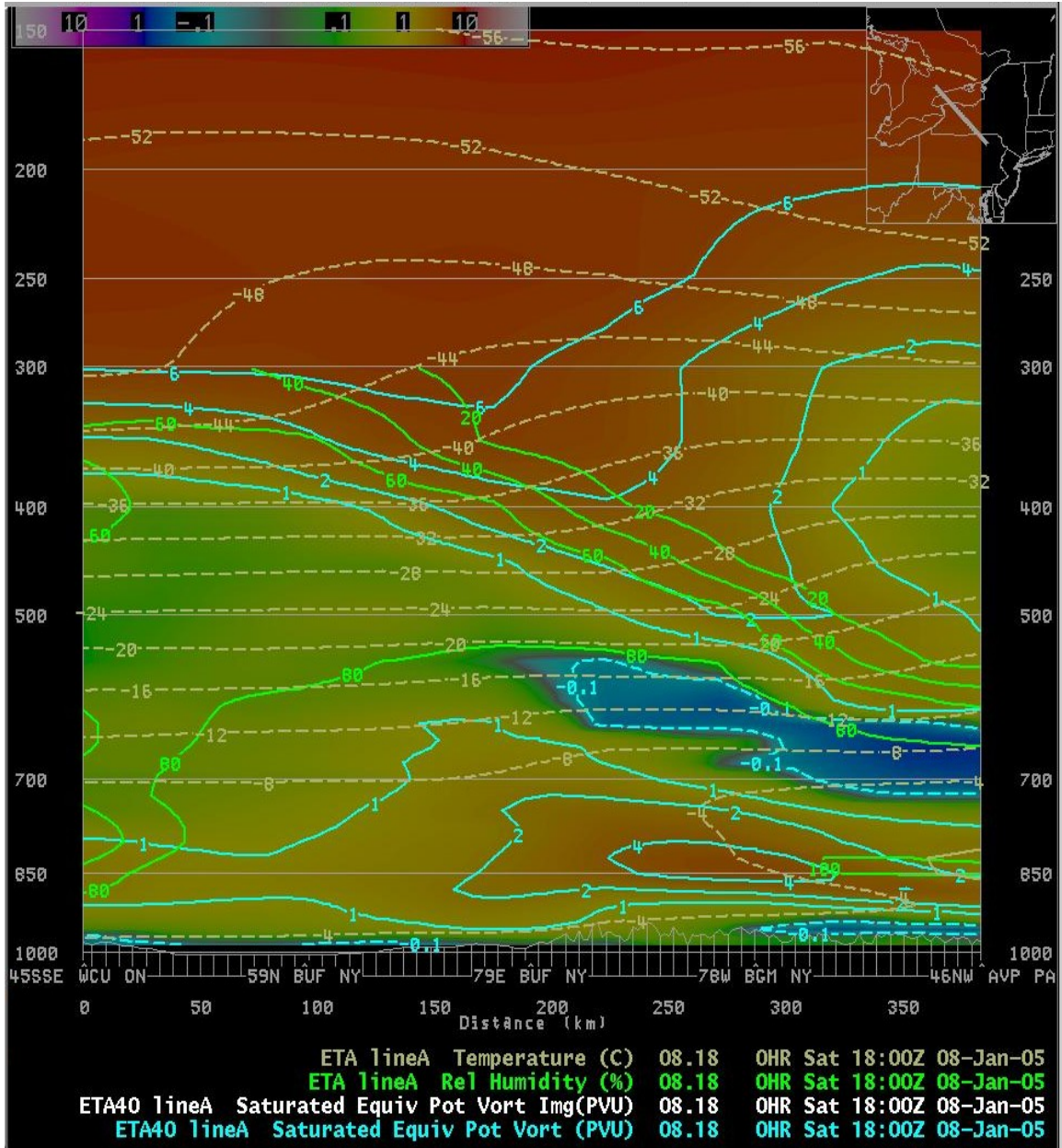


Fig. 4.22. As in Fig. 4.11 except for 8 January using the initialized 1800 UTC Eta.

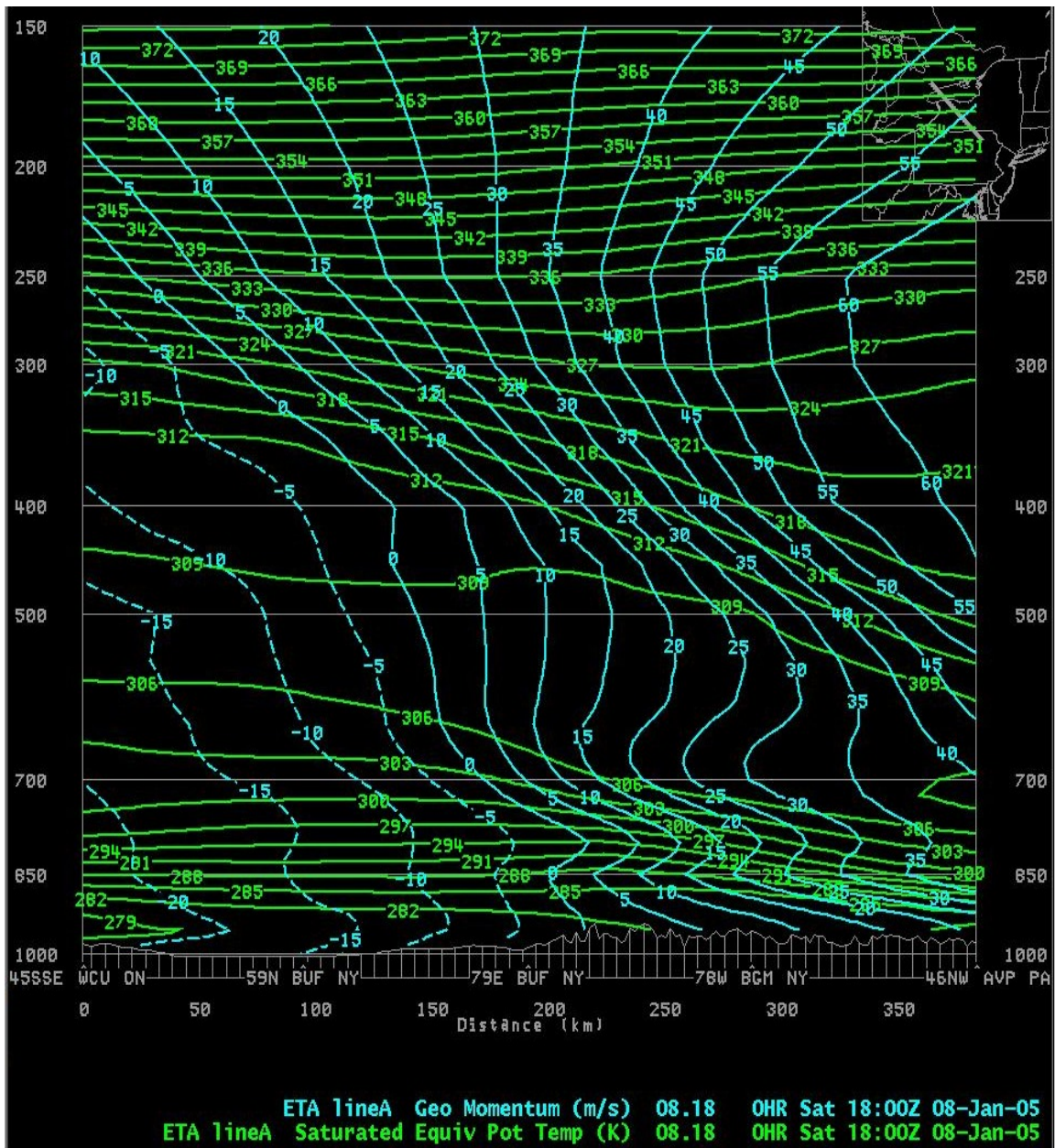


Fig. 4.23. 8 January initialized 1800 UTC Eta absolute geostrophic momentum (blue contours, m s^{-1}) and saturation equivalent potential temperature (green contours, K).

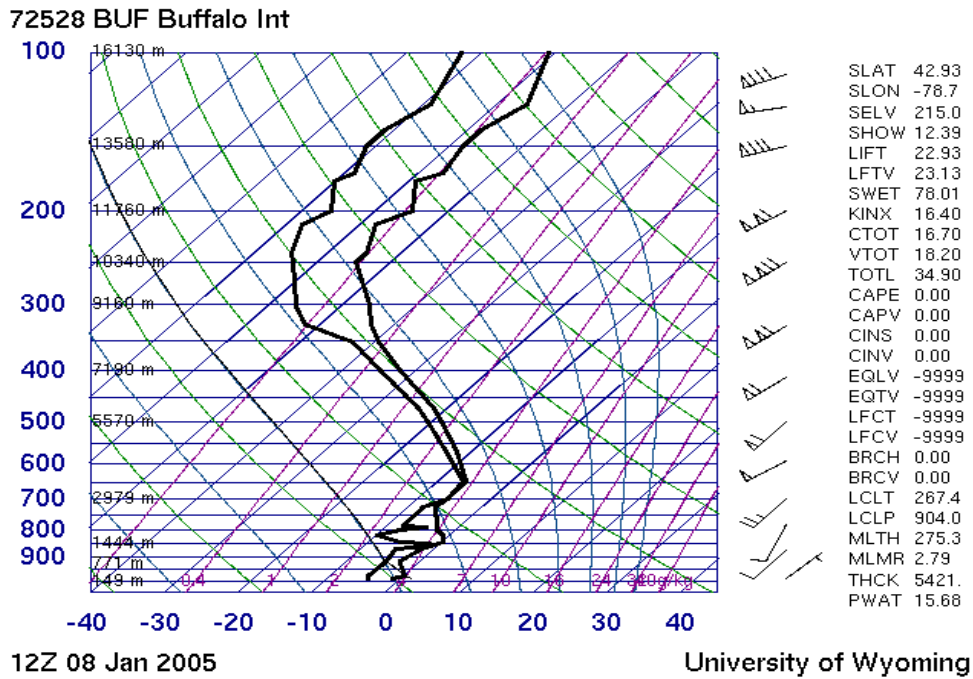


Fig. 4.24. As in Fig. 4.13 except at BUF on 8 January at 1200 UTC.

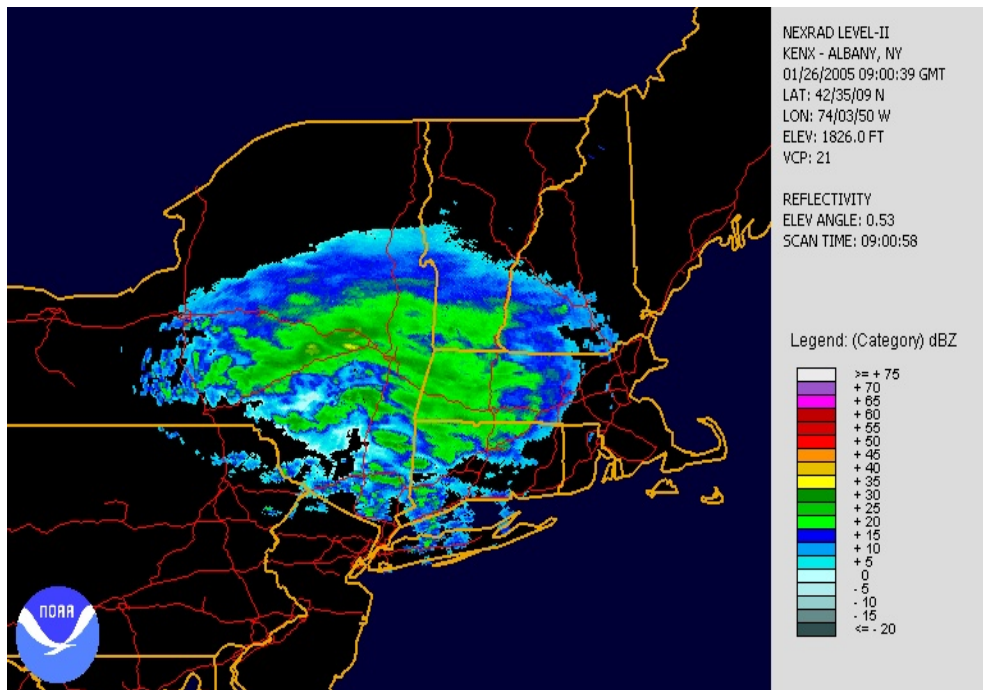


Fig. 4.25. As in Fig. 4.2 expect for 26 January 2005 at 0900 UTC.

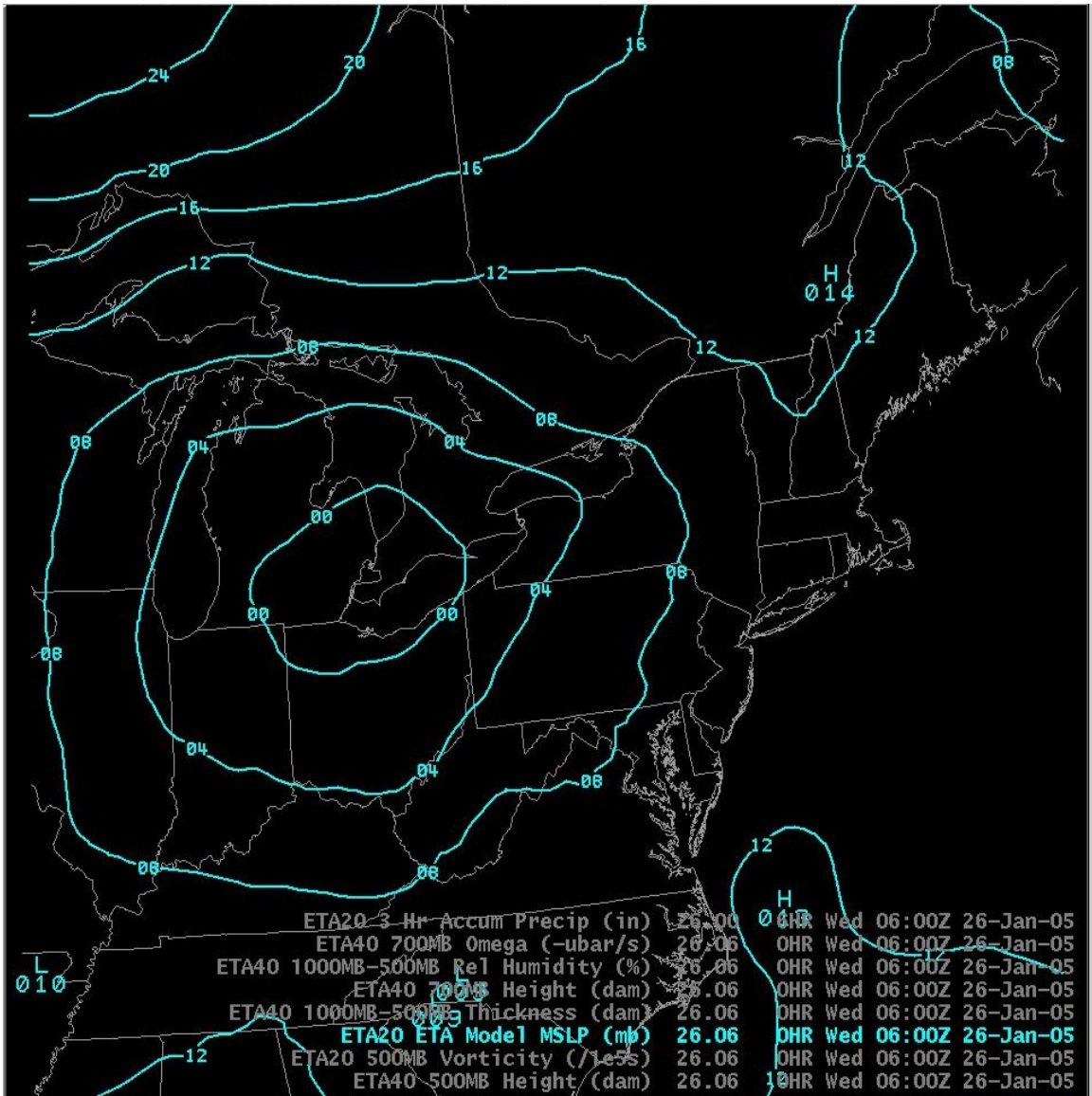


Fig. 4.26. As in Fig. 4.4 except for 26 January initialized 0600 UTC Eta.

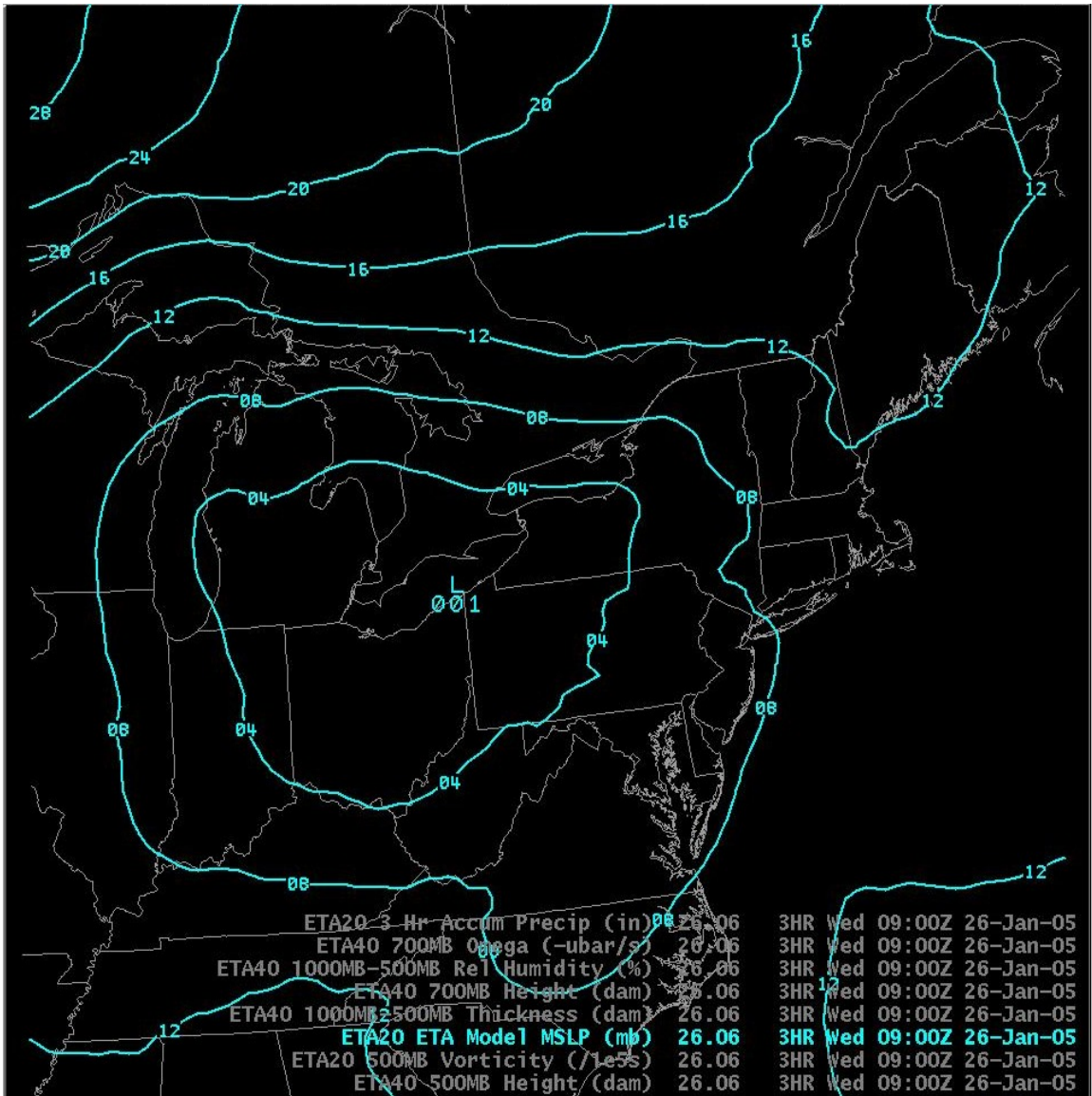


Fig. 4.27. As in Fig. 4.4 expect for 26 January 0600 UTC Eta 3-h forecast.

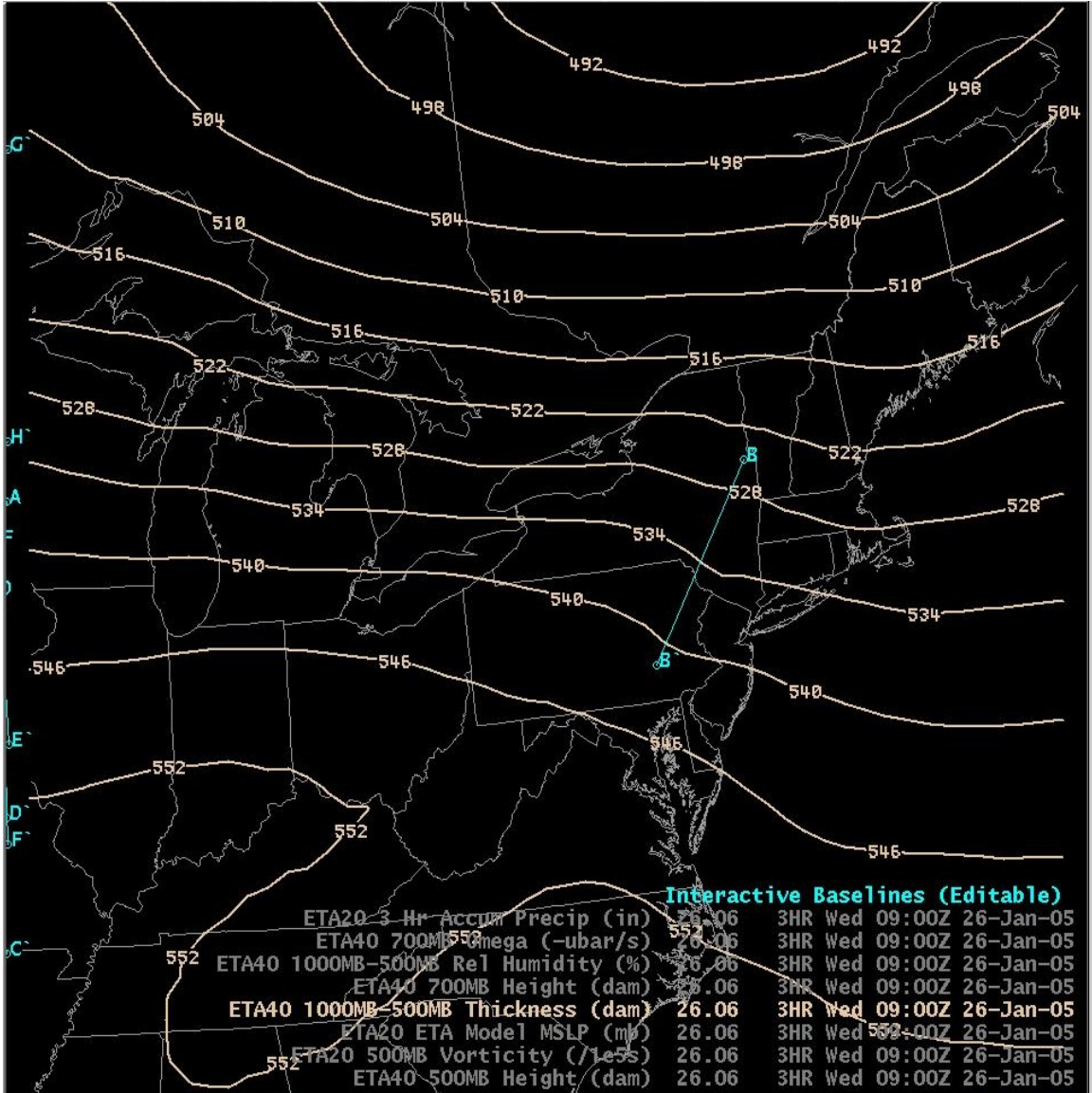


Fig. 4.28. 26 January 0600 UTC Eta 3-h forecast of 1000–500 hPa thickness (yellow contours, dam). Blue line marks location of cross section.

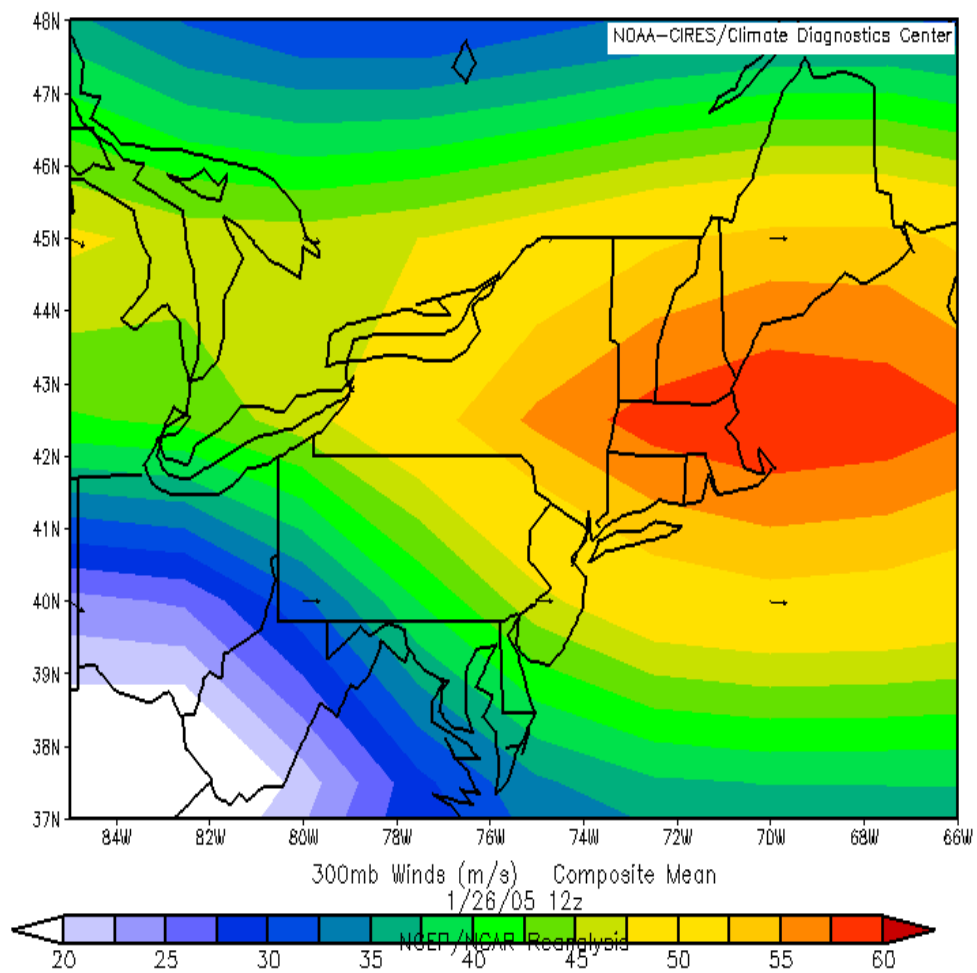


Fig. 4.29. As in Fig. 4.6 except for 26 January 1200 UTC.

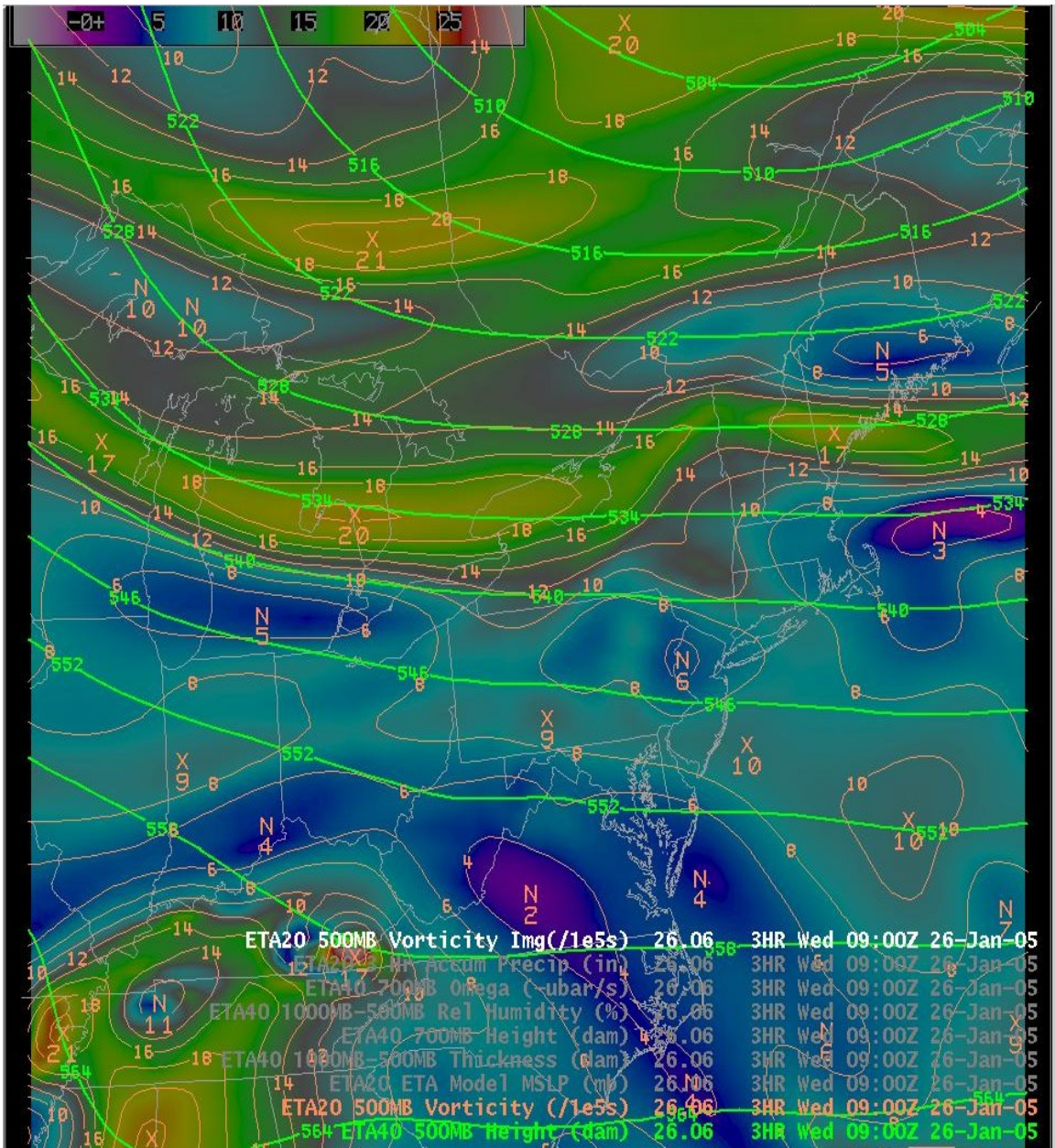


Fig. 4.30. As in Fig. 4.7 except for 26 January 0600 UTC Eta 3-h forecast.

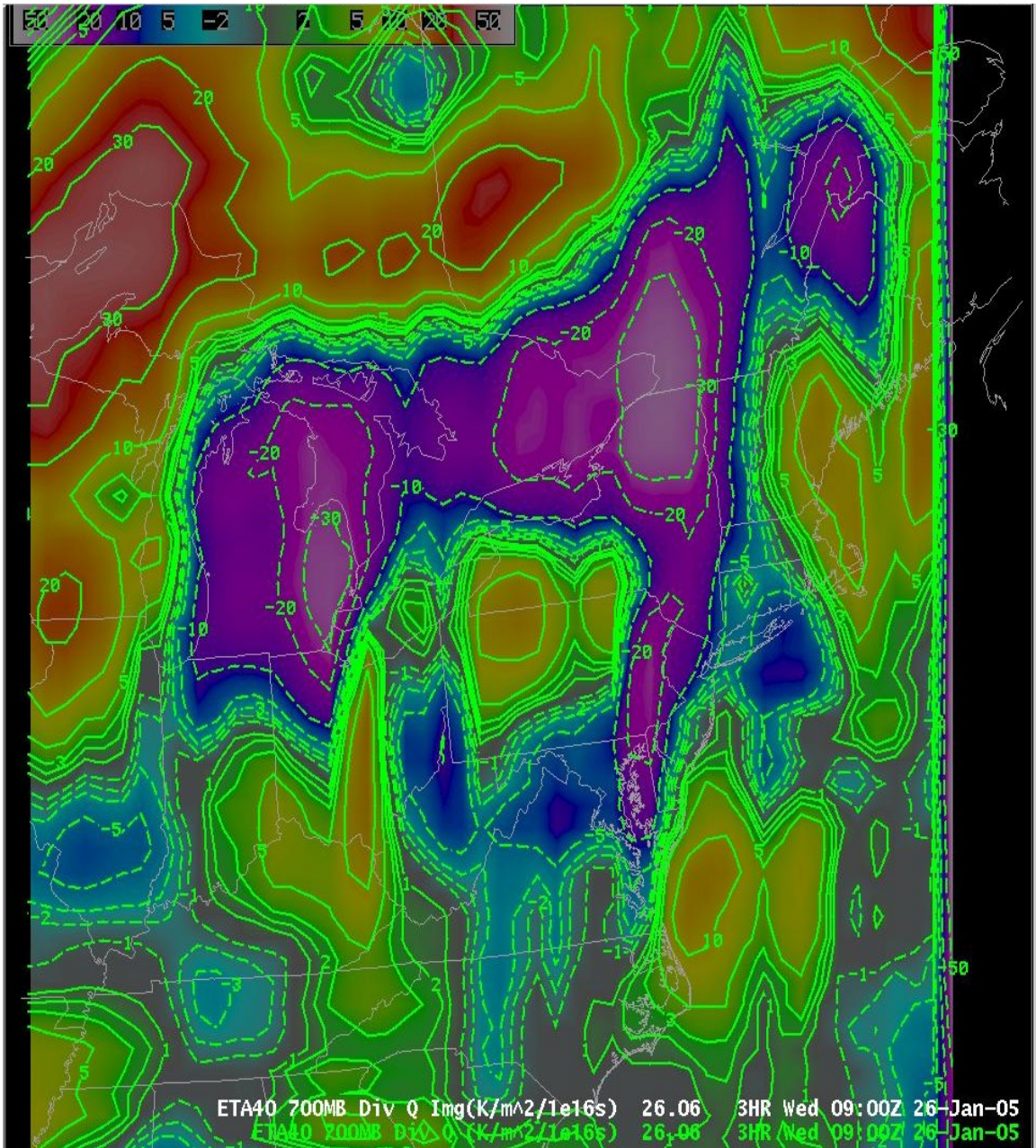


Fig. 4.31. As in Fig. 4.8 except for 26 January 0600 UTC Eta 3-h forecast evaluated at 700 hPa.

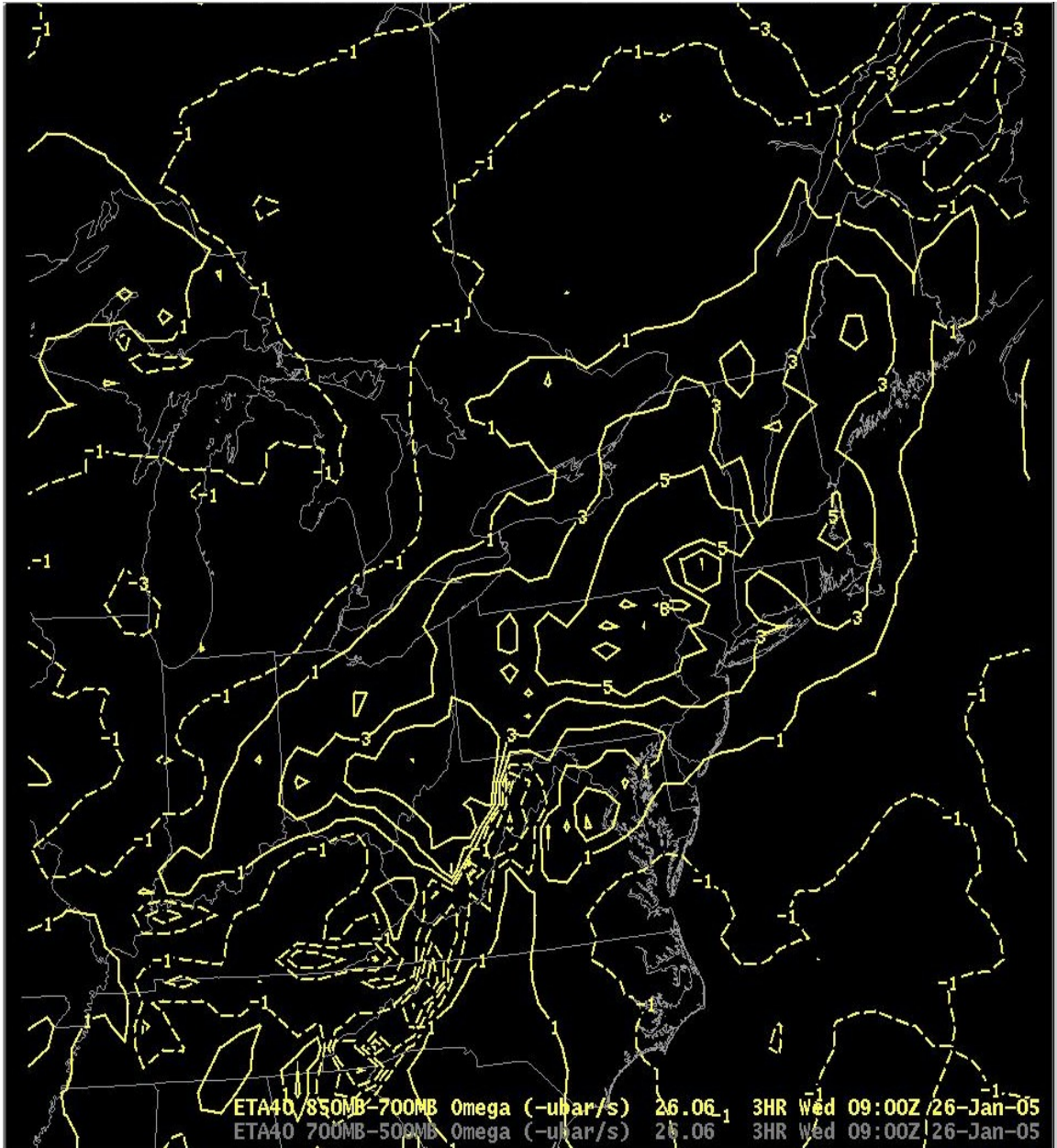


Fig. 4.32. As in Fig. 4.9 except for 26 January 0600 UTC Eta 3-h forecast.

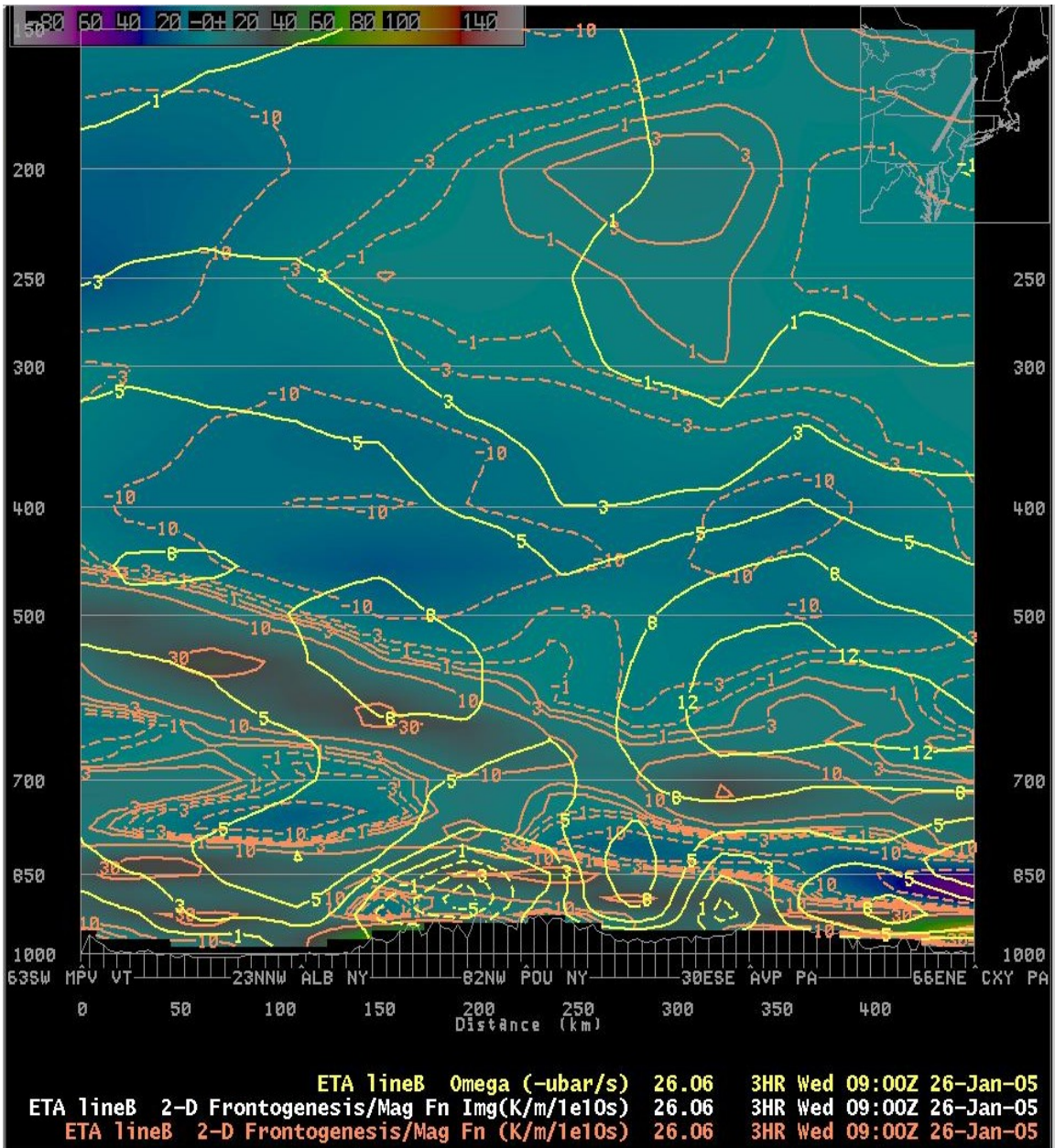


Fig. 4.33. As in Fig. 4.10 except for 26 January 0600 UTC Eta 3-h forecast.

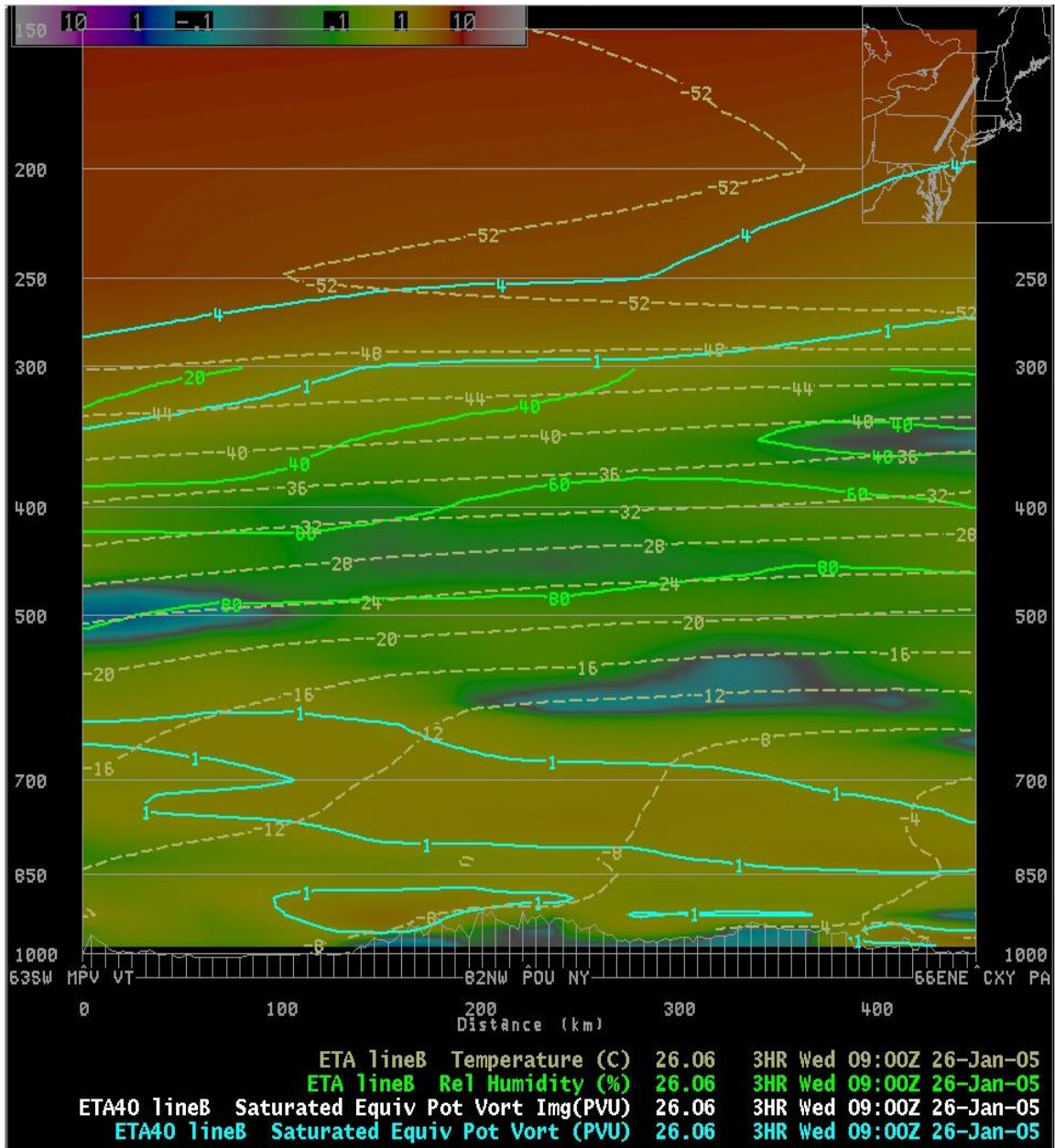


Fig. 4.34. As in Fig. 4.11 except for 26 January 0600 UTC Eta 3-h forecast.

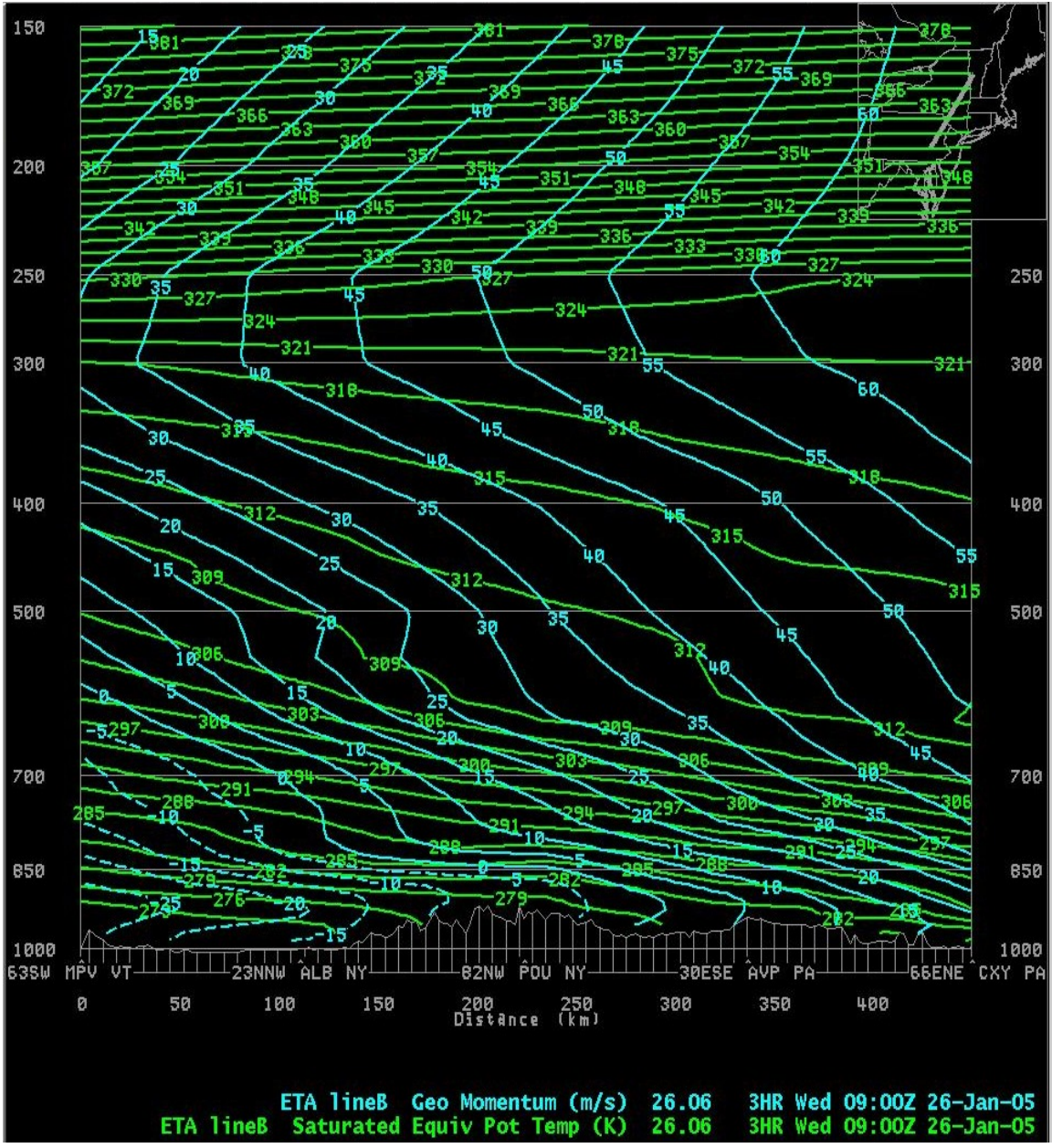


Fig. 4.35. As in Fig. 4.23 except for 26 January 0600 UTC Eta 3-h forecast.

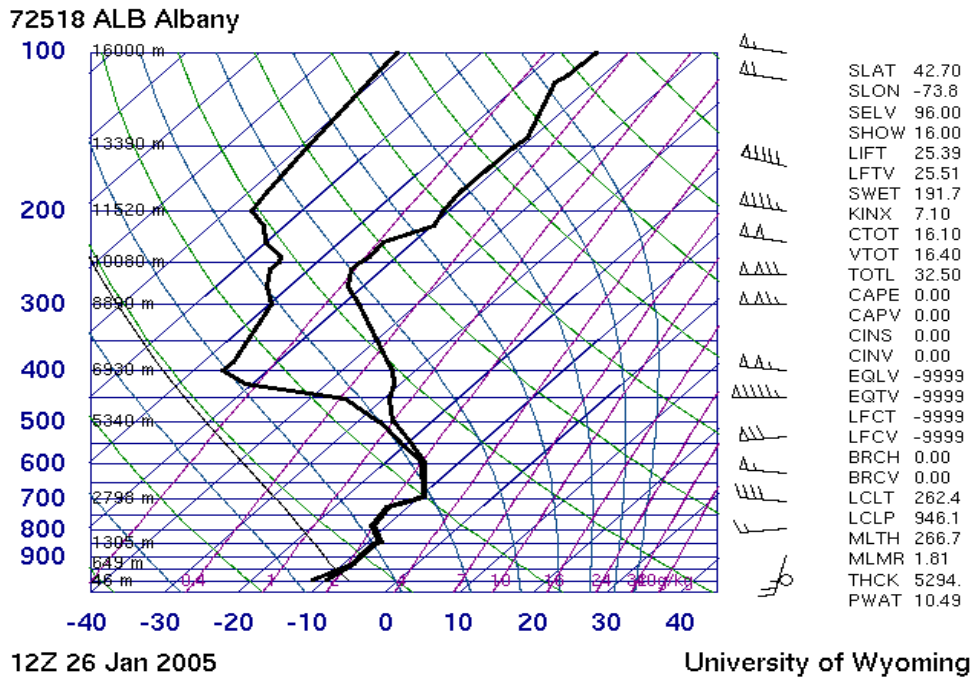


Fig. 4.36. As in Fig. 4.13 except at ALB on 26 January at 1200 UTC.

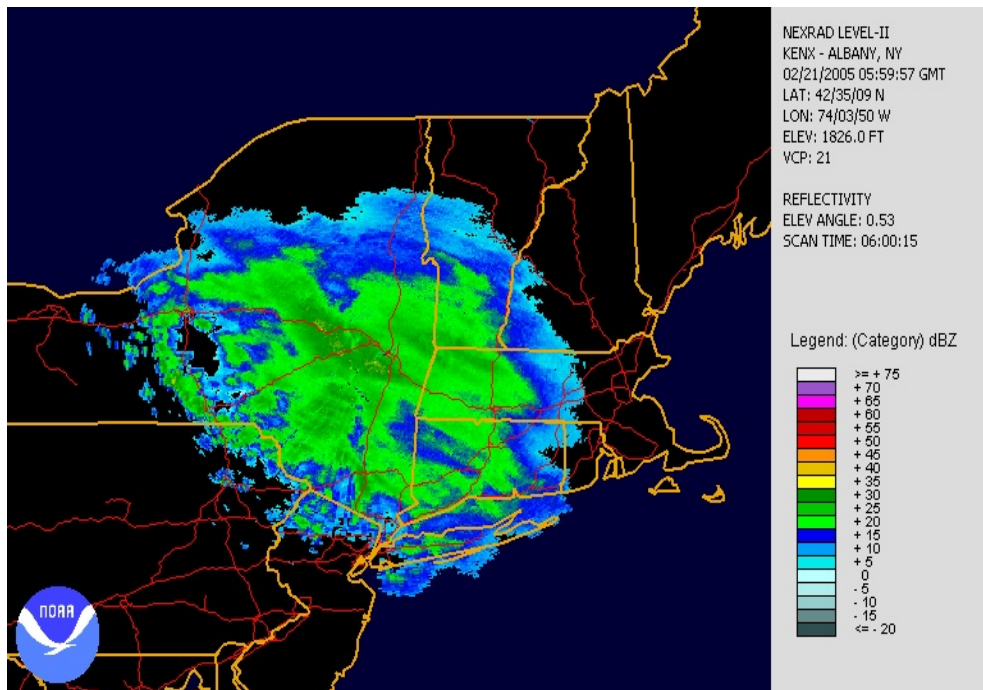


Fig. 4.37. As in Fig. 4.2 except for 21 February 2005 at 0600 UTC.

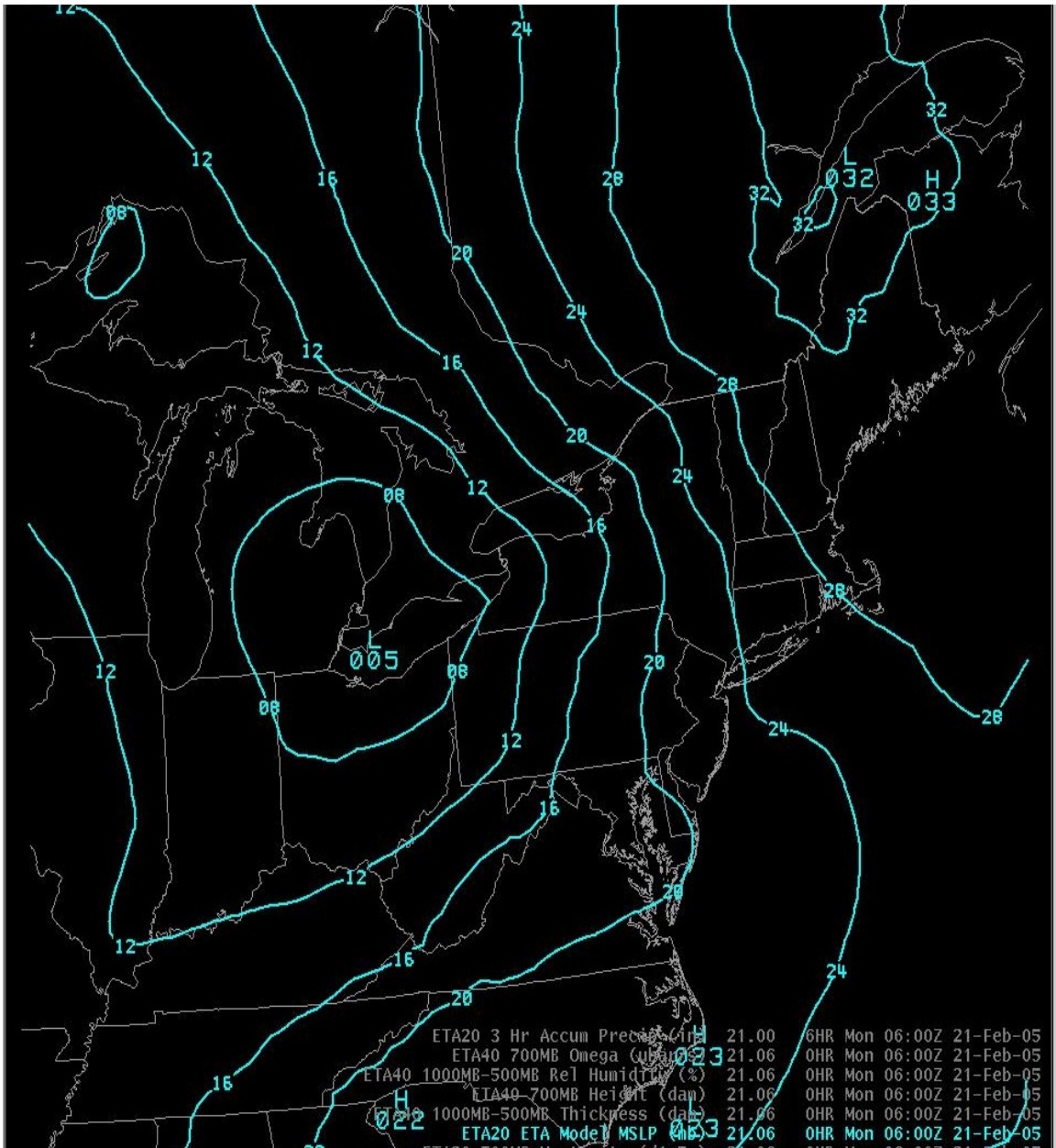


Fig. 4.38. As in Fig. 4.4 except for 21 February initialized 0600 UTC Eta.

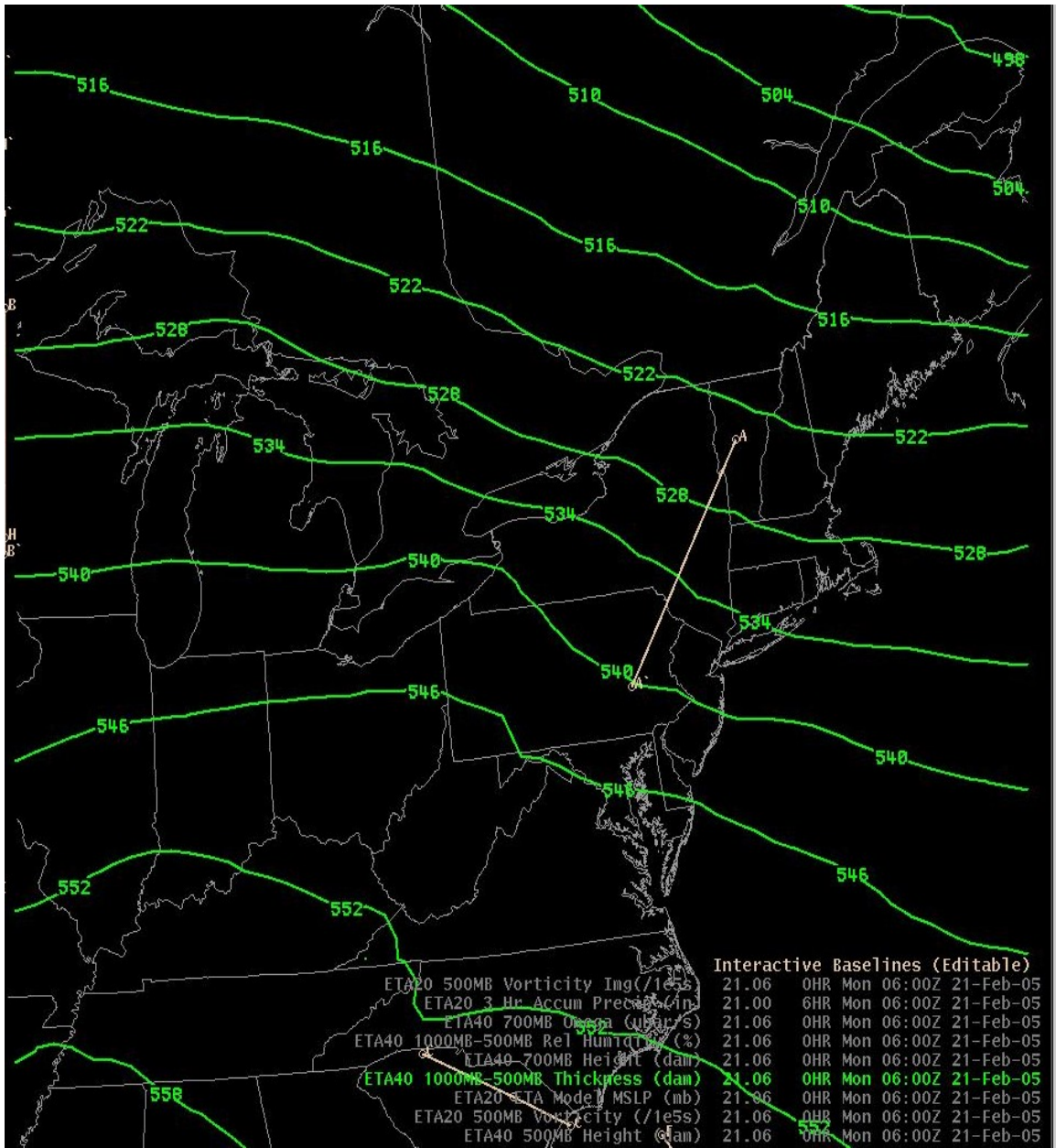


Fig. 4.39. As in Fig. 4.5 except for 21 February initialized 0600 UTC Eta. White line marks location of cross section.

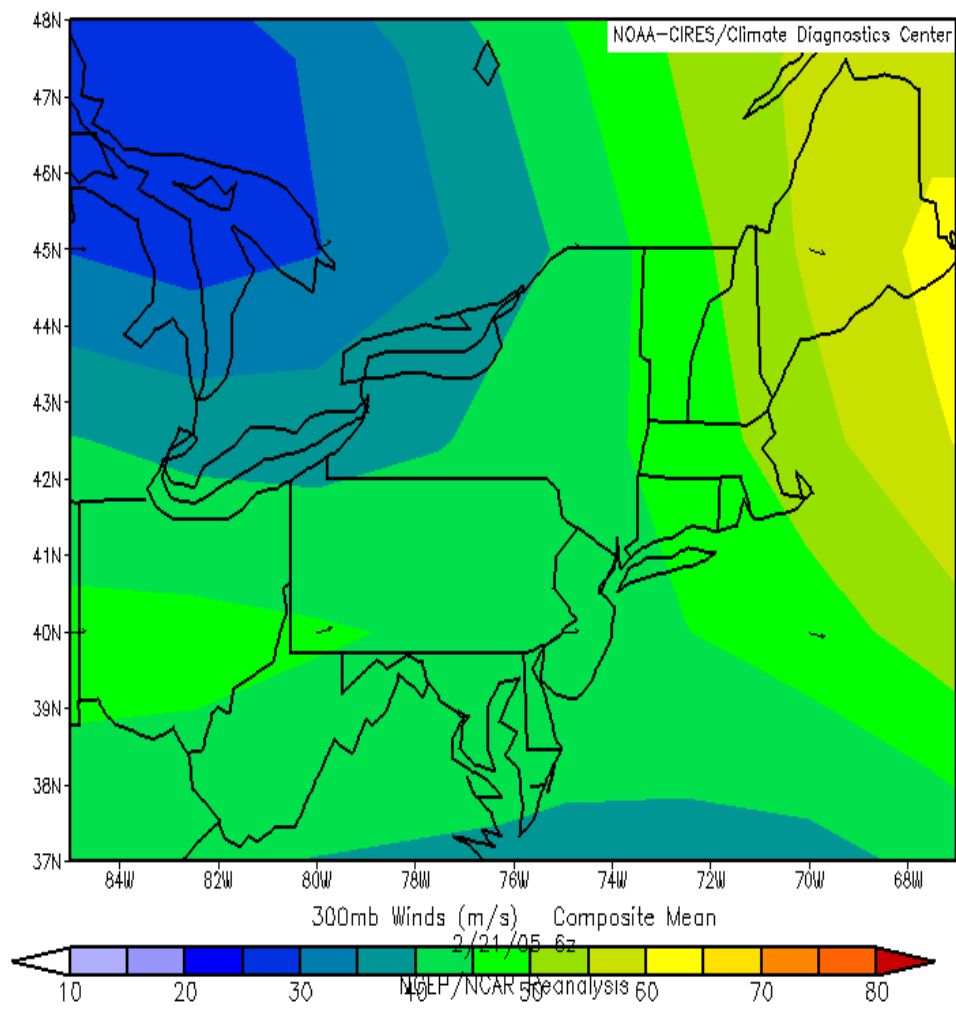


Fig. 4.40. As in Fig. 4.6 except for 21 February at 0600 UTC.

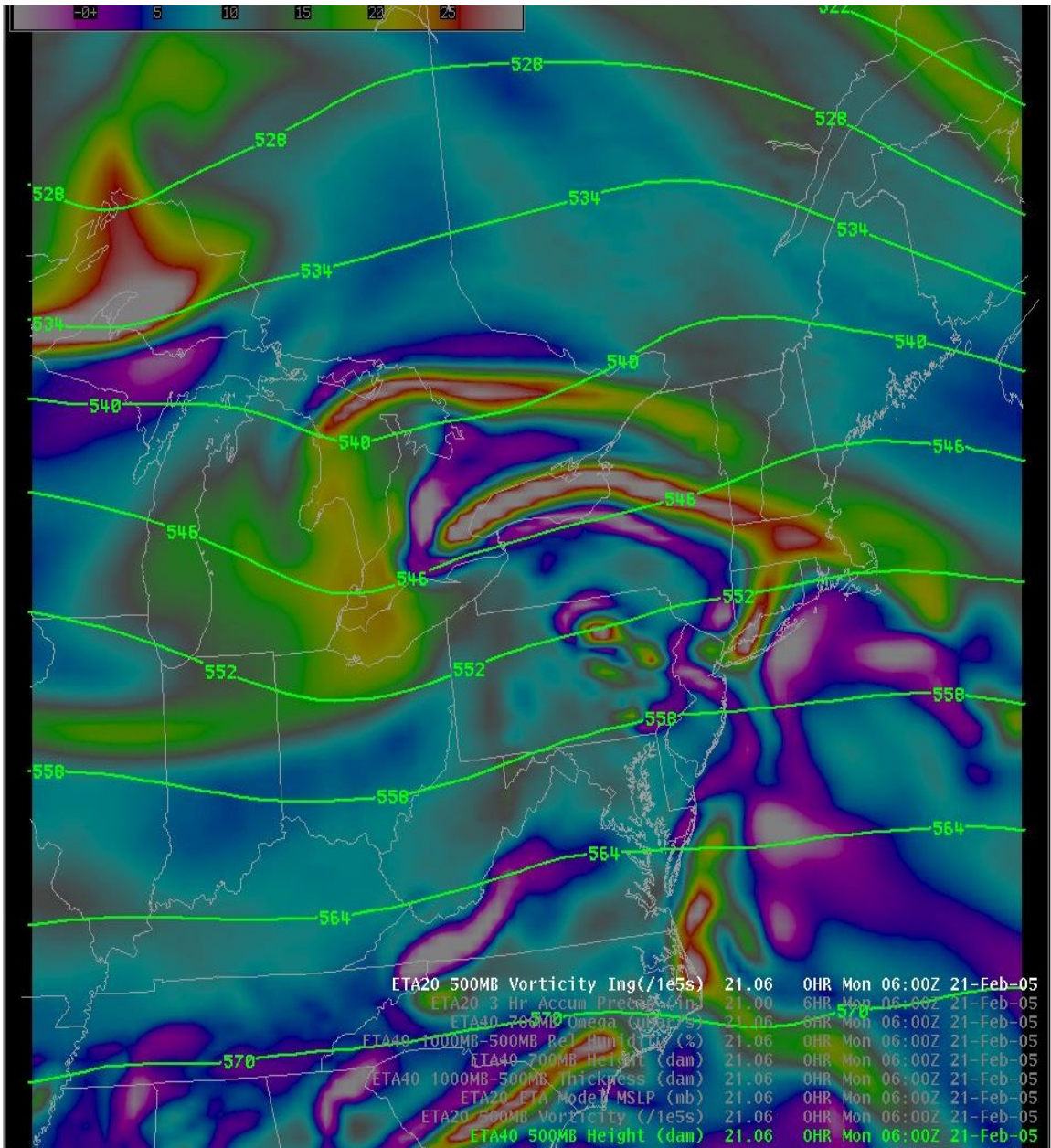


Fig. 4.41. 21 February initialized 0600 UTC Eta 500 hPa geopotential height (green contours, dam) and absolute vorticity advection (shaded, $10^{-5} s^{-1}$).

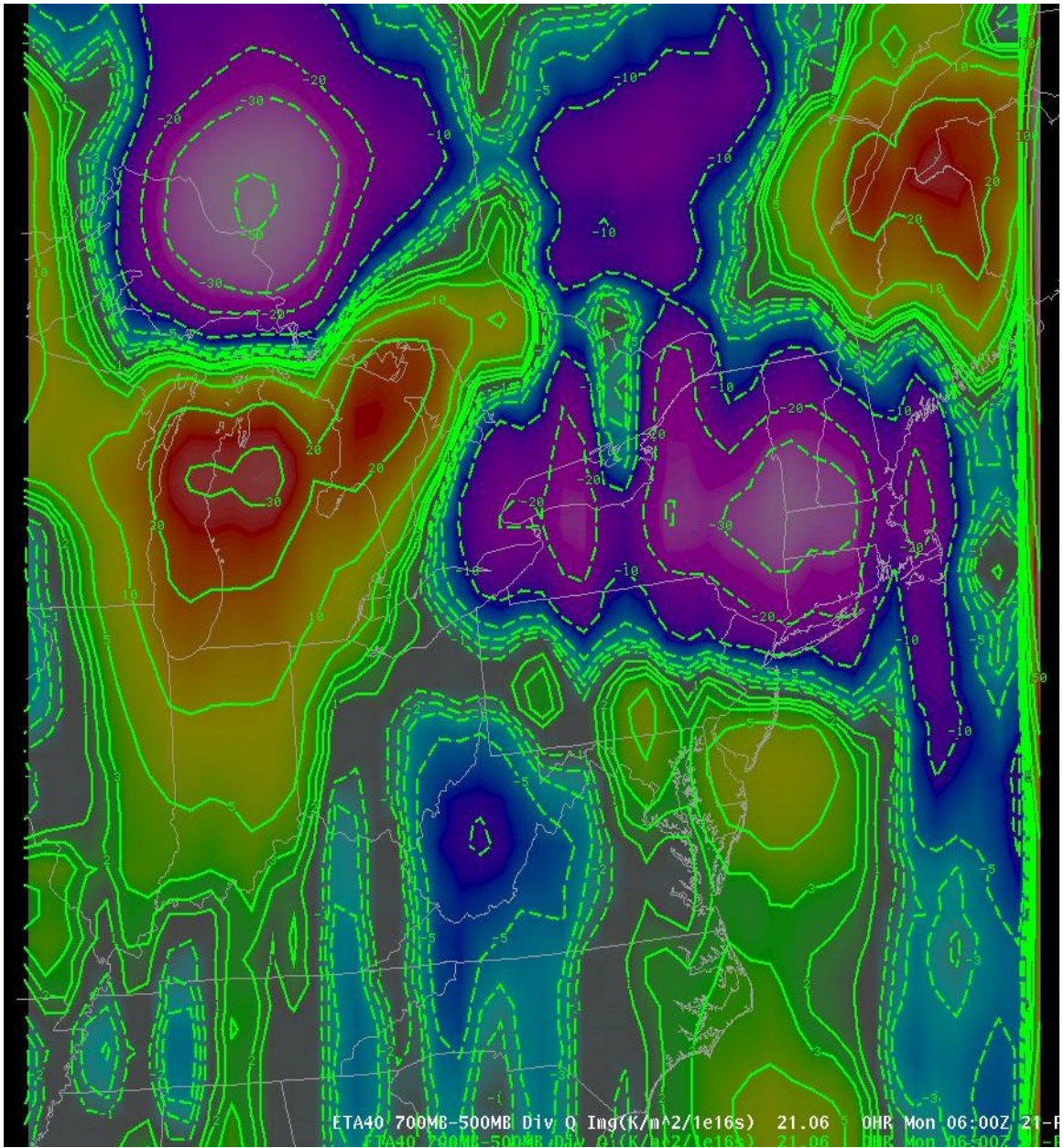


Fig. 4.42. As in Fig. 4.8 except for 21 February initialized 0600 UTC Eta 700–500 hPa average.

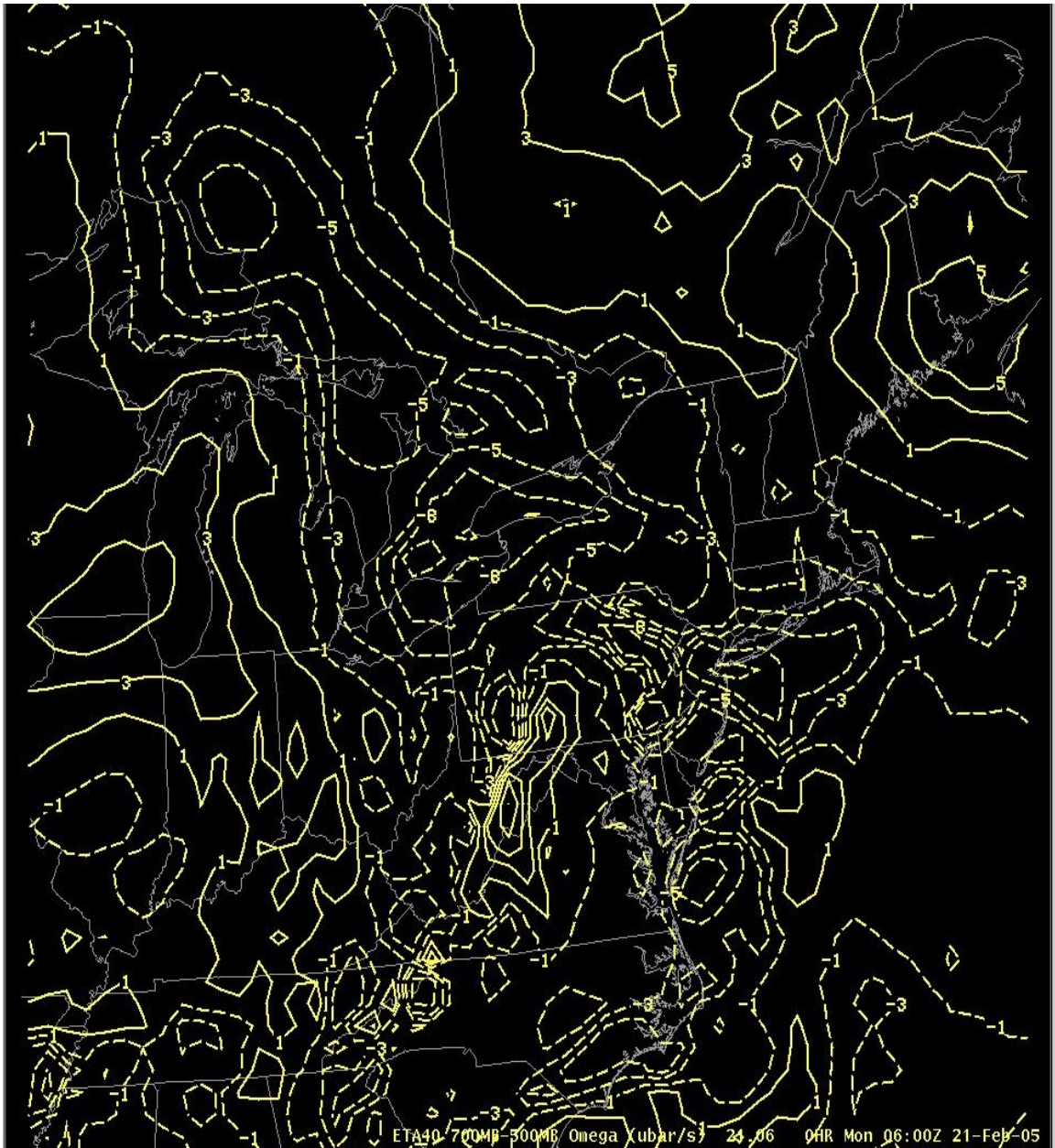


Fig. 4.43. 21 February initialized 0600 UTC Eta average 700–500 hPa average vertical velocity (yellow contours, $\mu\text{b s}^{-1}$). Dashed contours represent regions of upward vertical motion.

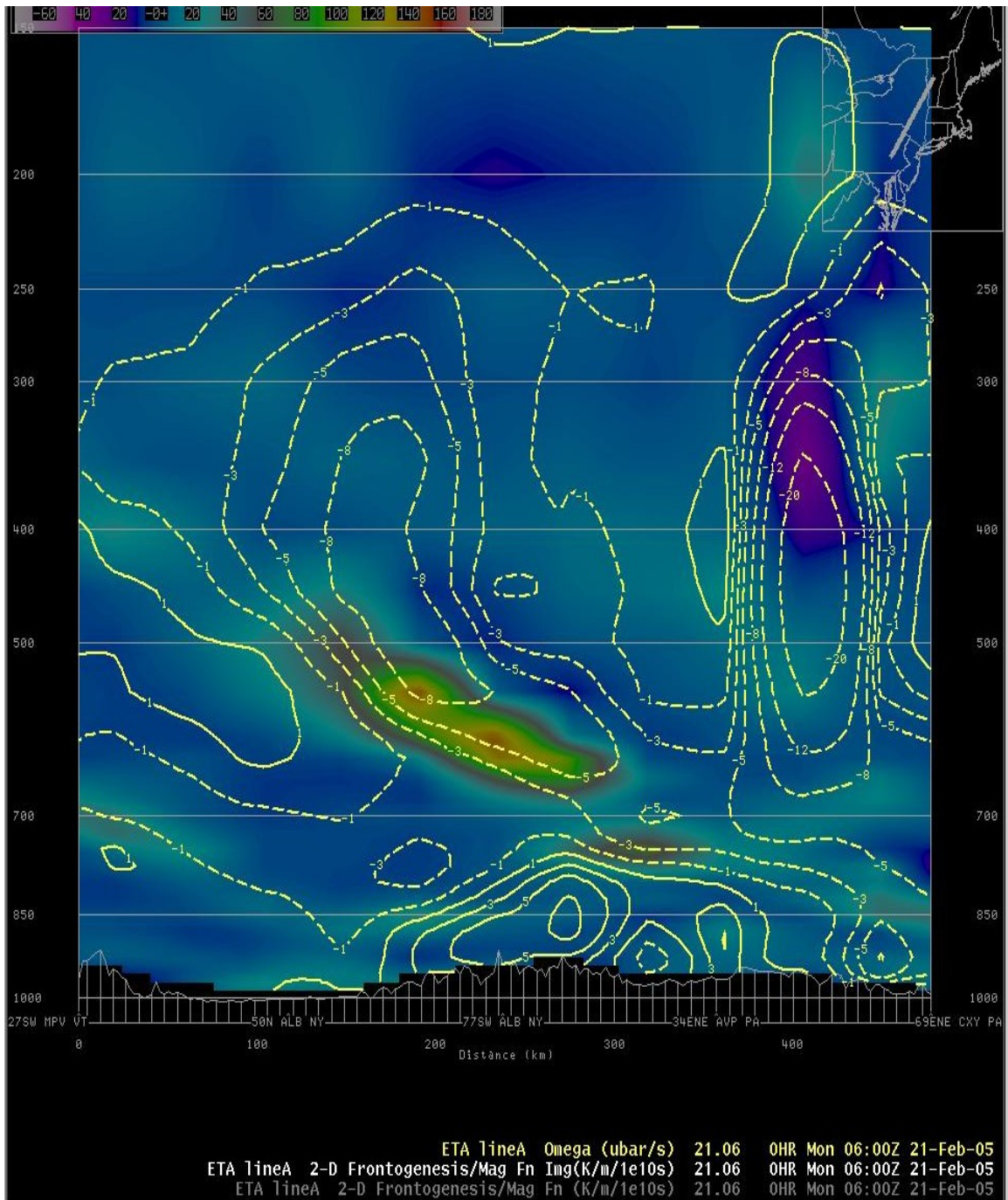


Fig. 4.44. As in Fig. 4.10 except for 21 February initialized 0600 UTC Eta. Frontogenesis is shaded only. Vertical velocity is given in $\mu\text{b s}^{-1}$. Dashed yellow contours represent upward vertical motion.

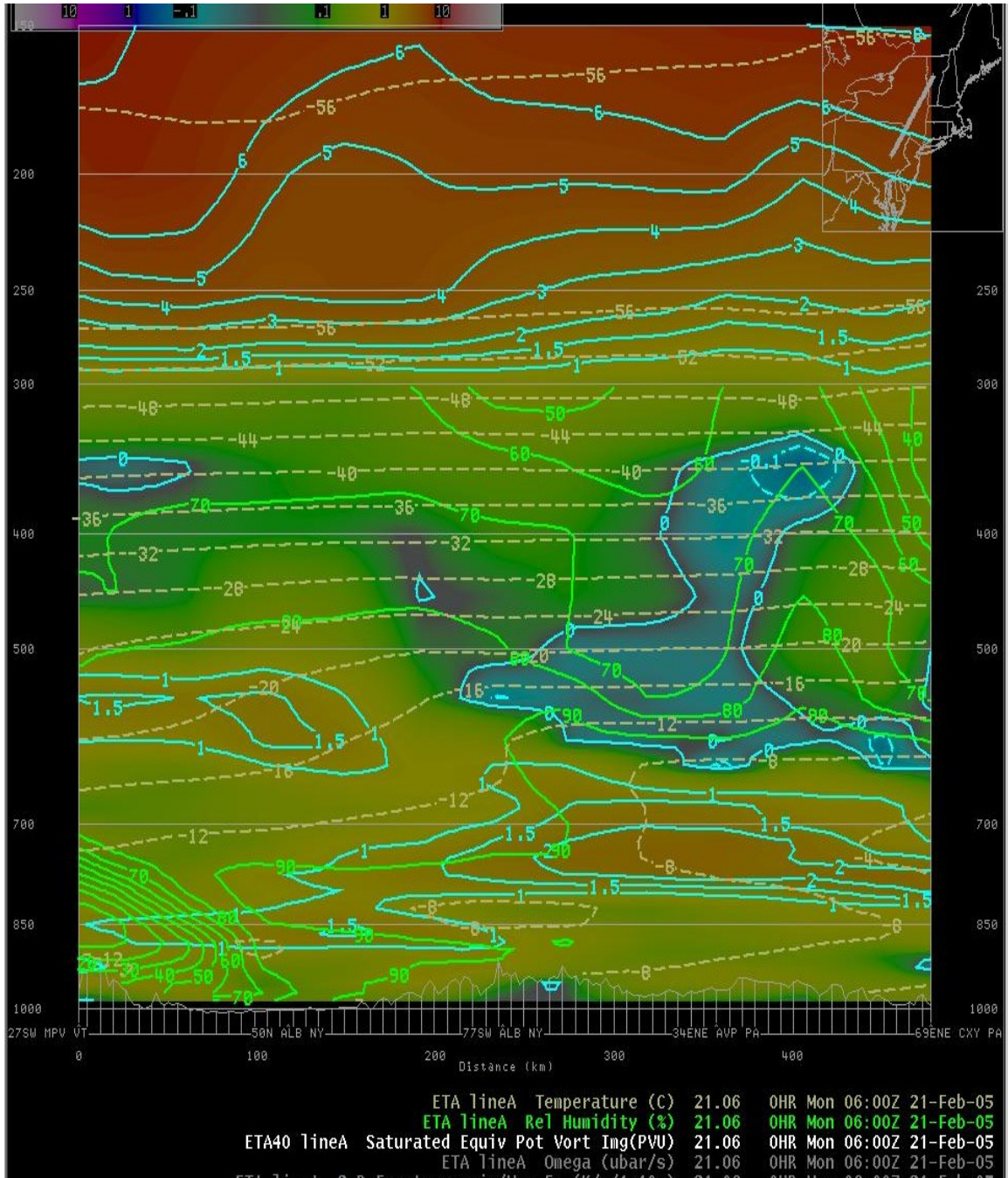


Fig. 4.45. As in Fig. 4.11 except for 21 February initialized 0600 UTC Eta.

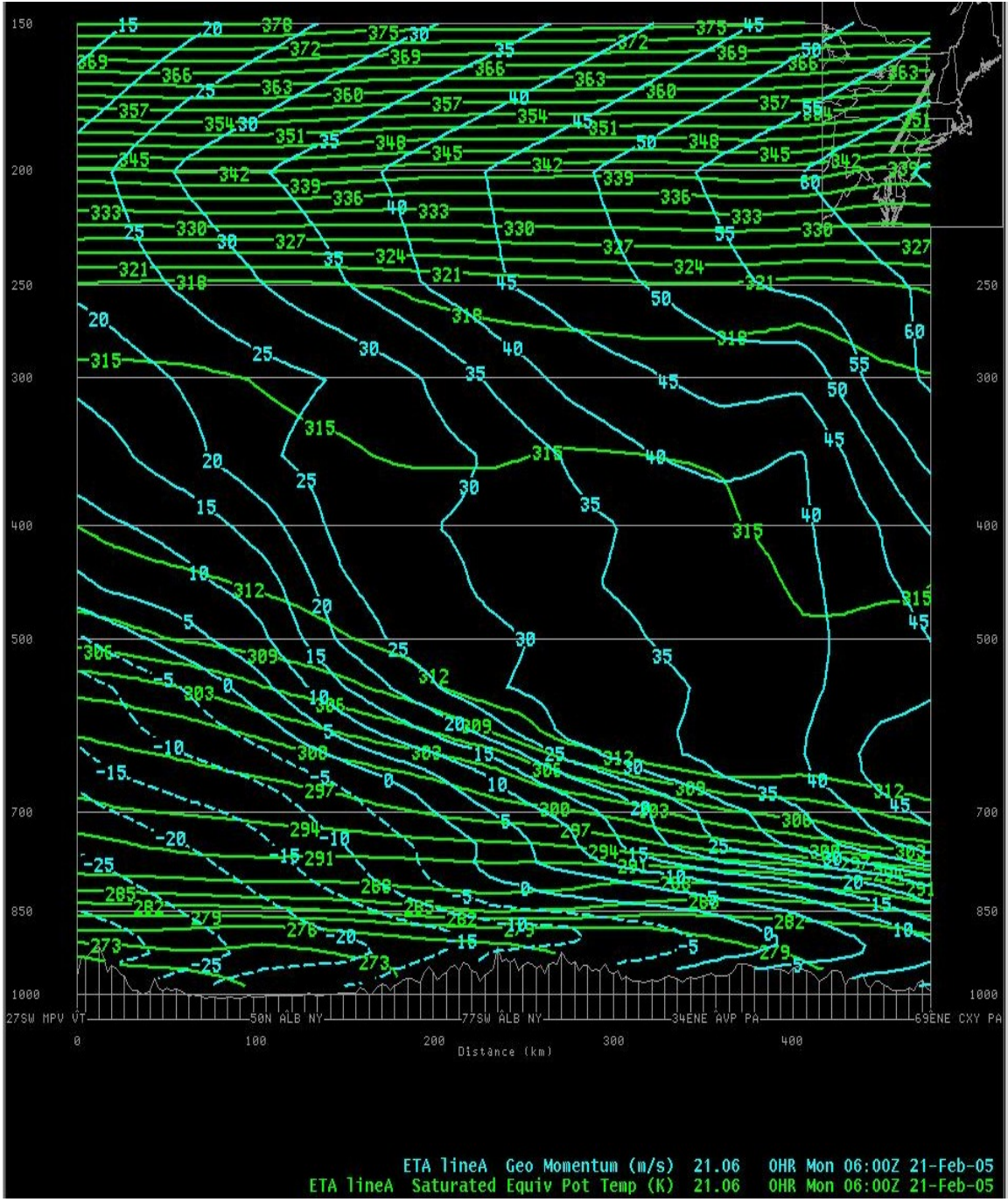
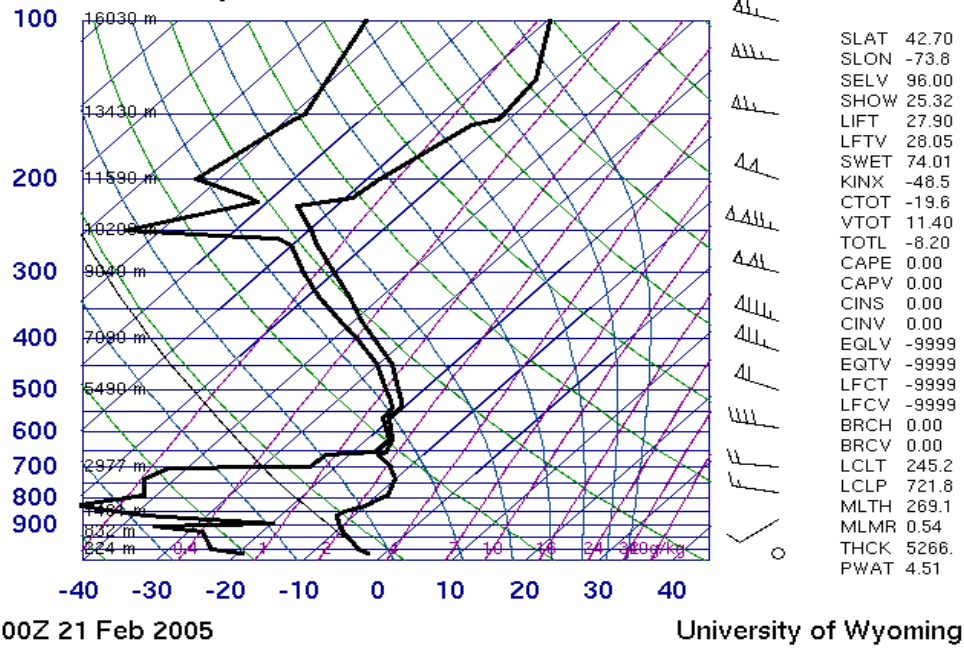


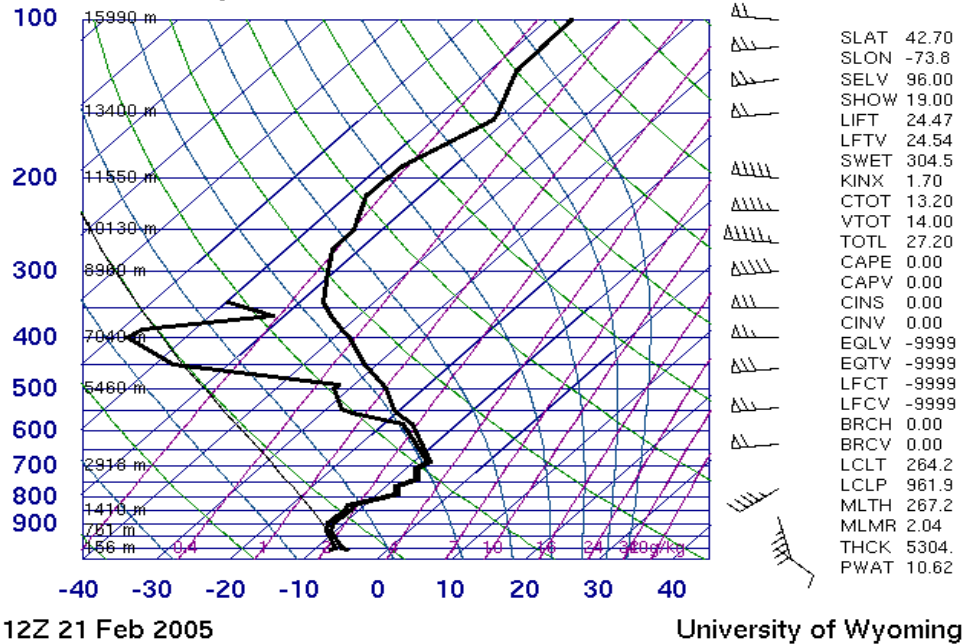
Fig. 4.46. As in Fig. 4.23 except for 21 February initialized 0600 UTC Eta.

72518 ALB Albany



a.

72518 ALB Albany



b.

Fig. 4.47a-b. As in Fig. 4.13 except at ALB on 21 February at: a) 0000 UTC and b) 1200 UTC.

5. Discussion

5.1 Climatology

5.1.1 Seasonal Trends

Section 3.1 revealed that variations in the frequency of occurrence of moderate precipitation events exist within the cool season. Frequency of occurrence for individual seasons (Figs. 3.1–3.4) show that large year-to-year variability exists for each month at any given location, but does little to determine any long-term trends in variability. The 10-yr monthly totals at BUF (Fig. 3.5) exhibit a peak in frequency of occurrence of moderate events during November–January. Niziol et al. (1995) showed that the difference between the mean air temperature and Lake Erie temperature at BUF was a maximum during this time period, with the peak difference occurring from December through early January. Lake-effect precipitation is known to occur when temperature differences between the lake surface and 850 hPa are at least 13°C. Although no climatology of these temperature differences has been produced, it can be inferred that they follow a similar trend as noted by Niziol et al. (1995). Therefore, the likelihood of lake-effect precipitation is greatest from the end of November through early January, which may explain the observed increase in frequency of moderate events at this time. The same can be said for any station that is downwind of Lakes Erie and Ontario. EKN exhibits a December–January peak (Fig. 3.5), which is likely a combined effect of moisture fluxes from Lake Erie and orographic lift. EKN also has a secondary peak in

March and April. One possible explanation for this peak at EKN is the tendency for showery precipitation to develop in association with cold air aloft over heated elevated terrain. The strong March–April sun heats the elevated terrain, which, when combined with cold air aloft, generates a steep lapse rate. This results in precipitation when forcing for ascent is present.

The combined 10-yr monthly totals for all stations in New York State (Fig. 3.8), Pennsylvania (Fig. 3.9), and Ohio (Fig. 3.10), along with the combined totals for all 35 stations (Fig. 3.11), have a remarkably similar pattern. In each of these regions, October has the fewest number of events. A sharp increase in frequency then occurs during November and continues into December, resulting in a December–January peak. A midwinter decrease occurs in February, followed by a secondary March–April peak, which is larger than the early winter peak for most locations with the exception of New York State. The decrease in frequency during February for the combined 35 stations is larger than can be explained by February having fewer days. Between 150 and 200 fewer events occurred in February than in January or March. Figure 5.1 is similar to Fig. 3.11 except that each month has been normalized to 30 days. A noticeable decrease in frequency of occurrence is still observed in February, but not to the extent indicated in Fig. 3.11.

The observed seasonal variations in frequency of moderate events may be the result of several factors. One factor, as discussed above, is lake-effect precipitation. During October and early November, lake-effect precipitation is not a significant factor since temperatures aloft are usually too warm. Late November through early January features the greatest climatological difference between lake surface temperatures and 850

hPa temperatures, increasing the possibility for moderate lake-effect events. Even stations that are not directly affected by lake-effect precipitation are often influenced by lake-enhanced moisture, which may result in precipitation through orographic lifting. Nearly all stations across the western part of the domain are subject to the possibility of lake-enhanced precipitation. By February, Lake Erie often begins to freeze over in most years. A frozen Lake Erie combined with the return of warmer air during March effectively shuts off most lake-effect precipitation. Thus, beginning in February, the Great Lakes usually play a much reduced role in precipitation production. Therefore, a portion of the observed distribution of frequency of moderate events is likely modulated by lake-effect precipitation, with October and February–April receiving very little contribution from the lakes.

A second factor in the observed seasonal variations in frequency are 500 hPa cutoff cyclones. Smith (2003, section 3.1.1b) showed that two to three times the number of cutoff cyclones occur during spring across the Northeast and eastern Great Lakes when compared to autumn. Fracasso (2004, section 3.1.1) showed that the average daily precipitation associated with cutoffs is often in the moderate range, especially across New England. Therefore, there is a much greater chance of having a cutoff cyclone that produces a moderate event during spring. Fracasso (2004) also found that 50–65% of climatological precipitation is associated with cutoff lows across the Northeast during autumn and spring. The percentage of climatological precipitation from cutoffs is much lower during winter. Therefore, a time of year that is less favorable for cutoffs and has a large percentage of its precipitation associated with them (autumn) is likely to have fewer moderate events, while a more favorable time of year for cutoffs that has a large

percentage of its precipitation associated with them (spring) is likely to have more moderate events.

A third factor that influences the frequency of moderate events is the synoptic-scale storm track. During autumn the main storm track is usually north and west of the domain, while during spring the main storm track extends across the Northeast and Great Lakes (e.g., Changnon et al. 1995). The location of the storm track may also play a role in the observed wintertime peak in occurrence of moderate events. The wintertime peak could be the result of the increased number of Alberta Clippers and Ohio Valley cyclones at this time of year. Additional impacts of the synoptic-scale storm track will be discussed in the next subsection.

These combined factors help describe the observed seasonal variations seen in Fig. 5.1. During October, the synoptic-scale storm track is too far north, cutoff frequency is at a minimum, and lake-effect precipitation is usually nonexistent, which results in fewer moderate events. In the November–January time frame, the synoptic-scale storm track shifts south across the Great Lakes and Northeast, cutoff frequency increases, and lake-effect precipitation potential reaches its maximum level, resulting in a peak in moderate event occurrence. During February, the synoptic-scale storm track shifts a little farther south, cutoff frequency is similar to early winter, and lake-effect precipitation begins to shut down, resulting in a decrease in the frequency of moderate events. During the March–April time frame, the main synoptic-scale storm track is once again located across the Northeast and cutoff frequency reaches its maximum. Although lake-effect precipitation is not a factor, the favorable synoptic-scale storm track and prevalence of cutoffs results in the largest frequency of moderate events during this time period.

5.1.2 Geographical Trends

Section 3.2 revealed that variations in frequency of occurrence of moderate events also exist over different geographic regions. A steady decrease in the observed number of events is evident as one travels east and south across New York State from BUF to LGA (Fig. 3.12). The three stations across northwestern New York (BUF, ROC, SYR) received over 160 moderate events during the 10-yr period, while the southeastern stations (JFK, LGA) received just over 100 events. Central/eastern New York stations (BGM, ALB) received 120–140 events. This pattern suggests that a general decrease in the number of events occurs as one moves east and south across the domain. These results are confirmed in Figs. 3.12–3.17, as northern and western stations have a higher frequency of occurrence than southern and eastern stations.

Figure 3.18 summarizes the results of the climatology by geographical region using a ratio of the number of events at each station to the mean number of events for all stations. Recall that the mean number of events is given by the 1.00 contour. The entire domain shows a general trend of decreasing frequency toward the southeast, with frequencies well above the mean to the north and west and well below the mean to the south and east. Enhanced frequency is observed south and east of Lakes Erie and Ontario, along the US/Canadian Border, and along the spine of the Appalachian. Detroit, MI (DTW), Akron, OH (CAK), and Bridgeport, CT (BDR), appear to be exceptions to the general trend.

The observed geographical variations may be explained using many of the same factors discussed in terms of seasonal variations. Assuming west to northwest surface winds are likely to occur often during the cool season, regions east and southeast of the Great Lakes have the greatest potential to receive moderate lake-effect or lake-enhanced precipitation. A clear lake-effect signal is seen east of Lake Erie in Fig. 3.18 and to a lesser extent southeast of Lake Ontario. BGM and ALB also experience lake-effect precipitation, but their distance from the lakes limits the impact. Lake-enhanced precipitation is also frequently observed across eastern Ohio, western Pennsylvania, and even northern West Virginia. Stations across northern New England and most stations located southeast of the 1.00 contour are not impacted by the Great Lakes. DTW is the only station in the western part of the domain that does not experience lake-enhanced precipitation. Accordingly, this station received only 85% of the mean number of moderate events. It is unclear why CAK received less than the mean number of events.

A second factor that may help explain the observed frequency of moderate events is the synoptic-scale storm track. The storm track shifts southward from Canada to the northeastern US by winter. During winter, Colucci (1976) noted that winter cyclone frequency maxima exist in a band off the Atlantic Coast from Cape Hatteras to Maine and in the eastern Great Lakes. The eastern Great Lakes maximum is likely due to the typical path taken by Alberta Clippers (e.g., Hutchinson 1995), which are known to often produce moderate precipitation across much of New York and northern New England. Changnon et al. (1995) showed that cyclones frequently occur near the Ohio Valley during winter as well. These are the Ohio Valley-type storms discussed in chapter 3. These systems are associated with light-to-moderate precipitation to the north or

northwest of the surface cyclone. A track up the Ohio Valley would lead to possible moderate precipitation for regions north and west of the 1.00 contour in Fig. 3.18. As shown by Smith (2003), cutoff cyclones occur most frequently across New England. Therefore, a large percentage of the observed moderate events in that region are likely due to cutoffs. The wintertime maximum in cyclone frequency along the Atlantic coast shown by Colucci (1976) may have a significant impact on the frequency of moderate events occurring there. Many storms that follow this track during winter are intense cyclones featuring heavy precipitation to the northwest of the surface center. Therefore, the observed frequency of occurrence of moderate events along the Atlantic coast may be below the mean due to the propensity of storms forming in that region to be associated with heavy precipitation.

Orography also appears to be a factor in the frequency of occurrence of moderate events. A distinct maximum is observed along the Appalachians at EKN (Fig. 3.18), where 134% of the mean number of events occurred. Moist unstable air is forced upward when it approaches the high terrain, resulting in precipitation. The moisture and instability may be the result of a northwest flow over Lake Erie in winter or cold air aloft over heated, elevated terrain during spring. Weak synoptic-scale systems capable of producing only light precipitation may also receive additional lift from the high terrain, thus producing moderate events. While EKN is located in a high mountain range, Fig. 3.18 shows that stations located near the elevated terrain extending through Pennsylvania and into eastern New York/northern New England are all within $\pm 10\%$ of the mean number of events. Worcester, MA (ORH), is the highest station in Fig. 3.14. Although all stations in Fig. 3.14 are below the mean number of events, ORH has the highest

frequency of occurrence of moderate events for nearby stations. Therefore, it appears that the height of the elevated terrain also impacts frequency of occurrence.

Combining the above factors leads to a better understanding of the observed distribution in Fig. 3.18. Across northern and western sections of the domain, lake-effect precipitation combined with synoptic-scale storm tracks that are conducive to moderate precipitation events result in a frequency of occurrence that is above the mean. Orographic enhancement along the Appalachians results in another peak in frequency of occurrence, while other elevated stations to the northeast are within 10% of the mean number of events. Stations along the Atlantic coast and in the southeastern part of the domain do not receive any lake-enhanced precipitation and are not in a favorable position to frequently receive moderate precipitation from Alberta Clippers or Ohio Valley cyclones. Also, many systems that affect this region are associated with heavy precipitation. These factors help explain why coastal and southeastern stations receive fewer than the mean number of moderate events.

5.2 Case Studies

Assuming saturation, for heavy cool season precipitation events to occur, one expects two general conditions to be satisfied. First, we expect moderate-to-strong synoptic-scale forcing to be present in the precipitation region. Features that are typically associated with strong synoptic-scale forcing include intensifying surface cyclones, strong 500 hPa troughs and associated vorticity maxima, intense upper-level jet streaks, and strong low-level Q-vector convergence. Second, we often expect to see intense

frontal-scale vertical circulations in the region of heaviest precipitation. The vertical circulation around intense, deep, and upright regions of frontogenesis is narrowed and intensified in the presence of a deep layer of WMSS or negative EPV* (Fig. 1.6). Although it is possible for synoptic-scale and mesoscale processes to act independently in producing heavy precipitation, usually a combination of moderate-to-strong synoptic-scale and mesoscale forcing leads to heavy precipitation. When using similar model resolutions as those used in this study, the combined forcing often leads to vertical velocities in excess of $-15 \mu\text{b s}^{-1}$. The synoptic-scale and mesoscale features are usually favorably aligned with each other. Also, mesoscale features are typically well aligned among themselves and often tend to persist over a given area.

5.2.1 27 December 2004 (Case I)

Case I, a high-end moderate snowstorm for ALB associated with an inverted trough, illustrates several differences in structure between moderate events and heavier events. As seen in Figs. 4.3–4.9, the synoptic-scale forcing is sufficient to correspond to light-to-moderate precipitation, but is not overly impressive. An intensifying surface cyclone (Figs. 4.3–4.4) is located well off the coast, with only a weak inverted trough extending across eastern New York. The 300 hPa winds (Fig. 4.6) reveal that a jet streak is present north of Maine, placing eastern New York in the left-entrance region of the jet, where descent is likely. A weak negatively tilted trough is also observed in Fig. 4.6. Negatively tilted troughs usually have more focused ascent than positively tilted troughs, but the trough is too weak in this case to induce significant ascent. Weak-to-moderate Q-

vector convergence (Fig. 4.8) over eastern New York indicates the region where the greatest ascent is likely. The feature that provides the most synoptic-scale lift is a strong 500 hPa trough and associated vorticity maximum (Fig. 4.7). Even with these features, low-level ascent across eastern New York is only $-5 \mu\text{b s}^{-1}$. Synoptic-scale features that would lead to the greatest forcing are not favorably aligned across eastern New York (e.g., the upper-level jet streak and surface cyclone are not in a position to enhance the ascent there). Therefore, synoptic-scale forcing for ascent for case I is present, but its magnitude is not sufficient to correspond to heavy precipitation.

Differences between the mesoscale aspects of case I and heavy precipitation events are also apparent. Typical magnitudes of frontogenesis for heavy precipitation are in excess of $15 \text{ K (100 km)}^{-1} (3 \text{ h})^{-1}$ at model resolutions similar to those used in this research. The low-level frontogenesis maximum for case I (Fig. 4.10) is not intense [approximately $1 \text{ K (100 km)}^{-1} (3 \text{ h})^{-1}$] and is very flat. As a result, the vertical circulation about the frontogenesis maximum is not as intense or upright as observed in typical frontal circulations. Thus, the maximum vertical velocity associated with the frontal circulation is only $-8 \mu\text{b s}^{-1}$, which is much weaker than expected for a heavy precipitation event. The regions of WMSS and negative EPV* (Fig. 4.11) that are associated with the frontogenesis maximum are also much thinner than typically seen in heavier events. With that said, thinner regions of reduced stability (or instability) still have the potential to enhance frontal circulations. However, the banding research of Novak et al. (2004), among others, suggests that the frontal-scale circulation drives banded precipitation, while WMSS and negative EPV* modulate the scale and strength of the ascent. If that circulation does not have a significant vertical component, then a

weaker vertical velocity can be expected. Therefore, although the ingredients seen in heavy events are present in case I, the weak, flat nature of the frontal circulation precludes the formation of heavier precipitation.

5.2.2 8 January 2005 (Case II)

Case II, a moderate precipitation event across much of New York associated with a weak Ohio Valley cyclone, has a very similar synoptic and mesoscale structure to case I, despite being a different type of synoptic system. Precipitation across western New York is associated with the wraparound moisture of a weak surface cyclone (Fig. 4.15) located off the New Jersey coast. As in case I, western New York is positioned in the descent region of a 300 hPa jet streak (Fig. 4.17). Weak low-level Q-vector convergence (Fig. 4.19) is occurring across western New York. Again, most of the synoptic forcing is provided by a 500 hPa short-wave trough with an associated potential vorticity (PV) hook structure (Fig. 4.18). These features combine to produce maximum low-level vertical velocities in the $-3 - -5 \mu\text{b s}^{-1}$ range across western New York. Therefore, once again, synoptic-scale forcing is present for case II, but it is not strong enough to produce heavy precipitation.

The mesoscale structure of case II is also similar to case I. The low-level region of frontogenesis (Fig. 4.21) is once again weak [approximately $2 \text{ K (100 km)}^{-1} (3 \text{ h})^{-1}$], thin, and has very little vertical tilt. The frontogenesis is slightly more upright than in case I, but it is far from what can be expected in a heavier event. Therefore, the vertical circulation about the frontogenesis maximum is not as intense or upright as typically seen

in heavier events. Thus, the maximum vertical velocity associated with the circulation is only $-5 \mu\text{b s}^{-1}$. A relatively thin layer of negative EPV* exists on the warm side of the frontal circulation. However, with a weak, nearly horizontal frontal circulation, the ascent in this region is unlikely to be enhanced by the presence of an unstable layer. Therefore, once again, mesoscale features typically found in heavy events are present in case II, but they are much less intense, shallower, and less upright in the moderate event.

5.2.3 26 January 2005 (Case III) and 21 February 2005 (Case IV)

Cases III and IV have very similar synoptic-scale patterns. Both cases feature a weak surface cyclone centered over Lake Erie (Figs. 4.27 and 4.38). Each case has a tight northeast–southwest thermal gradient with a weak thermal ridge (Figs. 4.28 and 4.39) across the eastern Great Lakes, suggestive of a warm advection pattern across much of New York. Forcing for ascent is enhanced across eastern New York for both cases as this region is located in the right-entrance region of 300 hPa jet streaks (Figs. 4.29 and 4.40). A 500 hPa short-wave trough and associated cyclonic vorticity maximum (Figs. 4.30 and 4.41) is located across the eastern Great Lakes in each case, with synoptic-scale ascent likely across much of New York. Weak-to-moderate low-level Q-vector forcing (Figs. 4.31 and 4.42) is present across eastern New York. For cases III and IV, the alignment of synoptic-scale features is more favorable for ascent than in cases I and II. However, the magnitude of the forcing is only sufficient to produce vertical velocities on the order of $-3 - -5 \mu\text{b s}^{-1}$ (Figs. 4.32 and 4.43) across eastern New York. Therefore,

synoptic-scale forcing is present, but once again it is not sufficient for the occurrence of heavy precipitation.

Differences between cases III and IV are apparent when the mesoscale features are examined. For case III, the region of frontogenesis at the northern end of the cross section (Fig. 4.33) is slightly more intense [$3 \text{ K (100 km)}^{-1} (3 \text{ h})^{-1}$], spans a greater horizontal distance, and has a more noticeable vertical tilt than in cases I or II. It appears as if the three frontogenesis maxima in Fig. 4.33 could be part of a single, sloping band of frontogenesis as is found in heavy events. However, the band of frontogenesis seems to break apart south of ALB, resulting in three separate maxima and thus three separate vertical velocity maxima. The forcing associated with these individual bands results in weaker vertical velocity associated with each piece. The regions of WMSS and negative EPV* along the cross section (Fig. 4.34) have the same fragmented appearance as the frontogenesis maxima. Also, they are not well aligned with the frontogenesis maxima. For example, the region of WMSS near 450 hPa over ALB is slightly more aloft and southeast of the region of maximum upward vertical velocity, while the region of negative EPV* at the northern end of the cross section is actually closer to the surface than the area of peak upward motion. Therefore, while a slightly more intense and more vertically tilted frontogenesis maximum exists, it is fractured into distinct pieces and still lacks significant vertical tilt. The regions of peak upward vertical motion associated with these pieces are not well aligned with regions of reduced symmetric stability, resulting in only moderate precipitation.

For case IV, a more intense and upright region of frontogenesis [approximately $13 \text{ K (100 km)}^{-1} (3 \text{ h})^{-1}$] is noted compared to cases I–III (Fig. 4.44). A narrow, sloping

region of $-8 \mu\text{b s}^{-1}$ vertical velocity is associated with the circulation around this frontogenesis maximum. Since the frontogenesis maximum has a stronger vertical component than the other cases, the region of peak upward vertical velocity has a more upright nature as well. Thus, we see a 200 hPa-deep layer of nearly upright ascent. This ascent was likely concentrated and enhanced by a region of reduced symmetric stability since it correlates well with a nearly 150 hPa-deep layer of WMSS and negative EPV* (Fig. 4.45). Therefore, case IV appears to have the potential to produce heavy precipitation, especially since synoptic-scale forcing is occurring as well. However, Fig. 5.2 shows Petterssen frontogenesis calculated 3 h later along the same cross section used in Fig. 4.44. Note that the frontogenesis maximum has significantly weakened and now has much less vertical tilt. The frontogenesis maximum now resembles those that were observed in cases I and II. As a result, only light precipitation occurred once the intense, fast-moving mesoscale forcing had passed by. Therefore, if features are intense and well aligned such that they are likely to produce heavy precipitation, but are transient or do not stay well aligned for more than a short period of time (i.e., a few hours), then moderate precipitation totals are likely.

5.2.4 Moderate Event Schematic Cross Section

Figure 5.3 shows a schematic vertical cross section through a typical moderate precipitation band. The location of the band of precipitation is denoted by the asterisk along the x-axis. Note that a weak, thin region of frontogenesis with minimal vertical tilt exists in lower or middle troposphere. A very thin layer of negative EPV* is found just

above and to the warm side of the frontogenesis maximum, but is shifted slightly toward the warmer air. A region of WMSS, which is also slightly displaced from the frontal circulation, exists above the area of negative EPV*. Due to the flat nature of the frontogenesis maximum, the circulation has a limited vertical component, and thus only moderate precipitation will occur.

5.3 Forecast Implications

The results of this climatology and case studies of cool-season moderate precipitation events across the Northeast should help improve forecasts of these challenging events. Forecasters should be aware of climatological regions that are most favorable for moderate events and the months of the cool season in which they are most likely to occur. With this general concept in mind, forecasters can identify synoptic or mesoscale systems that are likely to produce moderate events. Forecasters should also recognize that synoptic-scale forcing is usually present (with the exception of pure lake-effect precipitation), but is weaker during a moderate precipitation event. Also, mesoscale features such as frontogenesis and reduced symmetric stability found in more familiar heavy events are also present in moderate events. The difference is that in moderate events these ingredients are less intense, shallower, have less vertical tilt, are not well aligned, and are more transient, thus reducing the precipitation amount. It is the intent of the author that the results of this research will provide a better understanding and awareness of the synoptic and mesoscale features that govern the occurrence of cool-season moderate precipitation events, and thus improve their forecastability.

**Moderate Precipitation Events For All Stations
Normalized to a 30-day Month: 1994-2004**

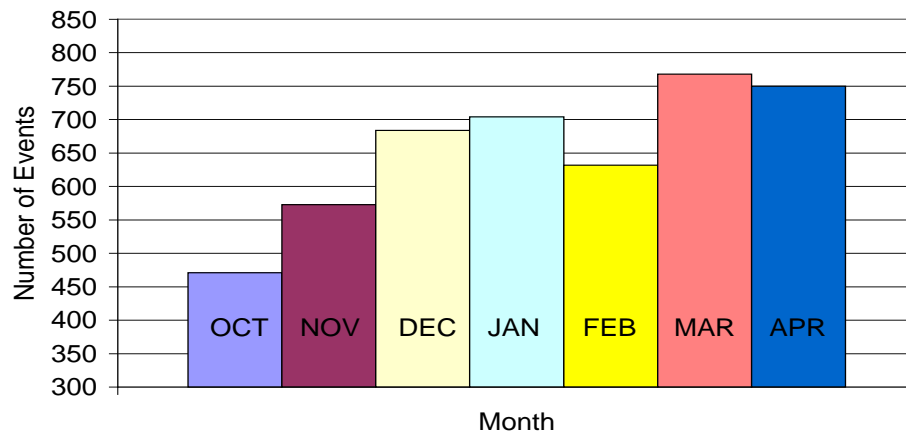


Fig. 5.1. Frequency of occurrence of moderate events for all 35 stations for the 10-yr period 1994–2004 using a normalized 30-day month.

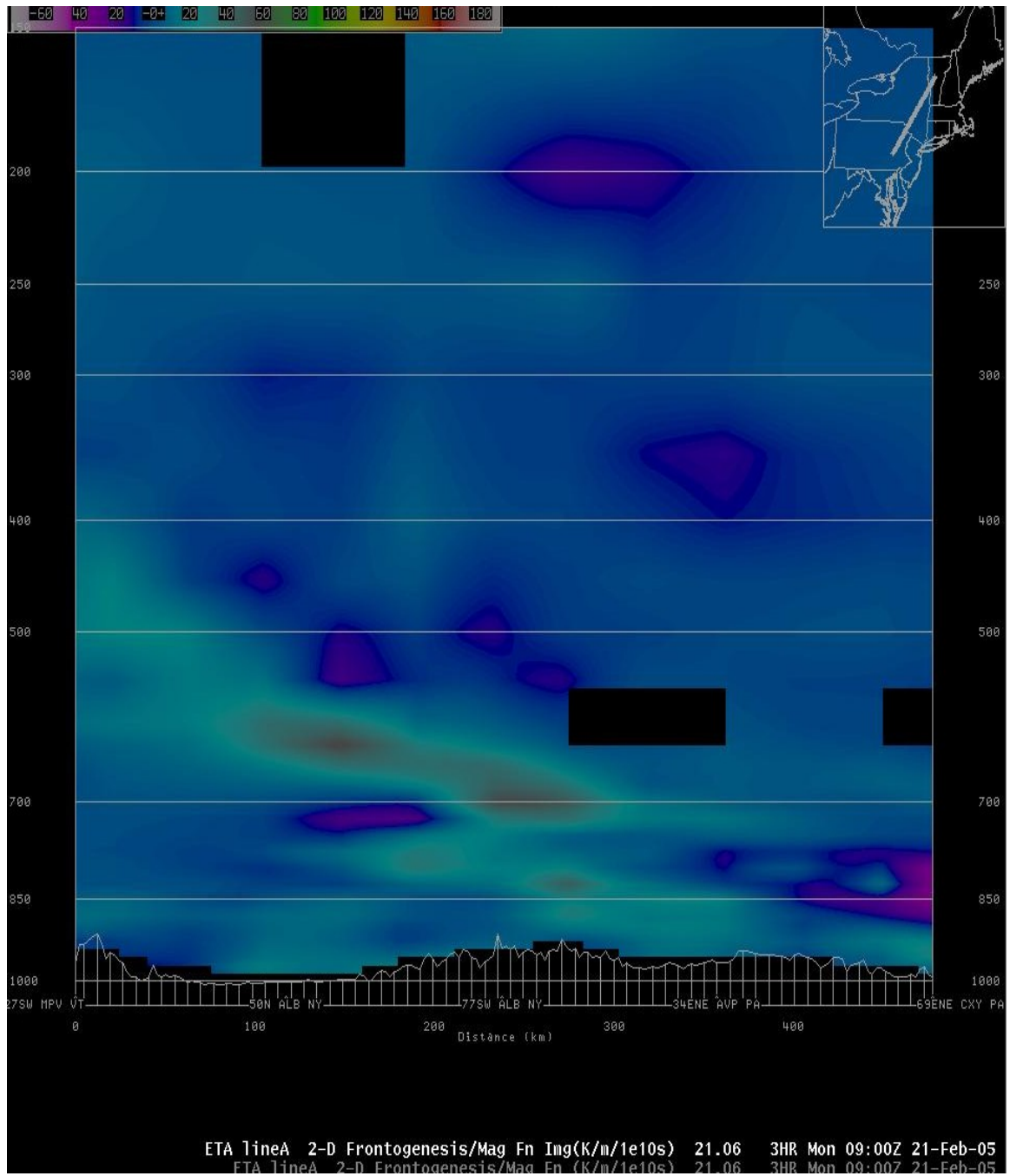


Fig. 5.2. 21 February 0600 UTC Eta 3-h forecast of Petterssen frontogenesis valid at 0900 UTC.

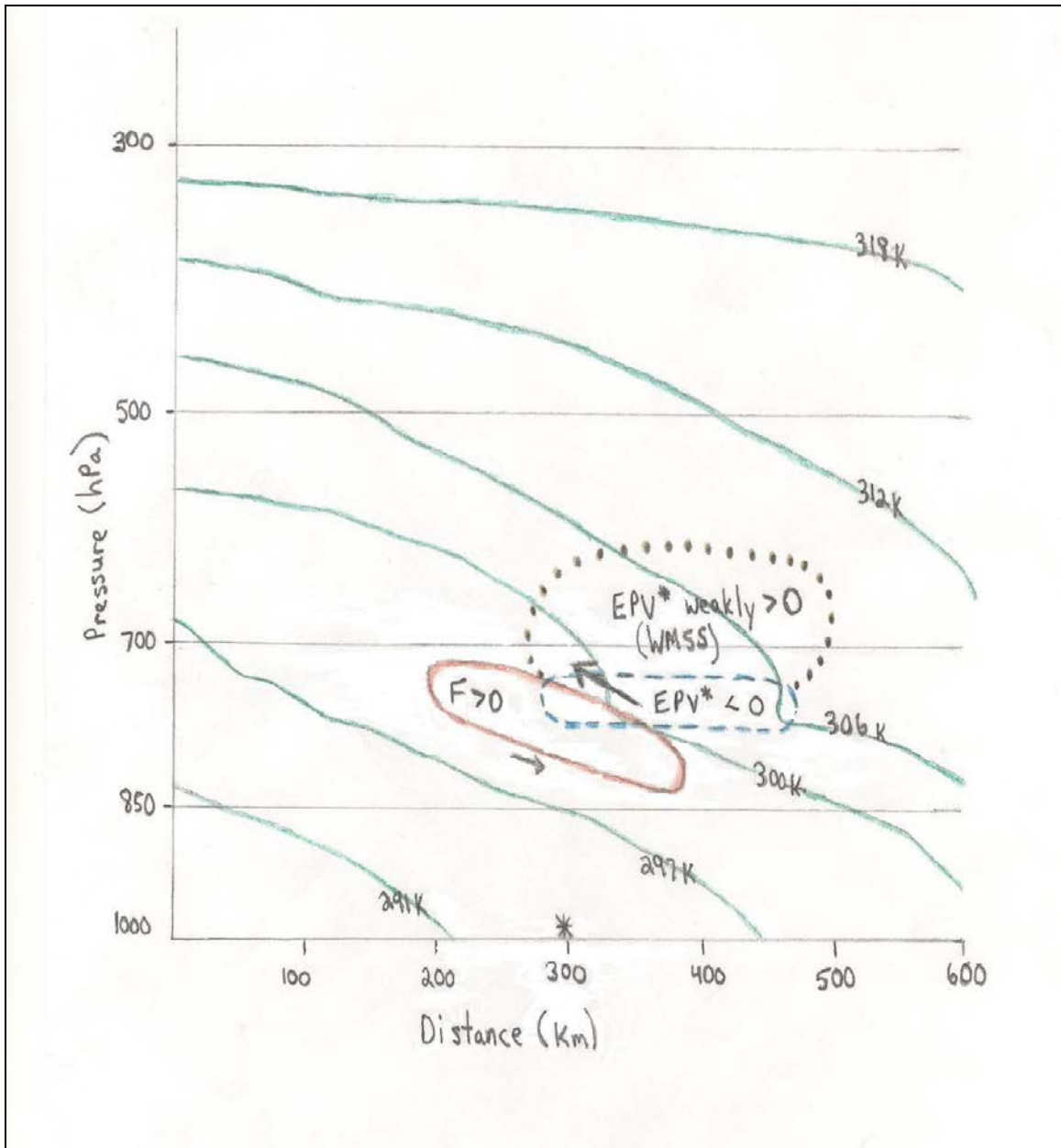


Fig. 5.3. Schematic cross section through a cool-season moderate precipitation band showing Petterssen frontogenesis (red ellipse), negative EPV* (dashed blue ellipse), WMSS (brown dotted region), saturation equivalent potential temperature (dark green contours), and transverse circulation (arrows).

6. Conclusions and Future Work

6.1 Conclusions

A 10-yr climatology (October 1994–April 2004) of cool-season moderate precipitation events across the northeastern US is presented. A moderate event was defined as an event liquid precipitation amount of 0.6–1.3 cm (± 0.1 cm) or an event snowfall total of 6.4–19.0 cm. Using NCDC daily and hourly precipitation data, 35 first-order stations were analyzed for each day within the cool season over the 10-yr period to determine if a moderate event had occurred. Histograms were then produced to summarize the findings by month, station, state, and geographic region.

Two main results emerged from the climatology of cool-season moderate precipitation events. First, there appear to be variations in frequency of occurrence of moderate events within the cool season. Individual stations often have large annual variability when considering the number of events that occur during a given month. A better defined pattern is established when monthly totals for the entire 10-yr period are considered on a state-by-state basis. For nearly all states, October receives the lowest number of moderate events, while peaks in frequency of occurrence are found during early winter and again in spring. This pattern is more clearly established when all 35 stations are combined. Two separate peaks in frequency of occurrence are noted. The first peak occurs in December–January, with a second and slightly larger peak in March–April. The December–January peak may be the result of several factors including: 1) an increased potential for lake-effect precipitation at that time of year, 2) an increased

frequency of Alberta Clippers and Ohio Valley cyclones due to a favorable synoptic-scale storm track, and 3) an increased cutoff cyclone frequency. The March–April peak may be the result of: 1) more showery springtime weather due to cold air aloft over heated and/or elevated terrain, 2) a synoptic-scale storm track that is located across the Northeast and eastern Great Lakes, and 3) the observed peak in frequency of cutoff cyclones.

Also, two distinct minima in frequency of occurrence are noted in October and February. October has over 100 fewer events than November, while February has over 130 fewer events than January or March. The latter difference is too large to be explained by the fact that February has fewer days, as normalizing each month to 30 days does not significantly affect the observed trend. October and February represent times when: 1) lake-effect precipitation is generally not as likely to occur because the air aloft is too warm (October) or Lake Erie begins to freeze over (February), 2) the synoptic-scale storm track is often shifted too far north (October) or south (February), and 3) cutoff cyclone frequency is at a minimum (October). Thus, synoptic-scale and mesoscale features are not as favorable for the occurrence of moderate events at these times. November appears to be a transition month as synoptic and mesoscale features quickly become more favorable for moderate events to occur.

Second, there are variations in the frequency of occurrence of moderate events based on geographical location. When compared to the mean number of events at all stations over the 10-yr period, moderate events occur most often for locations downwind of Lakes Erie and Ontario, across the northern part of the domain, and along the spine of the Appalachians. Other regions of elevated terrain experience a frequency of occurrence that is within $\pm 10\%$ of the mean number of events. Locations near the Atlantic coast and

in the southeastern part of the domain experience less than the mean number of events.

In general, the number of events is highest across the northern and western parts of the domain, and decreases to the south and east. Enhanced frequency of occurrence may be the result of: 1) proximity to the Great Lakes and thus an increased likelihood of lake-enhanced precipitation, 2) a synoptic-scale storm track that favors moderate precipitation events along the northern and western parts of the domain, and 3) orographic enhancement. Stations closer to the Atlantic coast and in the southeastern part of the domain generally do not receive lake-enhanced precipitation, are not in a favorable position to receive moderate precipitation from Alberta Clippers or Ohio Valley cyclones, and do not experience orographic enhancement. Also, since the midwinter storm track often favors heavy precipitation events along the Atlantic coast, the lack of moderate events there may signal that when these coastal stations receive precipitation it is more frequently of the heavy variety.

Four moderate event cases (27 December 2004: inverted trough; 8 January 2005: weak Ohio Valley cyclone; 26 January 2005: Alberta Clipper; and 21 February 2005: Alberta Clipper/Ohio Valley hybrid) were studied in order to determine the synoptic-scale and mesoscale forcing that governs when and where these events occur. The 27 December 2004 and 8 January 2005 moderate event cases featured weak synoptic-scale forcing with weak, thin, and flat frontal circulations, which precluded heavy precipitation from occurring. The 26 January 2005 case featured slightly stronger synoptic-scale and mesoscale forcing. However, regions of frontogenesis were broken into distinct segments instead of one sloping band, which decreased the intensity of the vertical motion and resulted in lighter precipitation. Also, regions of instability were not well

aligned with the individual frontogenesis maxima. The 21 February 2005 moderate event featured weak-to-moderate synoptic-scale forcing with a more intense and upright frontal circulation. However, the most intense mesoscale forcing quickly passed through eastern New York, limiting the precipitation totals.

As a point of reference, a schematic of heavy snowbands was consulted to determine how stability and lifting mechanisms contributed to the heavy event. These types of events typically feature moderate-to-strong synoptic-scale forcing and a deep layer of weak moist symmetric stability (WMSS) or negative saturation equivalent potential vorticity (EPV*) in conjunction with strong, upright low to midlevel frontogenesis. The moderate events from this study were then compared to heavy events. It was found that many of the same ingredients that appear in heavy events also appear in moderate events, except that their structure is different in the moderate case. Synoptic-scale forcing is present, but less intense in moderate cases. The moderate events generally have weaker low-level frontogenesis maxima, which are also much thinner and less upright than the heavy events. The regions of WMSS or negative EPV* are usually in a very thin layer as well and are not as well aligned with the frontogenesis maxima in moderate events. Also, the features in moderate events are often more transient. Therefore, even if the ingredients align themselves in a favorable manner, it usually is for a relatively short period of time. Weaker synoptic-scale and mesoscale forcing results in weaker upward vertical velocities, thus reducing precipitation totals.

6.2 Future Work

This research is one of the first to investigate the spatial and temporal characteristics of cool-season moderate precipitation events in the northeastern US and to examine the forcing that governs when and where these events occur. However, additional research on this topic will help to improve forecasts of these extremely challenging events. Some topics to be addressed in the future include:

- 1) Expand the climatology back several more years.
- 2) Include stations that are not considered first order in the climatology, provided that sufficient hourly data is present. The increased number of stations would provide a more detailed description of geographical variations.
- 3) Determine what type of system produced each moderate event and apply the event type to the climatology results.
- 4) Apply the techniques used in this research to additional moderate events to determine if similar synoptic-scale and mesoscale features are observed.
- 5) Determine what differences apply to null cases where moderate precipitation was forecast but never materialized. Similarly, cases where moderate precipitation was forecast, but heavy precipitation occurred should also be examined to determine what aspects of the storm resulted in the unexpected intensity.

LIST OF FIGURES

Fig. 1.1. Winter cyclone frequencies for January 1964–December 1973. Contour values should be multiplied by 10. Source: Colucci (1976), Fig. 1.

Fig. 1.2. Schematic vertical cross section illustrating symmetric instability. Solid lines represent absolute momentum, M , while dashed lines represent potential temperature. Letters show sample displacements (dashed) and accelerations (arrows). This configuration of absolute momentum and potential temperature is symmetrically unstable to the slantwise displacement shown for parcel C. Source: Sanders and Bosart (1985), Fig. 4.

Fig. 1.3. Stability regimes often observed near frontal zones. Contours represent typical values: M_g (thick black lines) and θ_e^* (θ_{es}) (thin gray lines). Source: Schultz and Schumacher (1999), Fig. 4.

Fig. 1.4. Vertical cross section of the vertical circulation around a sloping frontal zone (dashed line) in the presence of weak moist symmetric stability (to the right of the frontal zone). Source: Emanuel (1985), Fig. 5.

Fig. 1.5. Cross section through a heavy snowband depicting strong, upright frontogenesis (solid contours), saturation equivalent potential temperature (dashed contours), and saturation equivalent potential vorticity (negative values shaded) for a 12-h forecast valid at 0000 UTC 5 February 1995. Source: Nicosia and Grumm (1999), Fig. 5c.

Fig 1.6. Schematic cross section through a heavy snowband showing steeply sloped midlevel frontogenesis (solid purple ellipse) and conditionally unstable region (dashed blue line). Region of WMSS is shaded. X represents the dry conveyor belt. Arrows indicate sense of slantwise circulation. Source: Moore et al. (2005), Fig. 15b.

Fig 2.1. Location and three-letter identifier for all 35 first-order stations used in the cool-season moderate event climatology across the Northeast.

Fig. 3.1. Frequency of occurrence of moderate precipitation events at ALB for the 1999–2000 cool season.

Fig. 3.2. As in Fig. 3.1 except for 2000–2001.

Fig. 3.3. As in Fig. 3.1 except at BUF for 2001–2002.

Fig. 3.4. As in Fig. 3.3 except for 2003–2004.

Fig. 3.5. Frequency of occurrence of moderate events at BUF for the 10-yr period 1994–2004.

Fig. 3.6. As in Fig. 3.5 except at EKN.

Fig. 3.7. As in Fig. 3.5 except at ALB.

Fig. 3.8. As in Fig. 3.5 except for all seven first-order stations in New York State.

Fig. 3.9. As in Fig. 3.5 except for all five stations in Pennsylvania.

Fig. 3.10. As in Fig. 3.5 except for all five station in Ohio.

Fig. 3.11. As in Fig. 3.5 except for all 35 stations across the Northeast.

Fig. 3.12. Number of cool-season moderate events at each station in New York State for the 10-yr period 1994–2004.

Fig. 3.13. As in Fig. 3.12 except for northern New England.

Fig. 3.14. As in Fig. 3.12 except for southern New England.

Fig. 3.15. As in Fig. 3.12 except for the Washington, DC, area.

Fig. 3.16. As in Fig. 3.12 except for stations near the Atlantic coast.

Fig. 3.17. As in Fig. 3.12 except for the western region.

Fig. 3.18. Ratio of the number of events at each station to the mean number of events for all stations (132.5). Contours drawn about the mean at 0.20 intervals. The mean number of events is defined by the 1.00 contour.

Fig. 4.1. BGM WSR-88D (Level II) reflectivity image at 0300 UTC 27 December.

Fig. 4.2a–b. ALB WSR 88-D (Level II) reflectivity image on 27 December 2004 at: a) 0600 UTC and b) 0900 UTC.

Fig. 4.3. 26 December 1800 UTC Eta 9-h forecast of mean sea level pressure (hPa) valid at 0300 UTC on 27 December 2004.

Fig. 4.4. 27 December initialized 0600 UTC Eta mean sea level pressure (hPa). Dashed white line marks location of an inverted trough.

Fig. 4.5. 27 December initialized 0600 UTC Eta 1000–500 hPa thickness (green contours). Blue line marks location of cross section.

Fig. 4.6. 27 December 0600 UTC NCEP/NCAR reanalysis 300 hPa winds. Wind direction given by black arrows.

Fig. 4.7. 27 December initialized 0600 UTC Eta 500 hPa geopotential height (green contours, dam) and absolute vorticity (brown contours, shaded, 10^{-5} s^{-1}).

Fig. 4.8. 27 December initialized 0600 UTC Eta 850–700 hPa average Q-vector divergence (solid green contours, shaded, $10^{-16} \text{ K m}^{-2} \text{ s}^{-1}$). Q-vector convergence is given by dashed green contours.

Fig. 4.9. 27 December initialized 0600 UTC Eta 850–700 hPa average vertical velocity (yellow contours, $-\mu\text{b s}^{-1}$). Upward motion is given by solid contours.

Fig. 4.10. 27 December initialized 0600 UTC Eta Petterssen frontogenesis (red contours, shaded, $10^{-10} \text{ K m}^{-1} \text{ s}^{-1}$) and vertical velocity (yellow contours, $-\mu\text{b s}^{-1}$). Regions of frontogenesis are given by solid red contours and green shading. Upward vertical motion is depicted by solid yellow contours.

Fig. 4.11. 27 December initialized 0600 UTC Eta saturation equivalent potential vorticity (blue contours, shaded, PVU), relative humidity (green contours, %), and temperature (dashed orange contours, $^{\circ}\text{C}$). Regions of negative EPV* are shaded blue, while regions of WMSS are shaded dark green.

Fig. 4.12. 27 December initialized 0600 UTC Eta absolute geostrophic momentum (green contours, m s^{-1}) and saturation equivalent potential temperature (blue contours, K).

Fig. 4.13a–b. Atmospheric soundings taken at ALB on 27 December at: a) 0000 UTC and b) 1200 UTC.

Fig. 4.14a–b. BUF WSR 88-D reflectivity image on 8 January 2005 at: a) 1500 UTC and b) 1800 UTC.

Fig. 4.15. As in Fig. 4.4 except for 8 January initialized 1800 UTC Eta.

Fig. 4.16. 8 January initialized 1800 UTC Eta 1000–500 hPa thickness (blue contours, dam). White line marks location of cross section.

Fig. 4.17. As in Fig. 4.6 except for 8 January 1800 UTC.

Fig. 4.18. As in Fig. 4.7 except for 8 January using the initialized 1800 UTC Eta.

Fig. 4.19. As in Fig. 4.8 except for 8 January using the initialized 1800 UTC Eta.

Fig. 4.20. 8 January initialized 1800 UTC Eta 850–500 hPa average vertical velocity (yellow contours, $-\mu\text{b s}^{-1}$). Upward motion is given by solid contours.

Fig. 4.21. 8 January initialized 1800 UTC Eta Petterssen frontogenesis (red contours, shaded, $10^{-10} \text{ K m}^{-1} \text{ s}^{-1}$). Regions of frontogenesis are given by solid red contours and shaded warm colors.

Fig. 4.22. As in Fig. 4.11 except for 8 January using the initialized 1800 UTC Eta.

Fig. 4.23. 8 January initialized 1800 UTC Eta absolute geostrophic momentum (blue contours, m s^{-1}) and saturation equivalent potential temperature (green contours, K).

Fig. 4.24. As in Fig. 4.13 except at BUF on 8 January at 1200 UTC.

Fig. 4.25. As in Fig. 4.2 expect for 26 January 2005 at 0900 UTC.

Fig. 4.26. As in Fig. 4.4 except for 26 January initialized 0600 UTC Eta.

Fig. 4.27. As in Fig. 4.4 expect for 26 January 0600 UTC Eta 3-h forecast.

Fig. 4.28. 26 January 0600 UTC Eta 3-h forecast of 1000–500 hPa thickness (yellow contours, dam). Blue line marks location of cross section.

Fig. 4.29. As in Fig. 4.6 except for 26 January 1200 UTC.

Fig. 4.30. As in Fig. 4.7 except for 26 January 0600 UTC Eta 3-h forecast.

Fig. 4.31. As in Fig. 4.8 except for 26 January 0600 UTC Eta 3-h forecast evaluated at 700 hPa.

Fig. 4.32. As in Fig. 4.9 except for 26 January 0600 UTC Eta 3-h forecast.

Fig. 4.33. As in Fig. 4.10 except for 26 January 0600 UTC Eta 3-h forecast.

Fig. 4.34. As in Fig. 4.11 except for 26 January 0600 UTC Eta 3-h forecast.

Fig. 4.35. As in Fig. 4.23 except for 26 January 0600 UTC Eta 3-h forecast.

Fig. 4.36. As in Fig. 4.13 except at ALB on 26 January at 1200 UTC.

Fig. 4.37. As in Fig. 4.2 except for 21 February 2005 at 0600 UTC.

Fig. 4.38. As in Fig. 4.4 except for 21 February initialized 0600 UTC Eta.

Fig. 4.39. As in Fig. 4.5 except for 21 February initialized 0600 UTC Eta. White line marks location of cross section.

Fig. 4.40. As in Fig. 4.6 except for 21 February at 0600 UTC.

Fig. 4.41. 21 February initialized 0600 UTC Eta 500 hPa geopotential height (green contours, dam) and absolute vorticity advection (shaded, 10^{-5} s^{-1}).

Fig. 4.42. As in Fig. 4.8 except for 21 February initialized 0600 UTC Eta 700–500 hPa average.

Fig. 4.43. 21 February initialized 0600 UTC Eta average 700–500 hPa average vertical velocity (yellow contours, $\mu\text{b s}^{-1}$). Dashed contours represent regions of upward vertical motion.

Fig. 4.44. As in Fig. 4.10 except for 21 February initialized 0600 UTC Eta. Frontogenesis is shaded only. Vertical velocity is given in $\mu\text{b s}^{-1}$. Dashed yellow contours represent upward vertical motion.

Fig. 4.45. As in Fig. 4.11 except for 21 February initialized 0600 UTC Eta.

Fig. 4.46. As in Fig. 4.23 except for 21 February initialized 0600 UTC Eta.

Fig. 4.47a–b. As in Fig. 4.13 except at ALB on 21 February at: a) 0000 UTC and b) 1200 UTC.

Fig. 5.1. Frequency of occurrence of moderate events for all 35 stations for the 10-yr period 1994–2004 using a normalized 30-day month.

Fig. 5.2. 21 February 0600 UTC Eta 3-h forecast of Petterssen frontogenesis valid at 0900 UTC.

Fig. 5.3. Schematic cross section through a cool-season moderate precipitation band showing Petterssen frontogenesis (red ellipse), negative EPV* (dashed blue ellipse), WMSS (brown dotted region), saturation equivalent potential temperature (dark green contours), and transverse circulation (arrows).

TABLE OF CONTENTS

Abstract	ii
Acknowledgments.....	v
Table of Contents	vii
List of Figures	ix
1. Introduction	1
1.1. Overview	1
1.2. Literature Review	2
1.2.1. Precipitation Climatologies.....	2
1.2.2. Mechanisms for Precipitation Production.....	5
1.2.2.1. Moisture	5
1.2.2.2. Lifting Mechanisms	6
1.2.2.3. Instability	8
1.2.3. Ingredients-based Methodologies	13
1.2.3.1. History of Ingredients-based Methodologies	13
1.2.3.2. Empirical Use of IBMs.....	15
1.2.4. Heavy Snow in the Presence or Absence of an Intense Cyclone	17
1.2.4.1. Ingredients Applied to Intense Cyclones	17
1.2.4.2. Ingredients Applied to Weak or Nonexistent Cyclones	19
1.3. Research Goals and Thesis Synopsis	20
2. Data and Methodology	25
2.1. Data Sources.....	25
2.1.1. Climatology	25
2.1.2. Case Studies	25
2.2. Methodology	26
2.2.1. Climatology	26
2.2.2. Case Studies	28
3. Climatology Results	33
3.1. Seasonal Trends	33
3.2. Geographical Trends	34
4. Case Studies	47

4.1.	Overview	47
4.2.	Case I: 27 December 2004	47
4.2.1.	Synoptic Overview	48
4.2.2.	Mesoscale Aspects	49
4.3.	Case II: 8 January 2005	51
4.3.1.	Synoptic Overview	51
4.3.2.	Mesoscale Aspects	52
4.4.	Case III: 26 January 2005	54
4.4.1.	Synoptic Overview	54
4.4.2.	Mesoscale Aspects	55
4.5.	Case IV: 21 February 2005	57
4.5.1.	Synoptic Overview	58
4.5.2.	Mesoscale Aspects	59
5.	Discussion	106
5.1.	Climatology	106
5.1.1.	Seasonal Trends	106
5.1.2.	Geographical Trends	110
5.2.	Case Studies	113
5.2.1.	27 December 2004 (Case I)	114
5.2.2.	8 January 2005 (Case II)	116
5.2.3.	26 January 2005 (Case III) and 21 February 2005 (Case IV)	117
5.2.4.	Moderate Event Schematic Cross Section	119
5.3.	Forecast Implications	120
6.	Conclusions and Future Work	124
6.1.	Conclusions	124
6.2.	Future Work	127
	References	129

ABSTRACT

Moderate precipitation events contribute a significant percentage of all cool-season (1 October–30 April) precipitation in the northeastern United States. It is important to investigate the structure and causes of these moderate precipitation events because 1) they are relatively common, 2) they tend to occur in relatively weak synoptic-scale forcing regimes, and 3) they can be challenging to forecast. The purpose of this research, through use of a climatology and case studies, is to determine the spatial and temporal characteristics of cool-season moderate precipitation events in the Northeast, and to examine the synoptic-scale and mesoscale forcing that governs when and where these events occur. This research was conducted under the National Weather Service (NWS) Collaborative Science, Technology, and Applied Research (CSTAR) program.

A 10-yr climatology (October 1994–April 2004) of cool-season moderate precipitation events across the northeastern United States was constructed using hourly and daily precipitation data provided by the National Climatic Data Center (NCDC). A total of 35 first-order NWS stations across the Northeast were included in the study. The results of the climatology indicate that important variations in the frequency of occurrence of moderate precipitation events occur within the cool season. October received the lowest number of events during the 10-yr period, while a peak in frequency was observed in early winter and again in spring. These peaks in frequency of occurrence correspond to times when the synoptic-scale storm track is favorably located to produce moderate events across the Northeast (early winter and spring) and lake-effect precipitation is most likely (early winter). They also coincide with times during the cool

season when 500 hPa cyclone frequency is at a maximum (spring) and cold air aloft over heated and/or elevated terrain results in showery precipitation (spring).

Variations in frequency of occurrence also are observed based on geographical location. A general decrease in the number of moderate events occurs to the south and east across the domain. Regions of enhanced frequency are located downwind of the Great Lakes, across the northern section of the domain, and along the spine of the Appalachians. These regions likely experience a higher frequency of occurrence due to a favorable synoptic-scale storm track, lake-effect precipitation, and/or orographic enhancement.

Four moderate event cases were selected for further study in order to examine the synoptic and mesoscale forcing that led to the observed precipitation. It was found that moderate precipitation events have ingredients that are similar to heavier events. In moderate events synoptic-scale forcing is present but generally weaker than for heavy events. Also, mesoscale features such as frontogenesis and weak moist symmetric stability or negative saturation equivalent potential vorticity are not as intense, deep, upright, or well aligned as is typical for heavy events. These features also tend to be more transient in moderate events since the associated storm typically moves at a faster speed than for heavy events. Therefore, although ingredients observed in heavy events are also found in moderate events, they are weaker in the moderate events, thus reducing precipitation totals.

Cool-Season Moderate Precipitation Events in the Northeastern United States

1. Introduction

1.1 Overview

Expand upon opening paragraph of NROW VII abstract. Discuss positive and negative impacts moderate events may have on the population. Give brief description of why it is important to investigate moderate events. (Homan and Uccellini 1987; Call 2005; Evans 2006).

1.2 Literature Review

1.2.1 Precipitation Climatologies

Precipitation climatologies can help forecasting process (Brooks and Stensrud 2000).

Discussion of general climatologies:

Precip increased 10% across US since 1910. Increase in frequency for all categories of precipitation. Percentage of total precip from heavy events is increasing relative to moderate events (Karl and Knight 1998).

Groisman et al. (2005) confirm widespread increase in frequency of very heavy precip events (upper 0.3%) in last 50-100 years. Karl (2006) attributes this to climate warming.

Seasonal cycle of heavy rain and flash flood events is highest near the Gulf Coast during the cool-season and moves north to the Midwest/Northeast during the summer (Brooks and Stensrud 2000).

Heavy precip during winter shows a nocturnal max over the eastern and northern US while there is a max in lighter precip near sunrise (Wallace 1975).

Fracasso (2004) constructed a climatology of precipitation associated with 500 hPa cool-season cutoff lows and found that precip in the Northeast associated with these lows decreases in mid winter.

Discussion of climatologies of winter weather:

Freezing rain, sleet, and freezing drizzle have a large spatial variability across the United States. Changnon and Karl (2003) found national maximums of freezing rain to occur in parts of PA

and NY, the Midwest, eastern Appalachians, and the Pacific Northwest. Cortinas et al. (2004) show the distribution of freezing precip is affected by topography, proximity to water, and the synoptic storm track.

Several snow/winter cyclone climatologies available. Colucci (1976) looked at winter cyclone tracks and found highest concentration in a band from Cape Hatteras to New England and over the eastern Great Lakes (Fig. 1: important for my climatology results). Businger et al. (1990) constructed a storm following climatology and found the frequency of moderate-heavy precip was highest north of the low. Novak et al. (2004) produced a climatology of heavy banded snowfall in the Northeast and found that most heavy events were associated with banding northwest of the surface low.

Branick (1997) constructed a detailed climatology of significant winter weather events across the US. He found a yearly mean of 128 significant events somewhere across the US (eventually relate this to the frequency of moderate events occurring at each site). He also found a max frequency of events from late November to late January with a sharp rise from October to November (similar to trends seen in my moderate events).

1.2.2 Mechanisms for producing precipitation

3 main mechanisms for producing precip: moisture, lift, instability (e.g. Doswell et al. 1996).

1.2.2.1 Moisture

Importance of moisture noted in all case studies (e.g., Homan and Uccellini 1987) Nicosia and Grumm (1999); Jurewicz and Evans (2004)). Instabilities not released if air is too dry. (I will not say more than a short paragraph on moisture).

1.2.2.2 Lifting mechanisms

Brief discussion of the QG omega equation and Q vector omega equation from Holton (1992). Quick look at how QG omega equation can be reanalyzed into form where vertical motion is assessed by geopotential height and thickness contours (Trenberth 1978). Use of Q vectors by Gyakum (1987) to diagnose vertical velocity. QG forcing plays a role in affecting strength and depth of frontal circulations (Jurewicz and Evans 2004). Transition to frontal forcing.....

Definition of Petterssen 2D frontogenesis and how it works (Bluestein Vol. 2 1993; Nicosia and Grumm 1999). Present an alternative way to express it (Moore and Blakely 1988; Moore et al. 2005;). Discuss how frontogenesis leads to a vertical circulation (Sawyer 1956, Sanders and Bosart 1985).

1.2.2.3 Instability

Definitions and applications of gravitational (convective), inertial, and symmetric instabilities (Schultz and Schumacher 1999; Sanders and Bosart 1985, Fig 4; Seltzer et al. 1985).

Discuss a special kind of symmetric instability, CSI (S and S 1999). Give origins of the CSI theory (Bennetts and Hoskins 1979; Emanuel 1979; Emanuel 1983a,b; Snook 1992) and methods to analyze it (e.g. Moore and Lambert 1993; Wiesmueller and Zubrick 1998). Discuss atmospheric criteria that can result in CSI (Wiesmueller and Zubrick 1998). Make sure to show that CSI and slantwise convection are not the same thing. CSI is the instability, the other is the result of CSI being released (S and S 1999).

Present an easier method to diagnose CSI called the equivalent potential vorticity (EPV) (Moore and Lambert 1993). Show how this is properly used to diagnose CSI by using the saturated form (EPV*) (S and S 1999; Jurewicz and Evans 2004). McCann (1995) presents a 3D version of EPV that relates EPV to vertical and horizontal temperature gradients. Discuss how CSI can coexist with conditional instability, but with CI dominating (Moore and Lambert 1993). Snook (1992) states that EPV determines the potential of CSI regardless of the geostrophic wind shear, but be sure to note that in order to determine CSI vs. CI, EPV needs to be used in conjunction with the old method of CSI analysis. Show S and S (1999) fig. 4.

Emanuel (1985, Fig. 5) shows that the vertical circulation around a frontal zone, when in the presence of negative EPV* or even weakly positive symmetric stability (or EPV*), is concentrated and enhanced on the warm side of the frontogenesis max. These results are confirmed by Thorpe and Emanuel (1985). Similarly, Xu (1989) shows that frontogenesis in the presence of negative EPV can produce long lasting mesoscale bands. Will show how this applies to some past case studies in upcoming subsection.

1.2.3 Ingredients based methodology (IBM)

Potential benefits of an IBM (Wetzel and Martin 2001; Doswell et al. 1996).

Ingredients based methodology using the above ingredients for deep convection, severe thunderstorms, and cyclogenesis: moisture, lift, instability (McNulty 1978, 1995; Doswell 1987, Johns and Doswell 1992). Doswell et al. (1996) developed an IBM for flash flooding that accounts for previous hydrological conditions, total precipitation, precipitation rate, and duration. An IBM for cloud heads, a precursor of rapid cyclogenesis, was developed by Dixon et al. (2002). Their Vertically integrated extent of Realizable Symmetric instability (VRS) diagnostics included negative EPV*, high moisture, and strong vertical motion.

IBM for snowfall developed by Nietfeld and Kennedy (1998) assumes air temperature, snowfall rate, and snowfall duration are the three main ingredients. This did not have much operational utility. Janish et al. (1996) use an IBM for diagnosing the distribution of winter weather precipitation type through the use of composite charts. S and S (1999) develop an IBM for slantwise convection. Wetzel and Martin (2001) expand upon the concepts of Janish et al. (1996). They determine five key ingredients for a winter precipitation event as being QG forcing for ascent, moisture, instability, precipitation efficiency, and temperature. The first 3 ingredients have been discussed in detail above.

Brief description of cloud microphysics that produce heavy snow. Discuss ice crystal habits and show that dendrites have the lowest density (Power et al. 1964; Roebber et al. 2003). Show that high accumulations result from large snowflakes consisting of dendritic crystals where the max vertical motion occurs around -15°C (Mossop 1970; Auer and White 1982; Rogers and Yau 1989). Give a very brief description of temperature influence (Wetzel and Martin 2001).

Discuss some traditional operational forecast techniques that apply some ingredients of the above IBMs. Goree and Younkin (1966) used a synoptic climatology method to find favored areas of snow in relation to the 500 hPa vorticity max and surface low, while Browne and Younkin (1970) related snowfall to the track of the 850 hPa low. Cook (1980) showed that snow totals over the next 24-h would be roughly equal to the 200 hPa warm advection in $^{\circ}\text{C}$ during that period. Wetzel (2000) summarized the Garcia method, in which Garcia found that the 12 hour snowfall in inches equals twice the average mixing ratio on an isentropic surface that

intersects the forecast area between 700 and 750 hPa. Garcia (2000) updated his initial method to allow for high snow/liquid ratios and jet streak events. A “magic chart” was developed by Sangster and Jagler (1985) which relates snowfall amounts to the net vertical displacement of an air parcel over a 12-h period ending 24-hours after that parcel arrives at 700 hPa. Finally, Gordon (1998) developed a winter weather checklist in which he describes the LEMO technique, which relates snow totals to the speed of the absolute vorticity max.

1.2.4 Heavy snow in the presence or absence of an intense cyclone.

Give a very brief discussion of classic eastern US cyclogenesis as described by Kocin and Uccellini (1990, 2004) and Maglaras et al. (1995). Show how jet stream interactions can lead to enhanced snow during such events (Uccellini and Kocin 1987). State that the ingredients above usually come together best in cyclones such as these.

1.2.4.1 Application of some ingredients to intense cyclones

Brief introduction to precipitation structure within a cyclone (Bjerknes 1919). Show that heavy bands are often present to the northwest of the cyclone (Novak et al. 2004). Sanders (1986) found that lower tropospheric frontogenesis occurs in the banded region northwest of the surface low. Wiesmueller and Zubrick (1998) showed that frontogenetic forcing can make a region more prone to CSI. Sanders and Bosart (1985) confirmed in their case study the results from Emanuel (1985) that maximum ascent occurs in a band parallel to the axis of frontogenesis. The ageostrophic circulation around the frontogenesis max is narrowed and intensified in the presence of weak symmetric stability (WSS) (or CSI). Reuter and Yau (1990) offer evidence to show that slantwise convection is not a rare phenomenon as seven events occurred in a three month period near Nova Scotia. Several observational studies of bands within classic cyclones have found this to be true, as well as confirming the results of Emanuel (1985): (Seltzer et al. 1985; Wiesmueller and Zubrick 1998; Nicosia and Grumm 1999; Novak et al. 2004; Jurewicz and Evans 2004).

1.2.4.2 Application of ingredients to weak or nonexistent surface lows

Observations also show that heavy snow can occur without a strong surface low or even with no surface low at all (Seltzer et al. 1985; Moore and Blakely 1998; Jurewicz and Evans 2004; Novak et al. 2004; Moore et al. 2005 (show their Fig. 15b); Evans 2006).

Each of these studies found that the collocation of a sloping frontogenetical circulation in the presence of CSI or weak moist symmetric stability can lead to heavy snow just as in the classic cases described above. Novak et al. (2004) and Jurewicz and Evans (2004) showed in their cases with lower QPF that the frontogenetical forcing was weaker and less sloped. Gyakum (1987) and Homan and Uccellini (1987) looked at the problems associated with forecasting light to moderate snow events. Gyakum (1987) studied an unforecasted moderate snow event that was not associated with a surface cyclone or obvious front and found that it resulted from a thermally direct frontal circulation in a region of weak MSS.

1.3 Research goals and thesis synopsis

Show that the above literature review has discussed mechanisms for producing precipitation, especially in winter storms. State that the systems studied in this research are more like those of Gyakum (1987) and Homan and Uccellini (1987). To that end, the goals of this research are to 1) construct a climatology of cool-season moderate precipitation events in the Northeast and 2) determine the synoptic-scale and mesoscale features that determine when and where these events occur. The second goal will be accomplished using components of the IBM's above and applying them in a manner as discussed by the above case studies for heavy snow.

Present the organization of the rest of the thesis: Chapter 1: Overview and Literature Review; Chapter 2: data and methodology; Chapter 3: climatology results; Chapter 4: Case study results; Chapter 5: discussion and forecast implications; Chapter 6: summary and future work.

2. Data and Methodology

2.1 Data sources

2.1.1 Climatology

Data were obtained from NCDC's Local Climatological Data LCD and Hourly Precipitation Data (HPD). Discuss problem with some missing data (especially snowfall), but note that it is a minor issue.

2.1.2 Case Studies

Cases were selected based on the criteria that the event total precipitation at most stations were in the moderate range and that the precipitation was not obviously associated with a deep cyclone.

Data were used from several sources. All case studies made use of the 40-km Eta model, available at 3-h intervals, and displayed using the NWS Albany and Binghamton Weather Event Simulator (WES) version 4.0. Data for some large scale analysis was also obtained from NCEP/NCAR Reanalysis data at a $2.5^\circ \times 2.5^\circ$ resolution. Radar data are from NCDC archives. Soundings provided by the University of Wyoming.

2.2 Methodology

2.2.1 Climatology

Define the domain boundary and discuss the 1st order station selection process.

Define cool season.

Present criteria for a moderate event.

Show how daily data were used to identify a moderate event.

Show how hourly data were used to refine the case selection process for potentially ambiguous cases.

Histograms were produced similar to those of Cortinas et al. (2004) to show the distribution of moderate events by city, state, and geographic region.

2.2.2 Case Studies

Define the equation used by WES for Q-vector divergence (Holton 1992).

Define Petterssen frontogenesis as calculated by WES (Bluestein 1993; Nicosia and Grumm 1999) and show why it is better to use the real wind for this calculation.

Define EPV from Moore and Lambert (1993) and EPV* from S and S (1999) and Jurewicz and Evans (2004) as calculated by WES. Going against the recommendations of S and S (1999), Jurewicz and Evans (2004) give some reasons as to why the real wind should be used in calculating EPV*.

Determined that three types of systems often produce moderate events during the cool season across the Northeast: Alberta Clippers (Hutchinson 1995), weak Ohio Valley warm-advection lows (as in Homan and Uccellini 1987), and inverted troughs (Keshishian and Bosart 1987, Keshishian et al. 1994). These were the basic storm types chosen for study.

Plan view maps were produced for each case study to assess the synoptic situation. Examples include sea level pressure, 500 hPa geopotential heights and vorticity, 1000–500 hPa thickness, upper-

level (~ 250 hPa) heights and winds, and low-level Q vector forcing and the corresponding omega. Soundings were used for locations near the precipitation to determine the thermodynamic influence on the precipitation.

Cross sections were created for each case study to analyze the mesoscale impacts on the observed precipitation. Cross sections were taken through the precipitation region according to the methods described in section 1.2.2.3 in order to analyze various aspects of moisture, instability (either CSI or CI via EPV* and momentum-theta e), and lift (through frontogenetical forcing).

3. Climatology results

3.1 Seasonal trends

Show how there appear to be two distinct minima for many of the 35 stations: one in October and another in February. There also appear to be distinct peaks that occur during late autumn/early winter and again as spring arrives. Present several histograms to illustrate this point.

3.2 Geographic trends

ERI had the most events over the last 10 years (197) while BWI had the least (95). The histograms show that far more moderate events occurred over the northern, western, and Great Lakes regions of the domain than over the southern and eastern regions. The Atlantic coastal regions had the lowest overall frequency of occurrence. The high terrain had a frequency of occurrence at or slightly above the mean.

Present histograms for New York State and other geographic regions. Compare and contrast the stations with others in that region and in different geographic regions.

Show contour map of ratio of number of events at each site to the mean number of events for all sites.

4. Case studies

4.1 Overview

4.2 27 December 2004

Forecast for ALB called for very light snow with the main system well off to the southeast. Instead, over 15 cm of snow fell.

4.2.1 Synoptic overview

Deep cyclone well off the Atlantic Coast continuing to move off the coast. Weak inverted trough over the Northeast. Some QG forcing was present. A moderate band of snow developed over Albany producing over 15 cm of snow. Show maps that illustrate synoptic set up.

4.2.2. Mesoscale aspects

Weak, shallow region of frontogenesis and a flat, shallow region of negative EPV* results in a modest region of vertical motion. Thin layer of instability is CI, not CSI.

4.3 8 January 2005

Forecast for BUF called for a chance of snow showers with accumulations under 3 cm from a weak system passing by to the south. Instead, nearly three times that much snow fell.

4.3.1 Synoptic overview

A weak Ohio Valley low pressure with associated warm advection and some wrap-around precipitation affected much of New York state. QG forcing was present. Snow totals ranged from around 7.5 cm in BUF to just under 15 cm in ALB. Some mixing occurred in the main warm advection region near BGM, which resulted in lower snowfall totals. Show maps illustrating synoptic set up.

4.3.2 Mesoscale aspects

Frontogenesis similar to 26 December case: weak and shallow slope. Layer of instability was slightly deeper, but some of this may have been caused by rapid drying with height as seen in the cross section.

4.4 26 January 2005

This case was chosen to see how the mesoscale aspects of an Alberta Clipper compare with heavier events since Clippers often have relatively strong synoptic forcing and have less available moisture.

4.4.1 Synoptic overview

An Alberta clipper dropped down across the eastern Great Lakes and into New York State. Synoptic forcing was present in the form of Q-vector convergence and vorticity advection. Snow totals were in the 7–13 cm range across the state. Show synoptic maps.

4.4.2 Mesoscale aspects

Frontogenetical circulation a bit stronger in this case than previous two cases. A double frontogenesis max is noted. The max farther south was in a fairly stable region, while the northern most max (near ALB) was able to tap into a region of WSS. The frontogenesis max is still not as intense or upright as the heavy events discussed in the lit review, so the snow totals are much lower. The quick movement of the system also helped cut down on totals.

4.5 21 February 2005

This case was chosen because it had fairly strong synoptic and mesoscale forcing. The speed of the system may have resulted in lower snow totals.

4.5.1 Synoptic overview

This case is not covered in as much detail as the other three. A weak low and its associated warm advection moved eastward across New York State. Snow broke out in the warm advection region across eastern New York and New England. Good synoptic forcing was present. Snow totals were in the 7.5–15 cm range.

4.5.2 Mesoscale aspects

Fairly strong, upright region of frontogenesis and associated region of upward motion is present. This region of frontogenesis is also associated with a deep region of negative EPV* and WSS. Radar confirms that the precipitation band moved through rather quickly.

5. Discussion and forecast implications

5.1 Climatology

Discuss possible reasons for the observed seasonal distribution. For example, more Alberta Clippers occur around January, and perhaps more lake effect events in December and January. The March and April peak probably requires further study. The fact that February has two or three fewer days cannot explain the decrease in the frequency of events over the 10 year period. There would have to be a moderate event on almost every day that was missed to account for the difference. In order to discuss the topic of geographic distribution, the figure showing the ratio of the number of events at each station to the mean number of events will be revisited. The peaks in the northern and western sections could be explained by Alberta Clippers and lake effect precipitation. Also many Ohio Valley lows spread moderate precipitation across this region. Show how lake effect snow has a way of eliminating itself, although it is not explicitly excluded, as seen in the figure. The high terrain peak may be a

result of orographic enhancement of otherwise light events. Also, the minimum along the Atlantic Coast and southeastern portion of the domain may be related to the cyclone storm track discussed by Colucci (1976). The storm track would suggest that during the cool season, a larger percentage of storms along the coast are heavy events.

5.2 Case studies

Show how the synoptic scale was conducive for precipitation to develop in all four cases. The first three cases all exhibit similar frontal scale circulations and instability patterns. The key point is that the frontogenesis is not as strong or upright in these moderate cases as was seen in heavy snow cases. Therefore, even in the presence of a region of CI or WMSS, the resulting circulation is not as intense. Thus we see weaker updrafts and less intense precipitation. It appears that the depth of the unstable region is only a modulating effect, while it is the frontogenetical circulation that is driving the precipitation. The third case, which had more intense and upright frontogenesis, was still not as upright as heavier events. The quick movement of the system also plays a role in limiting precipitation, as evidenced by the fourth case. Therefore, it appears that moderate events have similar ingredients as heavier events. Synoptic forcing is present. There is a region of frontogenesis, a layer of instability or WMSS, and sufficient moisture, but these features are not as deep, upright, or well aligned as in heavier events. These features will be shown in a schematic cross section of moderate events. The features also appear to be more transient than they are in the northwest region of a classic intense cyclone. The strength, depth, tilt, and speed of these features has major implications for forecasters, as they can now recognize that these hard-to-forecast moderate events have similar structures as more familiar heavy events, but just to a lesser degree.

6. Summary and suggestions for future work

Tie up loose ends and summarize key findings from the climatology and case studies.

Offer suggestions for future work:

1. Expand the climatology to include a longer time period
2. Use data from COOP stations to provide a more detailed climatology
3. Determine what type of system caused each moderate event and apply the event type to the climatology results.
4. Apply the techniques used here to other moderate events to see if similar results are obtained.
5. See what differences apply to null cases where moderate precipitation was forecasted but never materialized.

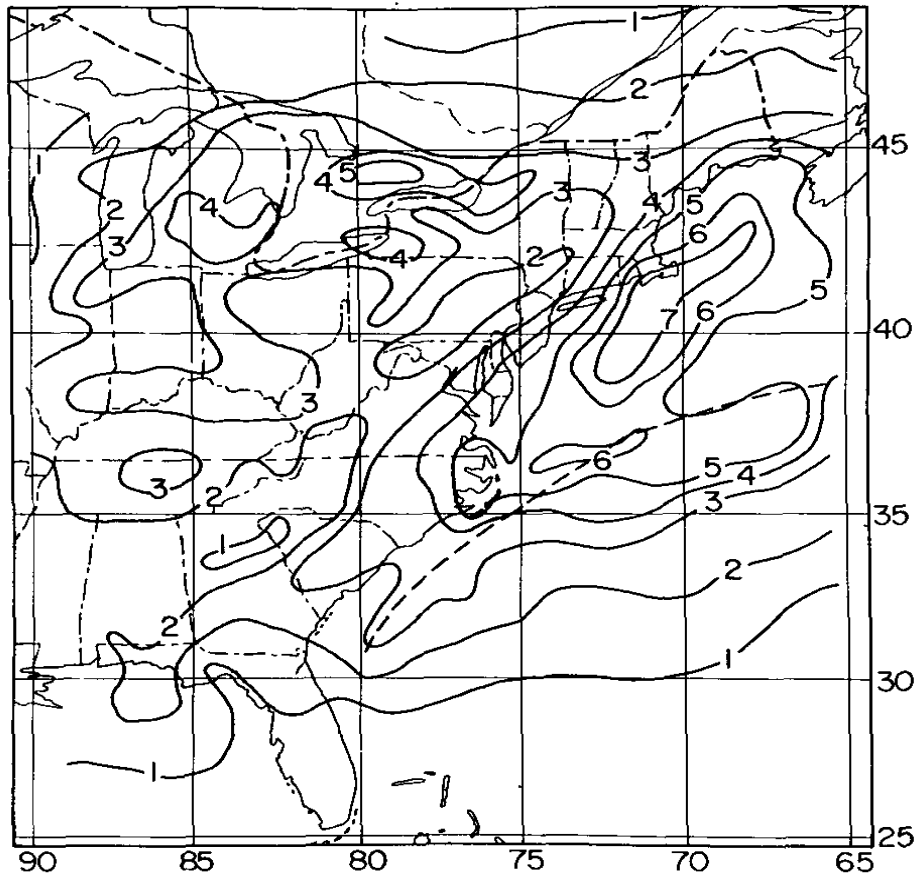


Fig. 1.1 Winter cyclone frequencies for January 1964–December 1973. Contour values should be multiplied by 10. From Colucci (1976).

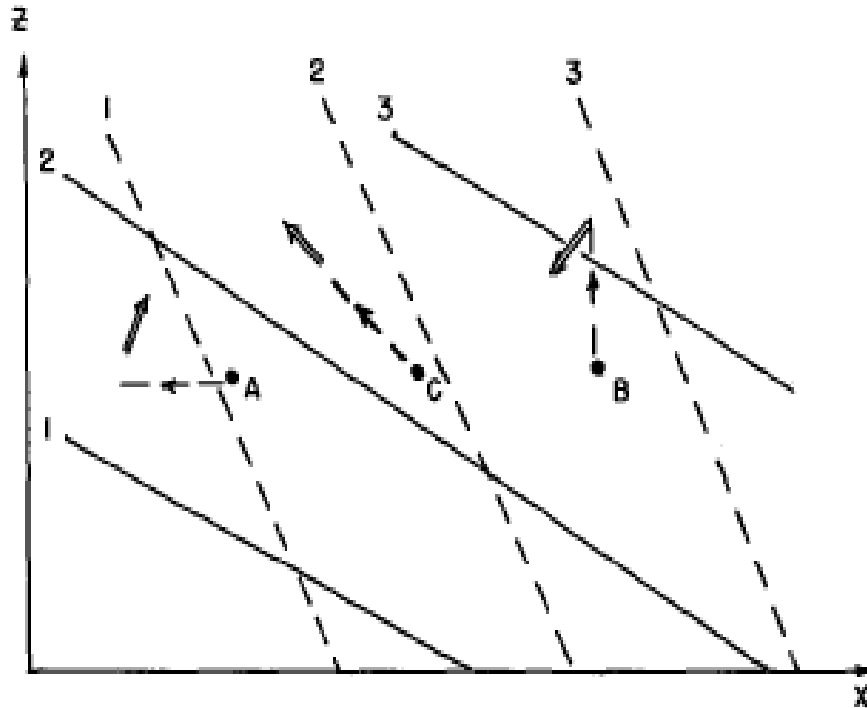
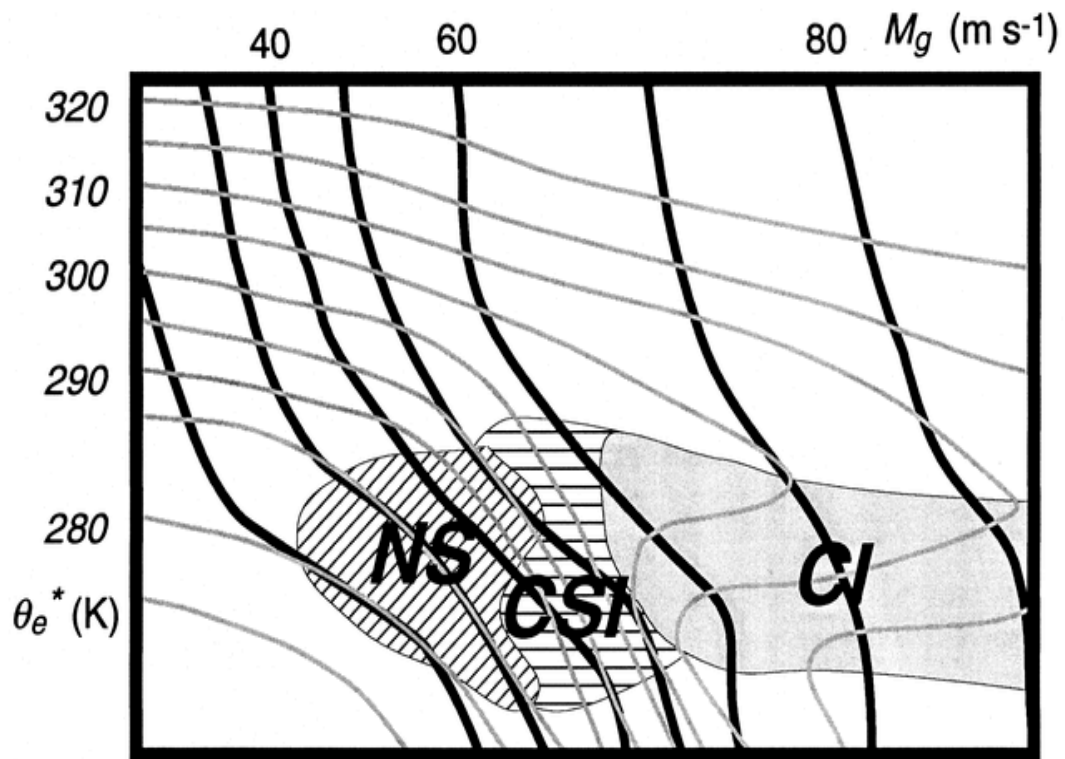


Fig 1.2. Schematic vertical cross section illustrating symmetric instability. Solid lines represent absolute momentum, M , while dashed lines represent equivalent potential temperature. Letters show sample displacements (dashed) and accelerations (arrows). From Sanders and Bosart (1985).



NS = neutral symmetric stability
CSI = conditional symmetric instability
CI = conditional instability

Fig 1.3. Stability regimes often observed near frontal zones. Contours represent typical values often present: M_g (thick black lines) and θ_e^* (thin gray lines). From Schultz and Schumacher (1999).

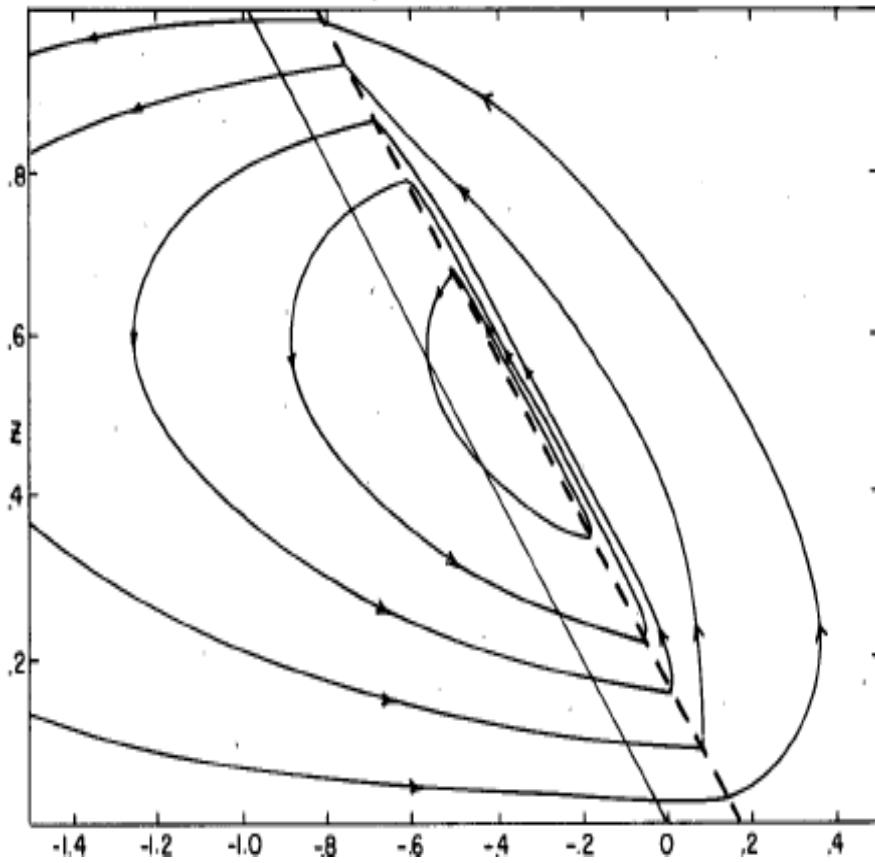


Fig. 1.4. Vertical cross section of the circulation around a sloping frontal zone (dashed line) in the presence of vanishing potential vorticity in the warm air (to the right of the frontal zone). From Emanuel (1985).

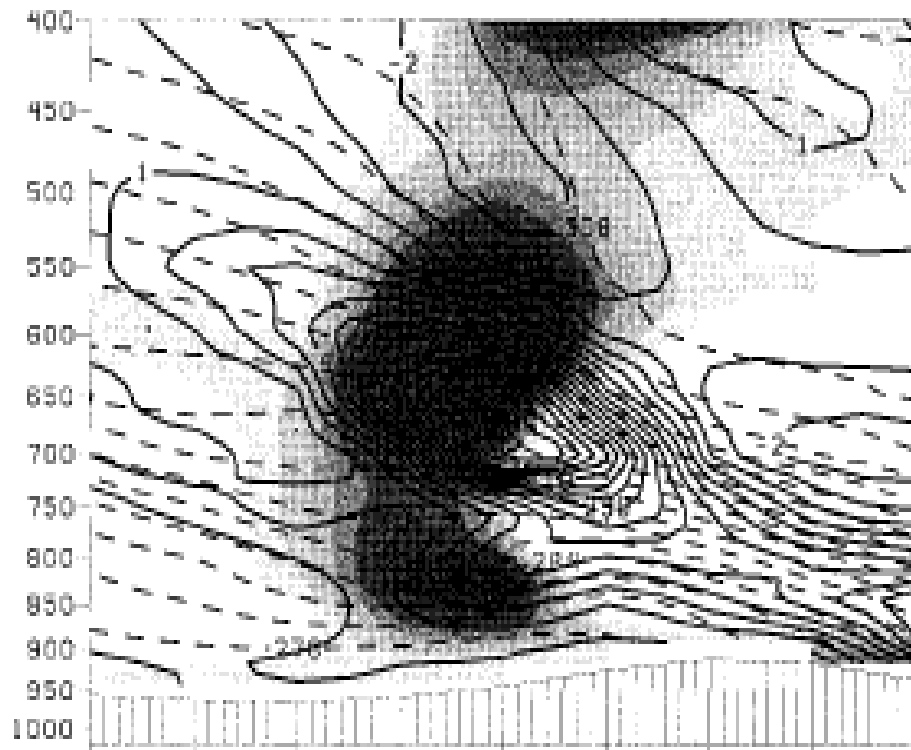


Fig. 1.5. Cross section through a heavy snow band depicting strong, sloped frontogenesis (solid contours), saturation equivalent potential temperature (dashed contours), and saturation equivalent potential vorticity (negative values shaded). 12-hr forecast valid at 0000 UTC 5 February 1995. From Nicosia and Grumm (1999).

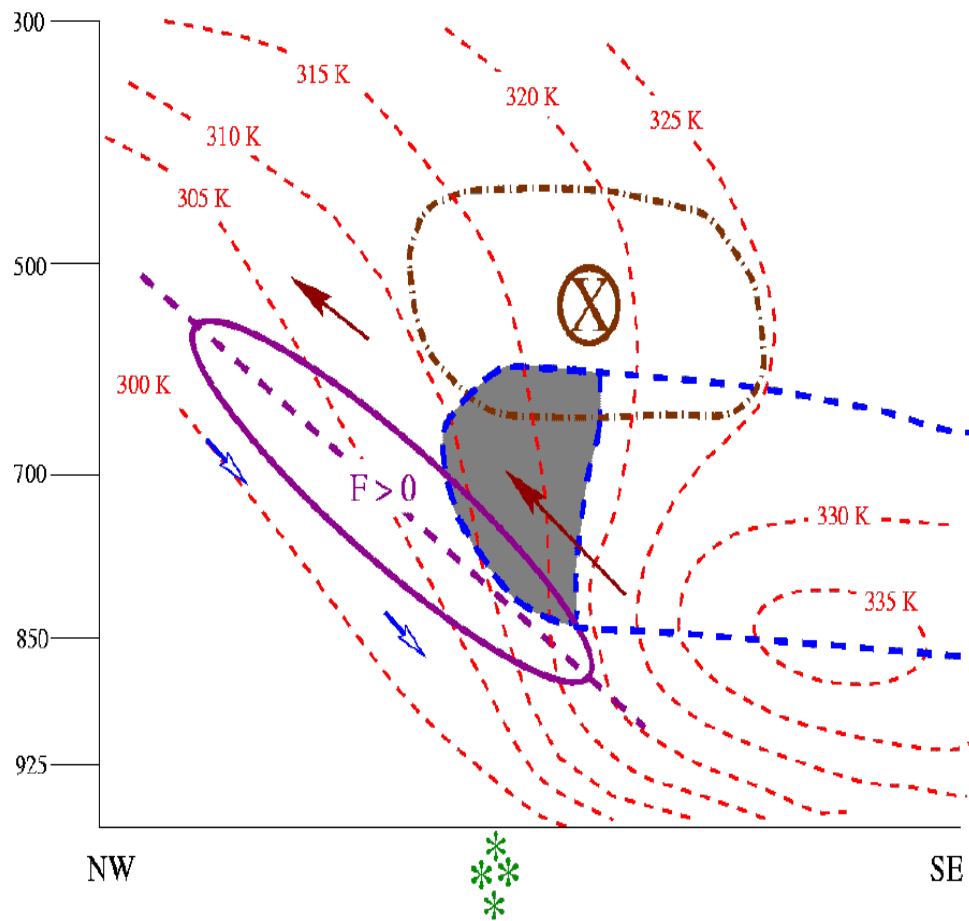


Fig 1.6. Schematic cross section (Moore et al. 2005) through a heavy snowband showing steeply sloped midlevel frontogenesis (solid purple ellipse) and conditionally unstable region (dashed blue line). Region of WMSS is shaded.

REFERENCES

- Auer, A. H. and J. M. White, 1982: The combined role of kinematics, thermodynamics and cloud physics associated with heavy snowfall episodes. *J. Meteor. Soc. Japan*, **60**, 500–507.
- Bennetts, D. A. and B. J. Hoskins, 1979: Conditional symmetric instability – a possible explanation for frontal rainbands. *Q. J. R. Meteorol. Soc.*, **105**, 945–962.
- Bjerknes, J., 1919: On the structure of moving cyclones. *Mon. Wea. Rev.*, **47**, 95–99.
- Black, T. L., 1994: The new NMC mesoscale Eta model: Description and forecast examples. *Wea. Forecasting*, **9**, 265–278.
- Bluestein, H. B., 1993: *Synoptic-Dynamic Meteorology in Midlatitudes*. Vol. 2, *Observations and Theory of Weather Systems*. Oxford University Press, 594 pp.
- Branick, M. L., 1997: A climatology of significant winter-type weather events in the contiguous United States, 1982–94. *Wea. Forecasting*, **12**, 193–207.
- Brooks, H. E. and D. J. Stensrud, 2000: Climatology of heavy rain events in the United States from hourly precipitation observations. *Mon. Wea. Rev.*, **128**, 1194–1201.
- Browne, R. F. and R. J. Younkin, 1970: Some relationships between 850-millibar lows and heavy snow occurrences over the central and eastern United States. *Mon. Wea. Rev.*, **98**, 399–401.
- Businger, S., D. I. Knapp, and G. F. Watson, 1990: Storm following climatology of precipitation associated with winter cyclones originating over the Gulf of Mexico. *Wea. Forecasting*, **5**, 378–403.
- Call, D. A., 2005: Rethinking snowstorms as snow events: A regional case study from upstate New York. *Bull. Amer. Meteor. Soc.*, **86**, 1783–1793.
- Changnon, D., J. J. Noel, and L. H. Maze, 1995: Determining Cyclone Frequencies Using Equal-Area Circles. *Mon. Wea. Rev.*, **123**, 2285–2294.
- Changnon, S. A. and T. R. Karl, 2003: Temporal and spatial variations of freezing rain in the contiguous United States: 1948–2000. *J. Appl. Meteor.*, **42**, 1302–1314.
- Colucci, S. J., 1976: Winter cyclone frequencies over the eastern United States and adjacent western Atlantic, 1964–1973. *Bull. Amer. Meteor. Soc.*, **57**, 548–553.
- Cook, B. J., 1980: A snow index using 200 mb warm advection. *Natl. Wea. Dig.*, **5**, 29–40.

- Cortinas, J. V., Jr., B. C. Bernstein, C. C. Robbins, and J. W. Strapp, 2004: An analysis of freezing rain, freezing drizzle, and ice pellets across the United States and Canada: 1976–90. *Wea. Forecasting*, **19**, 377–390.
- Crum, T. D., R. L. Alberty, and D. W. Burgess, 1993: Recording, archiving, and using WSR-88D data. *Bull. Amer. Meteor. Soc.*, **74**, 645–653.
- Dixon, R. S., K. A. Browning, and G. J. Shutts, 2002: The relation of moist symmetric instability and upper-level potential-vorticity anomalies to the observed evolution of cloud heads. *Q. J. R. Meteorol. Soc.*, **128**, 839–859.
- Doswell, C. A., III, 1987: The distinction between large-scale and mesoscale contribution to severe convection: A case study example. *Wea. Forecasting*, **2**, 3–16.
- , H. E. Brooks, and R. A. Maddox, 1996: Flash flood forecasting: An ingredients-based methodology. *Wea. Forecasting*, **11**, 560–581.
- Emanuel, K. A., 1979: Inertial instability and mesoscale convective systems. Part I: Linear theory of inertial instability in rotating viscous fluids. *J. Atmos. Sci.*, **36**, 2425–2449.
- , 1983a: The Lagrangian parcel dynamics of moist symmetric instability. *J. Atmos. Sci.*, **40**, 2368–2376.
- , 1983b: On assessing local conditional symmetric instability from atmospheric soundings. *Mon. Wea. Rev.*, **111**, 2016–2033.
- , 1985: Frontal circulations in the presence of small moist symmetric stability. *J. Atmos. Sci.*, **42**, 1062–1071.
- Evans, M. S., 2006: An analysis of a frontogenetically forced early-spring snowstorm. *Bull. Amer. Meteor. Soc.*, **87**, 27–32.
- Fracasso, A. R., 2004: Case studies of cool season 500 hPa cutoff cyclone precipitation distribution. Masters of Science thesis, Department of Earth and Atmospheric Sciences, University at Albany/SUNY, Albany, NY, 121 pp.
- Garcia, C., Jr., 2000: Forecasting snowfall using mixing ratios on an isentropic surface: An update. NOAA Tech. Memo. NWS CR-116, 13 pp. [Available from NOAA/National Weather Service Central Region Headquarters, Kansas City, MO 64106-2897.]
- Gordon, J. D., 1998: A comprehensive winter weather forecast checklist. Scientific Services Division Applied Research Paper 18-08, NWS Central Region Headquarters. [Available from NOAA/National Weather Service Central Region Headquarters, Kansas City, MO 64106-2897.]

- Goree, P. A. and R. J. Younkin, 1966: Synoptic climatology of heavy snowfall over the central and eastern United States. *Mon. Wea. Rev.*, **94**, 663–668.
- Groisman, P. Y., R. W. Knight, D. R. Easterling, T. R. Karl, G. C. Hegerl, and V. N. Razuvaev, 2005: Trends in intense precipitation in the climate record. *J. Climate*, **18**, 1326–1350.
- Gyakum, J. R., 1987: Evolution of a surprise snowfall in the United States Midwest. *Mon. Wea. Rev.*, **115**, 2322–2345.
- Holton, J. R., 1992: *An Introduction to Dynamic Meteorology*. 3d ed. Academic press, 511 pp.
- Homan, J and L. W. Uccellini, 1987: Winter forecast problems associated with light to moderate snow events in the Mid-Atlantic States on 14 and 22 February 1986. *Wea. Forecasting*, **2**, 206–228.
- Hutchinson, T. A., 1995: An analysis of NMC's Nested Grid Model forecasts of Alberta Clippers. *Wea. Forecasting*, **10**, 632–641.
- Janish, P. R., C. A. Crisp, J. V. Cortinas Jr., R. L. Holle, and R. H. Johns, 1996: Development on an ingredients based approach to forecasting winter weather in an operational environment. Preprints, *15th Conf. On Weather Analysis and Forecasting*, Norfolk, VA, Amer. Meteor. Soc., 56–59.
- Johns, R. H. and C. A. Doswell III, 1992: Severe local storms forecasting. *Wea. Forecasting*, **7**, 588–612.
- Jurewicz, M. L., Sr. and M. S. Evans, 2004: A comparison of two banded, heavy snowstorms with very different synoptic settings. *Wea. Forecasting*, **19**, 1011–1028.
- Kalnay, E., M. Kanamitsu, R. Kistler, W. Collins, D. Deaven, L. Gandin, M. Iredell, S. Saha, G. White, J. Woollen, Y. Zhu, A. Leetmaa, B. Reynolds, M. Chelliah, W. Ebisuzaki, W. Higgins, J. Janowiak, K. C. Mo, C. Ropelewski, J. Wang, R. Jenne, and D. Joseph, 1996: The NCEP/NCAR 40-year reanalysis project. *Bull. Amer. Meteor. Soc.*, **77**, 437–471.
- Karl, T. R., 2006: Changes in very heavy and extreme precipitation events: What do we know? *18th Conference on Climate Variability and Change. AMS forum: Enviromental Risks and Impacts on Society: Success and Challenges. Severe Local Storms Special Symposium*. Atlanta, GA.
- and R. W. Knight, 1998: Secular trends of precipitation amount, frequency, and intensity in the United States. *Bull. Amer. Meteor. Soc.*, **79**, 231–241.

- Keshishian, L. G. and L. F. Bosart, 1987: A case study of extended east coast frontogenesis. *Mon. Wea. Rev.*, **115**, 100–117.
- , ———, and W. E. Bracken, 1994: Inverted troughs and cyclogenesis over interior North America: A limited regional climatology and case studies. *Mon. Wea. Rev.*, **122**, 565–607.
- Kistler, R., E. Kalnay, W. Collins, S. Saha, G. White, J. Woolen, M. Chelliah, W. Ebisuzaki, M. Kanamitsu, V. Kousky, H. Van den Dool, R. Jenne, and M. Fiorino, 2001: The NCEP-NCAR 50-year reanalysis: Monthly means CD-ROM and documentation. *Bull. Amer. Meteor. Soc.*, **82**, 247–267.
- Kocin, P. J. and L. W. Uccellini, 1990: *Snowstorms along the Northeastern Coast of the United States: 1955-1985*. Meteor. Monogr., No. 44, Amer. Meteor. Soc., 280 pp.
- and ———, 2004a: *Overview*. Vol. 1. *Northeast Snowstorms*. No. 54. Amer. Meteor. Soc., 296 pp.
- and ———, 2004b: *The Cases*. Vol. 2. *Northeast Snowstorms of the 20th Century*. Meteor. Monogr., No. 54. Amer. Meteor. Soc., 522 pp.
- Maglaras, G. J., J. S. Waldstreicher, P. J. Kocin, A. F. Gigi, and R. A. Marine, 1995: Winter weather forecasting throughout the eastern United States. Part I: An overview. *Wea. Forecasting*, **10**, 5–20.
- McCann, D. W., 1995: Three-dimensional computations of equivalent potential vorticity. *Wea. Forecasting*, **10**, 798–802.
- McNulty, R. P., 1978: On upper tropospheric kinematics and severe weather occurrence. *Mon. Wea. Rev.*, **106**, 662–672.
- , 1995: Severe and convective weather: A central region forecasting challenge. *Wea. Forecasting*, **10**, 187–202.
- Moore, J. T. and P. D. Blakely, 1988: The role of frontogenetical forcing and conditional symmetric instability in the Midwest snowstorm of 30–31 January 1982. *Mon. Wea. Rev.*, **116**, 2155–2171.
- , C. E. Graves, S. Ng, and J. L. Smith, 2005: A process-oriented methodology toward understanding the organization of an extensive mesoscale snowband: A diagnostic case study of 4–5 December 1999. *Wea. Forecasting*, **20**, 35–50.
- and T. E. Lambert, 1993: The use of equivalent potential vorticity to diagnose regions of conditional symmetric instability. *Wea. Forecasting*, **8**, 301–308.

- Mossop, S. C., 1970: Concentrations of ice crystals in clouds. *Bull. Amer. Meteor. Soc.*, **51**, 474–479.
- Nicosia, D. J. and R. H. Grumm, 1999: Mesoscale band formation in three major northeastern United States snowstorms. *Wea. Forecasting*, **14**, 346–368.
- Nietfeld, D. D. and D. A. Kennedy, 1998: Forecasting snowfall amounts: An ingredients-based methodology supporting the Garcia method. Preprints, *16th Conf. On Weather Analysis and Forecasting*, Phoenix, AZ, Amer. Meteor. Soc., 385–387.
- Niziol, T. A., W. R. Snyder, and J. S. Waldstreicher, 1995: Winter weather forecasting throughout the eastern United States. Part IV: Lake effect snow. *Wea. Forecasting*, **10**, 61–77.
- Novak, D. R., L. F. Bosart, D. Keyser, and J. S. Waldstreicher, 2004: An observational study of cold season-banded precipitation in northeast U.S. cyclones. *Wea. Forecasting*, **19**, 993–1010.
- , J. S. Waldstreicher, L. F. Bosart, and D. Keyser, 2006: A forecast strategy for anticipating cold season mesoscale band formation within eastern U.S. cyclones. *Wea. Forecasting*, **21**, 3–23.
- Petterssen, S., 1956: *Weather Analysis and Forecasting*. Vol. 1. McGraw-Hill, 428 pp.
- Power, B. A., P. W. Summers, and J. D`Avignon, 1964: Snow crystal forms and riming effects as related to snowfall density and general storm conditions. *J. Atmos. Sci.*, **21**, 300–305.
- Reuter, G. W. and M. K. Yau, 1990: Observations of slantwise convective instability in winter cyclones. *Mon. Wea. Rev.*, **118**, 447–458.
- Roebber, P. J., S. L. Bruening, D. M. Schultz, and J. V. Cortinas Jr., 2003: Improving snowfall forecasting by diagnosing snow density. *Wea. Forecasting*, **18**, 264–287.
- Rogers, R. R. and M. K. Yau, 1989: *A Short Course in Cloud Physics*. Pergammon Press, 293 pp.
- Sanders, F., 1986: Frontogenesis and symmetric stability in a major New England snowstorm. *Mon. Wea. Rev.*, **114**, 1847–1862.
- and L. F. Bosart, 1985: Mesoscale structure in the megalopolitan snowstorm of 11–12 February 1983. Part I: Frontogenetical forcing and symmetric instability. *J. Atmos. Sci.*, **42**, 1050–1061.
- Sangster, W. E. and E. C. Jagler, 1985: The (7WG, 8WT) “magic” chart. CR Tech. Attachment 85-1, NOAA/NWS Central Region, Kansas City, MO, 5 pp.

- Sawyer, J. S., 1956: The vertical circulation at meteorological fronts and its relation to frontogenesis. *Proc. Royal. Soc. London*, **A234**, 346–362.
- Schultz, D. M. and P. N. Schumacher, 1999: The use and misuse of conditional symmetric instability. *Mon. Wea. Rev.*, **127**, 2709–2732.
- Seltzer, M. A., R. E. Passarelli, and K. A. Emanuel, 1985: The possible role of symmetric instability in the formation of precipitation bands. *J. Atmos. Sci.*, **42**, 2207–2219.
- Smith, B. A., 2003: Cutoff cyclones: A global and regional climatology and two case studies. Masters of Science thesis, Department of Earth and Atmospheric Sciences, University at Albany/SUNY, Albany, NY, 165 pp.
- Snook, J. S., 1992: Current techniques for real-time evaluation of conditional symmetric instability. *Wea. Forecasting*, **7**, 430–439.
- Thorpe, A. J. and K. A. Emanuel, 1985: Frontogenesis in the presence of small stability to slantwise convection. *J. Atmos. Sci.*, **42**, 1809–1824.
- Uccellini, L. W. and P. J. Kocin, 1987: The interaction of jet streak circulations during heavy snow events along the east coast of the United States. *Wea. Forecasting*, **2**, 289–308.
- Wallace, J. M., 1975: Diurnal variations in precipitation and thunderstorm frequency over the conterminous United States. *Mon. Wea. Rev.*, **103**, 406–419.
- Wetzel, S. W., 2000: Investigation of the dynamical and thermodynamical ingredients for mid-latitude winter season precipitation. Masters of Science thesis, Department of Atmospheric and Oceanic Sciences, University of Wisconsin-Madison, Madison, WI, 158 pp.
- and J. E. Martin, 2001: An operational ingredients-based methodology for forecasting mid latitude winter season precipitation. *Wea. Forecasting*, **16**, 156–167.
- Wiesmueller, J. L. and S. M. Zubrick, 1998: Evaluation and application of conditional symmetric instability, equivalent potential vorticity, and frontogenetic forcing in an operational forecast environment. *Wea. Forecasting*, **13**, 84–101.
- Xu, Q., 1989: Extended Sawyer-Eliassen equation for frontal circulations in the presence of small viscous moist symmetric stability. *J. Atmos. Sci.*, **46**, 2671–2683.

Cool-Season Moderate Precipitation Events
in the Northeastern United States

*A thesis presented to the Faculty
of the University at Albany, State University of New York
in partial fulfillment of the requirements
for the degree of
Master of Science
College of Arts & Sciences
Department of Earth and Atmospheric Sciences*

Keith R. Wagner
2006